

NORTHWESTERN UNIVERSITY

Polyelectrolyte Complexes of Random Copolymers and their Applications in Environmental
Remediation

A DISSERTATION

SUBMITTED TO THE GRADUATE SCHOOL
IN PARTIAL FULFILLMENT OF THE REQUIREMENTS

for the degree

DOCTOR OF PHILOSOPHY

Field of Material Science and Engineering

By

Jeremy Wang

EVANSTON, ILLINOIS

March 2023

Abstract

Polyelectrolyte Complexes of Statistical Copolymers and their Applications in Environmental Remediation

Jeremy Wang

As polymer science has advanced as a field, so too have the uses for polymeric materials. We encounter polymers and plastics on a daily basis, and while their presence has greatly improved our quality of life, they have also had a profound and often negative impact on our environment. Plastic waste and pollution are currently problems of great concern, and recent trends in terms of micro- and nanoplastic pollution, and chemical pollution of water continue to exacerbate such worries. In this thesis, we explore how polyelectrolyte complexes of random copolymers can be used to effectively address some of these environmental concerns. The combination of charged interactions and disorder of polymer sequence can provide a novel combination of interactions which are well suited for removing contaminants from water, and even promoting the enzymatic degradation of plastic. The results obtained demonstrate that this research into new polymeric materials not only advances our understanding of fundamental polymer properties but yields relevant applications to the issues we encounter in the present day.

Acknowledgements

I certainly would not have been able to reach this point without the help and support of all the people that I have met throughout all the circumstances of my life.

I would like to thank my parents, who as immigrants have had to work tirelessly to support me throughout my educational career.

I would like to thank my research advisors, who have watched over my scientific endeavors with care. This includes my undergraduate advisor, who continues to be a role model for me to this day.

And I would like to thank my friends, who have supported me and kept me going even through difficult times. This includes those who stuck with me through thick and thin over the years, and those who have only briefly but no less meaningfully been part of my life.

In terms of financial support funding my work throughout my Ph.D career, I would like to acknowledge the Sherman Fairchild Foundation and their grant to the Prof. Olvera de la Cruz, which has allowed me the academic freedom to pursue studies of my interest.

Table of Contents

Abstract	2
Acknowledgements.....	3
Table of Contents.....	4
List of Tables, Illustrations, Figures, or Graphs.....	7
1 Chapter 1: Introduction and Motivation.....	10
2 Chapter 2: Background.....	21
Section: Polymer synthesis and polymer sequences.....	21
Subsection: Polymer synthesis.....	21
Subsection: Copolymers and Composition.....	28
Section: Polyelectrolytes and Polyelectrolyte complexes.....	38
Section: Protein complexes and membraneless organelles.....	41
3 Chapter 3: Polyelectrolyte Complexes of Random Copolymers for Removing Organic Contaminants from Water.....	45
Introduction.....	46
Results and Discussion.....	50
Polymerization and Characterization of Random Copolymers.....	50
Polyelectrolyte complex formation and dye filtration.....	52
Confirmation of dye encapsulation and micelle formation in anionic copolymer.....	55
Simulations of Polymers and Dyes.....	56
Conclusion.....	66
Methodology.....	68
Materials.....	68
Copolymer characterization.....	70
Quantification of dye and contaminant removal.....	72
Coarse Grain Simulations.....	73
Coarse Grain Model.....	74
MARTINI Model.....	77

4	Chapter 4: Tailoring Interactions of Random Copolymer Polyelectrolyte Complexes to Remove Nanoplastic Contaminants from Water	80
	Introduction.....	80
	Experimental results.....	85
	Copolymer characterization	85
	Nanoplastic Remediation	86
	Copolymer adsorption.....	88
	Conclusion	91
	Methodology.....	93
	Materials	93
	Polymer synthesis	93
	Polymer NMR characterization	95
	Polymer molecular weight characterization.....	98
	Nanoplastic Synthesis and Characterization.....	101
	SEM image preparation	101
	Remediation procedure	103
	Fluorescence measurements of nanoplastic concentration	104
	Lead ion adsorption and removal.....	105
	Quartz Crystal Microbalance (QCM) tests	106
	Martini Simulations of Random Copolymer Adsorption	107
	Simulations of Polyelectrolyte Complexes.....	109
5	Chapter 5: Random Copolymer Complexes with PETase for Enhanced Enzymatic Degradation of PET	112
	Introduction.....	113
	Results and Discussion	116
	PETase Structure at Elevated Temperature	116
	Enzyme-Polymer Complexation.....	119
	Stability of the Complexed Enzyme	123
	PETase-copolymer complexes with suppressed aggregation	125
	Activity of Enzyme-Polymer Complexes on Small Molecule and Solid Substrates	127

Conclusions and Outlook.....	129
Methodology.....	130
Materials.....	130
Copolymer synthesis.....	131
Copolymer molecular weight characterization.....	132
Copolymer composition characterization.....	132
PETase expression and purification.....	133
PETase activity against p-nitrophenyl acetate after thermal challenge.....	136
PETase activity on PET films.....	137
PET degradation product calibration curve construction.....	138
Atomistic Simulations.....	139
GoMartini PETase Only Simulations.....	140
Calculation of Hydrphobic Surface Fraction.....	142
Martini Simulations of PETase and Random Copolymers.....	143
Definition of Polymer-Protein Contacts.....	144
6 Chapter 6.....	146
Outlook for enzyme copolymer complexes.....	146
Outlook for polyelectrolyte complexes for water remediation.....	152
Conclusion.....	157
References.....	159
Vita.....	171

List of Tables, Illustrations, Figures, or Graphs

Figure 1.1 Examples of amino acids.....	16
Figure 1.2 Components of a DNA polymer.. ..	18
Figure 2.1 Three steps of polymerization, with associated rate equations.....	24
Figure 2.2 Step Growth polymerization of polyethylene terephthalate.	27
Figure 2.3 An illustration of random copolymerization in a mixture of A and B monomers.	30
Figure 2.4 Four possible reactions in a two monomer copolymerization	32
Figure 2.5 An illustration of random copolymers that optimally adsorb onto a patterned surface.....	35
Figure 2.6 Chemical structure of random copolymer used in Reference 42.....	37
Figure 2.7 A phase diagram of polyelectrolyte complex formation with respect to salt concentration and polyelectrolyte concentration.	40
Figure 3.1 Schematic of random copolymer and contaminants with simulation models	49
Figure 3.2 Filtration and absorbance results	55
Figure 3.3 Probability of a chain clustering	59
Figure 3.4 Simulation results on copolymer complex charge distribution	61
Figure 3.5 Simulation results of molecular encapsulation.	64
Figure 3.6 NMR assignments for the cationic copolymer of HEMA and TMAEMA	71
Figure 3.7 NMR assignments for the anionic copolymer of EHMA, PEGMEMA, and SPMA.	71
Figure 3.8 MARTINI parameters for the random anionic copolymers.....	77
Figure 4.1 Schematic of polymer complexes and polymer adsorption onto PET.	85
Figure 4.2 Image of PET nanoplastics and remediation rates from water.	87
Figure 4.3 Polymer adsorption onto PET vs hydrophobic fraction FH with experiments and simulation.	88
Figure 4.4 Simulation results for polyelectrolyte complexes with varying hydrophobic fraction	90
Figure 4.5 Lead ion removal results with remediation technique.	92

Figure 4.6 Anionic copolymer NMR spectrum and peak assignments	96
Figure 4.7 Cationic copolymer NMR spectrum and peak assignments.	97
Figure 4.8 Serial dilution plot for Sample 3.	100
Figure 4.9 Correlation function and Intensity distribution from DLS measurements of PET nanoplastics.	102
Figure 4.10 Calibration curves for PET nanoplastic solutions as a function of percentage of stock solution.	105
Figure 4.11 QCM data for polymer adsorption experiments of samples 1-4.	107
Figure 5.1 Description and models of PETase and the random copolymers.	115
Figure 5.2 Comparison of the GoMartini PETase to atomistic simulations	118
Figure 5.3 Random copolymer complexation with PETase protein for different mean polymer compositions	119
Figure 5.4 Hydrophobic interactions affect PETase-random copolymer complexation.	121
Figure 5.5 Contact of negatively charged monomers with positive surface domains.	122
Figure 5.6 Active site stabilization by polymer contacts.	124
Figure 5.7 DLS measurements of PETase aggregation and copolymer solution behavior.....	126
Figure 5.8 DLS curves for PETase copolymer solutions after 20 minutes heating.	127
Figure 5.9 Activity of PETase and PETase/copolymer complexes	128
Figure 5.10 Hydrogen nuclear magnetic resonance of RAFT-synthesized random copolymer.....	133
Figure 5.11 DNA sequence encoding PETase.....	133
Figure 5.12 Amino acid sequence of PETase	134
Figure 5.13 Sodium dodecyl sulfate polyacrylamide gel electrophoresis (SDS-PAGE) stained with Coomassie blue on final purified PETase protein product.....	135
Figure 5.14 Calibration curve used to convert absorbance at 347 nm to p-nitrophenol concentration.....	137
Figure 5.15 Calibration curve used to convert absorbance at 242 nm to mass of PET degraded	138
Figure 6.1 Monomers for possible PET binding motif.	151

Table 3.1 Copolymer Characterization.....	52
Table 3.2 Non-Bonded Parameters for the Coarse-Grain forcefield.....	75
Table 3.3 Bond Parameters for the MARTINI Forcefield	78
Table 3.4 Angle Parameters for the MARTINI Forcefield	79
Table 4.1 Anionic Copolymer Compositions	86
Table 4.2 Anionic copolymer Molecular Weights	99
Table 4.3 Anionic Copolymer dn/dc values	100
Table 4.4 Cationic polymer solution added for flocculation	103
Table 6.1 Degradation of Treated PET samples	150

Chapter 1: Introduction and Motivation

As a class of materials, polymers occupy a vast space of properties, characteristics, and applications.¹ Unlike metals, with atoms held together by shared delocalized electrons, and ceramics, with a network of ionic and covalent bonding, polymer properties are determined by more than just the nature of interatomic bonds. Polymers are generally regarded as individual chemical units, or monomers, which are bonded together in a chain-like fashion, typically through covalent means. It is this interconnectivity of monomers which imparts many of the unique characteristics of polymer materials.

Perhaps the most well-known of polymer materials are plastics, which finds use in nearly every aspect of modern-day life. One defining feature of plastics is a combination of structural durability and ease of processing, which makes it an ideal material for packaging and containers.² Unlike metals and ceramics, the structural properties of plastic are derived from the steric repulsion and intermolecular interactions of a tangle of polymer chains. At room temperature, these polymer chains are typically immobile or glassy, leading to a material that is solid and impact-resistant. However, with relatively mild heating, the polymer chains become mobile and can rearrange in conformation, leading to a state that is rubbery and easily deformed, in some cases reaching an endpoint of liquid-like flow. This is in stark contrast to metals and ceramics, whose melting temperatures are generally an order of magnitude higher than that of plastics due to the high energy needed to break their atomic bonds. Thus, the shaping and manipulation of plastic materials are relatively facile, compared to that of metals, which require high energy and force inputs for melting and machining or drawing processes. Ceramics are even more difficult to handle, with its

brittleness posing challenges to forming complex shapes and even its usage as a container without breaking the material.

Adding to the fact that plastics are quite lightweight, being made of mostly carbon and hydrogen atoms compared to the heavier metal atoms further down the periodic table and can be made from natural resources that are readily exploited such as oil, it is little wonder that most objects or products whose main function is some form of structural durability is made of plastic. This applies not only packaging and containers but all sorts of trinkets, toys, furniture, mechanical parts, appliances, and construction materials. The list could most certainly go on. Plastic materials can also be processed into forms other than a dense solid. They can be blown into foam materials, such as Styrafoam, which is a polystyrene foam used for insulation, or woven into fibers to make fabrics and clothes. Polyester clothing is made from polyethylene terephthalate, the same material used in water bottles, and accounts for a significant and leading fraction of all textile fibers produced worldwide.³ Plastic materials can also be applied as a thin coating to alter the surface properties of an object, as in the case of water-repellent glass windows and non-stick pans.⁴

A closely related class of polymer materials to plastics are rubbers. Rubbers are also composed of a tangle of polymer chains, but these chains are mobile at room or operating temperatures, leading to a soft and deformable material. In most cases, rubbers are cross-linked, where the polymer chains have interconnected covalent bonds to form a percolated network structure. In this regard, rubbers have structural integrity and are difficult to permanently deform, as the underlying network structure is difficult to change. They traditionally cannot enter a liquid-like flow state, and if they are deformed, such as in the case of a rubber band, they tend to recover their original dimensions

in a timely manner. Rubber objects are prevalent in our lives, from tires and spatulas to gloves and shoes and a whole host of commercial and industrial products.

It is quite clear that a modern lifestyle as we know it would not be possible without polymer materials, particularly those made of synthetic polymer materials around which we have built massive industries and supply chains. They have brought an unprecedented level of quality of life and convenience, made possible by their particular properties and economics. However, as it has been with many human endeavors, progress is uneven and the consequences of our success have been difficult to deal with. Just as industrialization and the burning of coal and fossil fuels enabled the rapid development of many societies, it has also been a main driver of climate change that poses to exact heavy costs, particularly on less developed countries less able to adapt to changing weather patterns.⁵ The proliferation of plastic usage comes with its own set of costs to society and the environment. Most packaging materials, especially for foodstuff, are by design single-use items that are thrown away after the product is consumed. This has led to a large amount of plastic waste being generated, much of it going into landfill.^{6,7} However, waste management in many places is not perfect, and is inadequate in others. Large portions of plastic waste end up in the environment and the oceans where they exert negative consequences on marine life and potentially human life as well. Large plastic debris can have lethal interactions with various marine organisms such as fish, turtles, seals and whales through entanglement or ingestion. There is also a demonstrated impact on human economic activity, with an estimated \$6-19 billion dollar loss in tourism and aquaculture industries in 2018.⁸

There are further concerns related to smaller plastic particles as well. When larger pieces of plastic are subjected to environmental conditions such as the constant abrasion of wave motion and

exposure to UV light from the sun, smaller plastic particles are produced on the micron to millimeter scale.⁹ Small plastic particles are also produced for commercial or industrial use, such as in facial cleansers or in resins. These particles are considered microplastics and are a topic of current concern. Due to their high surface area to volume ratio, they are quite effective at adsorbing chemicals and heavy metal ions onto their surface and can act as a vector to transfer these chemicals and heavy metals into marine organism tissue.¹⁰ This not only affects the health of marine organisms but also humans who consume microplastic-contaminated seafood. The issue extends to plant life and vegetation as well, which have been shown to uptake microplastics from the surrounding soil.¹¹ Even smaller plastic particles that are under the micron scale, known as nanoplastics, can have potentially more pronounced effects due to even higher surface to area ratios and the ability to pass through biological membranes.¹²

Other modes of contamination also contribute to the externalities of industrial polymer production. The byproducts and intermediary compounds involved in the polymer manufacturing process can be detrimental to human health. For example, Bisphenol A is a common monomer used for a variety of purposes, such as the production of polycarbonate plastics.¹³ Another purpose is as part of the inner epoxy lining of soda cans to prevent acidic degradation of the aluminum metal. Studies have shown that Bisphenol A in polymer materials can leech out from the coating and contaminate water sources that come into contact with the materials.¹⁴ Bisphenol A is known to be an endocrine disruptor and can interfere with normal hormonal processes, and has been associated with obesity, diabetes, reproductive disorders, and cancer.¹⁵ While the daily exposure of Bisphenol A for most people is well below established safe levels, there is concern that fetuses, infants and children can be particularly sensitive to Bisphenol A as their livers have not fully developed the

ability to break down such chemicals. There also remains some controversy on the effects of being exposed to low dosages of endocrine disruptors like BPA, and whether a lower safe exposure limit should be established.

For the case of Bisphenol A, contamination of water sources from urban runoff does occur, as when rain falls upon exposed construction or automotive materials and carries BPA into municipal water supplies.¹⁶ Fortunately, BPA naturally degrades in environmental conditions over the course of a few days, and water treatment plants are quite effective at removing it through filtration processes like activated carbon.¹⁷ Thus the bulk of BPA exposure for humans comes from packaged food products and not from potable water. However, there are other chemicals used in polymer production that exhibit much more concerning behavior. One such type of chemical are perfluorinated alkyl substances, or PFAS, which are used to make polymers such as polytetrafluoroethylene (PTFE), otherwise known as Teflon, commonly used in non-stick coatings and lubricants.¹⁸

One type of PFAS that has been heavily used in the past few decades, perfluorooctanoic acid (PFOA), does not degrade under natural conditions, are difficult to remove from water sources using traditional water treatment techniques, and are thought to act as endocrine disruptors.¹⁹ Similar to BPA, PFAS and PFOA have been shown to leech out from coatings when exposed to water, such as from non-stick pans and some types of food containers. There have also been some documented cases of improper disposal of PFAS materials from certain manufacturers and discharge from industrial sites, including military bases and airports.²⁰ Taken together, PFAS contamination of water sources is widespread and relevant, with some locations having noticeably higher PFAS concentrations. Nearly everyone has detectable levels of PFAS in their blood, a

profound and somewhat morbid demonstration of how the presence of polymer materials and their byproducts can alter the environment and literally become a part of our lives.²¹ The health effects of PFAS exposure, particularly at typical concentrations encountered, have not been fully explored, with much controversy and debate over what a safe limit of PFAS in water should be. It is generally agreed upon that PFOA and PFAS are chemicals of concern and that remediation techniques should be investigated.

While there could be many more examples of how polymers, particularly synthetic polymers, have greatly impacted the environment, society, and our lived experience, it can be further instructive to consider natural polymer systems. Natural polymers present an entirely different set of properties with the possibility of complex behaviors that can only be found in living systems. The influence and ubiquity of natural polymers is no less than and can arguably be greater than that of synthetic polymers. One common natural polymer is cellulose, which is essentially many sugar molecules that are chained together and is quite common in plant life. Depending on the context, cellulose-based materials can have vastly different properties. Cotton is one such example, being composed of over 90% cellulose in a fibrous form, with another 8 percent being water.²² After polyester, cotton is one of the most common fibers used to make clothing and other fabrics. Wood is also another common material made mostly of cellulose, and has been used extensively throughout history as construction material and as a fuel source.²³

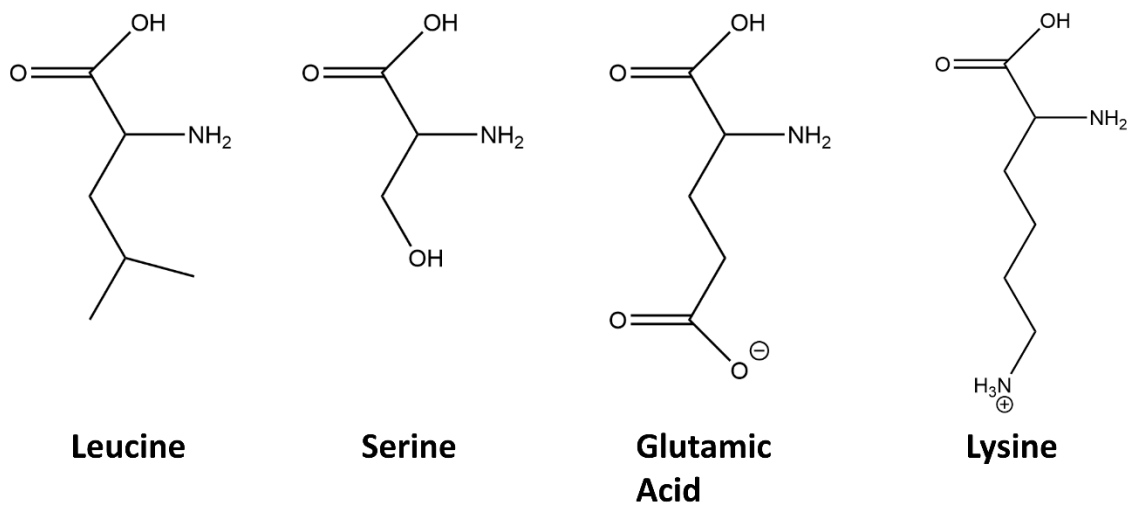


Figure 1.1 Examples of amino acids. Leucine is hydrophobic, serine is hydrophilic, glutamic acid is typically negatively charged and lysine is typically positively charged.

Perhaps the more interesting natural polymers are the ones that are not designed for bulk structural purposes, but for biological functions. This class of polymers include proteins and nucleic acids, are fundamental to living systems such as ourselves. The monomeric unit of proteins are amino acids, chemicals with both an amine and carboxylic acid group. Twenty two different amino acids are used to make proteins, and they can broadly be classified into four types, being hydrophobic, hydrophilic, positively charged or negatively charged.

Proteins are incredibly complex and precise entities. Starting from just a sequence of amino acids, a protein will, in many cases, fold and settle into a determinate structure in response to a combination of the interactions between monomers and the surrounding molecular environment, typically an aqueous buffer that is characteristic of biological media.²⁴ The structure and interactions of folded proteins give way to the myriad of biological functions we observe. At the chemical level, enzymes are a classic example of a functional protein, with an active site that is designed to fit and interact with specific molecular substrates and catalyzing their reactions.²⁵

Nearly all relevant biological reactions are mediated by enzymes. Not only do they accelerate reactions, but they also play a role in regulating reactions as well. There are several mechanisms by which enzymes can be activated or deactivated. One such example is allosteric activation and inhibition, in which an activator or cofactor binds to the enzyme away from the active site, but then induces a conformational change such that the active site is also changed. This change in the active site allows or prevents interaction with the enzyme's intended substrate. These sorts of feedback mechanisms are important in maintaining the incredibly complex network of reactions that living systems depend on.

Aside from regulating chemical reactions, proteins are integral to sensing and signaling functions.²⁶ Receptor proteins populate cell surfaces and membranes and act as sensor to external conditions. They typically are designed to bind strongly to a specific ligand molecule. Instead of catalyzing any chemical reaction, the proteins themselves change their conformation and characteristics, which then induces a response in the cell. One common example of this is endocytosis, in which small vesicles are formed to encapsulate and transport objects from outside the cell to the inside of the cell. When a particular receptor protein on a cell surface binds to a ligand, the interior portion of the protein changes conformation such that it can bind to clathrin proteins, which form a polyhedral lattice and induces membrane bending.²⁷ This is also the mechanism by which many viruses enter cells, as viral protein spikes bind strongly to receptor proteins. It can be noted that interfering with this binding process is the basis for various classes of antiviral drugs design to fight various diseases such as HIV and influenza.²⁸

Proteins are also very involved in our own senses that we use to experience the world. As an example, rhodopsin is a protein located at the nerve endings in the eye, and changes conformation once excited by light due to the photoisomerization of retinal (a form of Vitamin A).²⁹ This change in conformation leads to the release of a retinal that was otherwise bonded to the protein. The retinal activates the neural signaling process, and the aggregate information from this visual phototransduction pathway is processed by the brain to provide sight.³⁰ Similar processes happen with smell and taste, where receptor proteins in the nasal cavity and tongue change conformations when they bind to specific molecules that are associated with certain odors and flavors.³¹ The same principle also applies to hearing and touch, where certain proteins exhibit a mechanistic response to vibrations and pressure. These are known as mechanoreceptors and activate neural signaling processes based on displacement or force. One mechanism by which this occurs is that the receptor proteins change the conformation in way that permits ion flow through the membrane to activate the action potentials involved in nerve signaling.²⁶

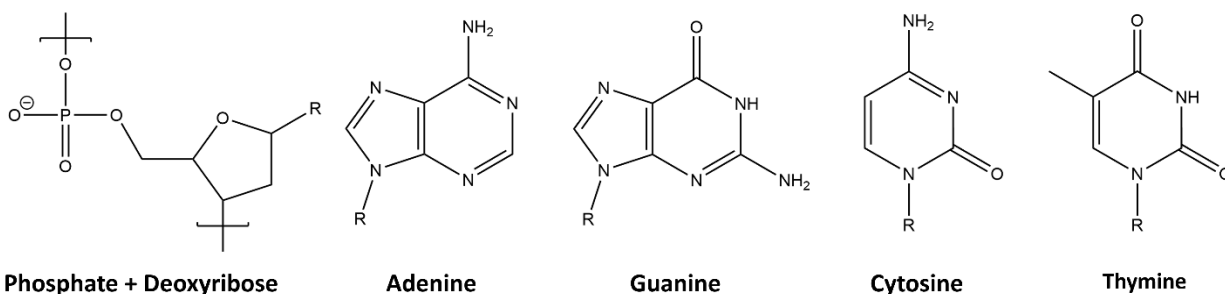


Figure 1.2 Components of a DNA polymer. The phosphate and deoxyribose backbone is shown on the left, while the four nitrogen bases are shown on the right.

Another class of biological polymers are the nucleic acids, which are just as essential in maintaining living processes. Deoxyribonucleic acids (DNA) and Ribonucleic acids (RNA) are

the most prominent of nucleic acids, being composed of nucleotides, monomers with a 5-carbon ring, a phosphate group, and a nitrogenous base.

DNA is well-known as the method which all living organisms store genetic information. Although DNA only has four monomer components, the sequence of these four components contains all the information necessary for cells to function and develop over time. DNA accomplishes this feat by encoding information necessary to manufacture all the proteins that a living organism can produce. Every three base pairs corresponds to a single amino acid in a protein sequence. Through a transcription process, an RNA version of the DNA sequence is made, which is then fed into a ribosome, a type of protein complex that will read the RNA sequence and synthesize the corresponding protein peptide sequence. This type of complex molecular machinery and process is present in nearly all living cells.²⁶

From all the above discussion it is quite evident that polymers are capable of accomplishing a great many tasks and function, and polymer properties and behaviors underlie much of how we experience and go about living our lives, whether in a good way or bad way, and in matters big and small. The study of polymer science has traditionally focused on synthetic polymers, with a focus on industrial application. While advances in this area has yielded many benefits and innovations, it does appear that we, as a society, are struggling to address the negative consequences of our usage of polymers, particularly in the case of environmental contamination and degradation. It is a main motivating factor of the work in this thesis to draw upon polymer science focusing on some of the complex behavior of polymers, such as those seen in biological systems, in order to try and address some of the environmental problems that can be caused by polymer production and usage. In particular, the ability of protein and other biological complexes,

such as membraneless organelles, to sequester molecules and enhance enzyme activity is quite relevant. Designing a polymer system that exhibits such a functionality could be very helpful in dealing with issues in water remediation and plastic waste management.

This thesis demonstrates such a feat is possible by studying a particular statistical copolymer system that is based around a polymer with hydrophobic, hydrophilic, and anionic monomers. In this sense, the anionic copolymer displays some similar characteristics to proteins in terms of its solubility and folding behavior. By utilizing the ability of this copolymer to form complexes with other polymers and proteins, significant results for environmental remediation are realized. This work draws upon various concepts in polymer science, from traditional polymer statistics, to the phase behavior of polyelectrolyte complexes, and the formation and functions of protein complexes. Chapter 2 delves further into this background and provides details that are important to understanding the key concepts of the thesis work.

Chapter 3 details the results of a study that demonstrates the ability of a random copolymer polyelectrolyte complex to remove chemical contaminants, including PFOA, from water. The results of this study has been published.³² Chapter 4 extends the work of this copolymer system, and shows that nanoplastics can be effectively removed from solution using the same technique. The results of this study has been submitted for publication at the time of writing this thesis. Chapter 5 explores how a complex of the anionic copolymer and PETase, a plastic degrading enzyme, can provide enhanced enzymatic activity for decomposing PET. The results of this study has been published.³³

Chapter 6 discusses future outlook on the potential research directions for the work presented and concludes the dissertation.

Chapter 2: Background

Section: Polymer synthesis and polymer sequences

As noted in the previous chapter, polymers are monomers that bonded together, and it is this connectivity that contributes to many polymer properties. Typically, the monomers are chemical units that are covalently bonded, although it is interesting to note there are exceptions such as polymers made of colloidal monomers bonded through interparticle interactions,³⁴ or supramolecular polymers with monomers bonded by non-covalent means.³⁵ In this section we will take a closer look at the process of forming covalent bonds and some of the statistics of that process.

Subsection: Polymer synthesis

The formation of a covalent bond is an inherently chemical process in which an electron pair is shared between two atoms. There are two main methods by which this can occur, either by a reaction involving an unpaired electron, known as a free radical, or by the reaction of two functional groups, molecular motifs with predictable and relatively consistent chemical behavior. The first mechanism is the basis for chain-growth polymerization, and the second mechanism is the basis for step-growth polymerization.

Sub-subsection: Chain-growth polymerization

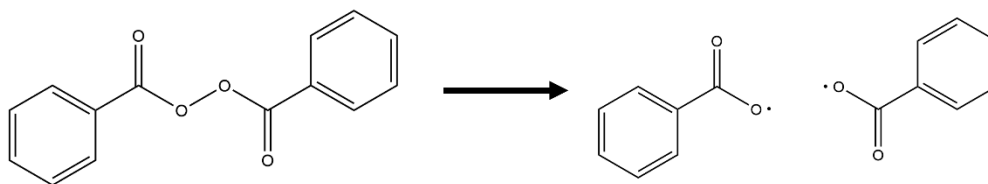
The process of chain-growth polymerization involves a few distinct steps. The first step is known as initiation, where a free radical is formed from a molecule known as an initiator. Initiators tend not to be very stable compounds, and will typically decompose and form free radicals when exposed to elevated temperatures or UV light.³⁶ One common initiator is benzoyl peroxide, which effectively decomposes at temperatures higher than 50 C. There are other initiators that can be selected depending on the desired temperature of decomposition.

Once a free radical is formed, it can react with a monomer by essentially ripping off an electron from an existing bond to form a new bond and new free radical. Carbon-carbon double bonds are particularly susceptible to this process as there is a significant difference in the strength of a sigma bond and a pi bond.³⁷ Thus, most monomers involved in chain-growth polymerization contain a carbon-carbon double bond. It should be noted that free radicals are very reactive, and in most cases not all free radicals formed from the decomposition of the initiator will end up reacting with a monomer.

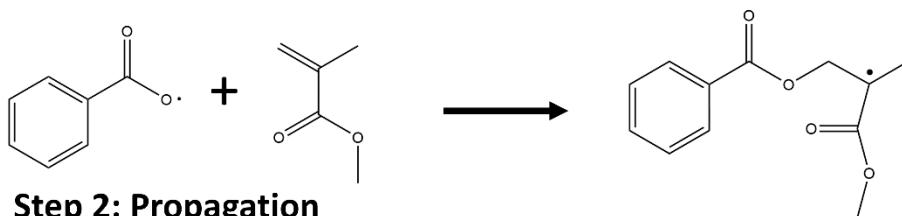
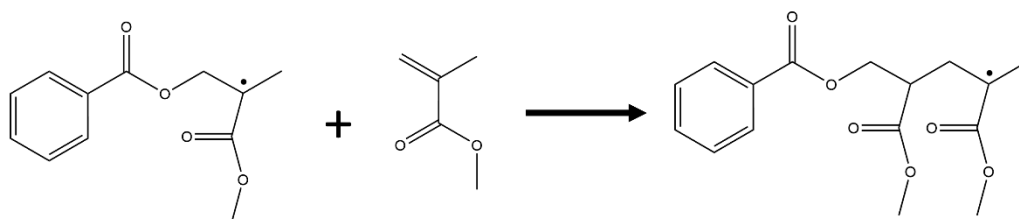
The second step is chain propagation. After initiation, we have an activated monomer with a free radical that is capable of repeating the bond formation process and adding more monomers to the chain. This is where the chain-growth portion of the polymerization process occurs. The rate at which monomers are added to polymer chains is generally independent of the chain length. The final step is chain termination. Chain propagation does not continue indefinitely, and eventually the free radical at the end of a growing chain will participate in reactions in which another free radical is not generated.

The most common of these reactions is when the free radical at a chain end meets another free radical. If this free radical is also at the end of another growing polymer chain, the two polymers can combine in a process called recombination. The free radical can also steal a hydrogen from a carbon-hydrogen bond from another polymer or compound, resulting in a carbon-hydrogen bond at the end of the polymer, and a carbon-carbon double bond where the hydrogen was taken from. This process is known as disproportionation. These termination reactions typically occur within less than a second of chain initiation.³⁸

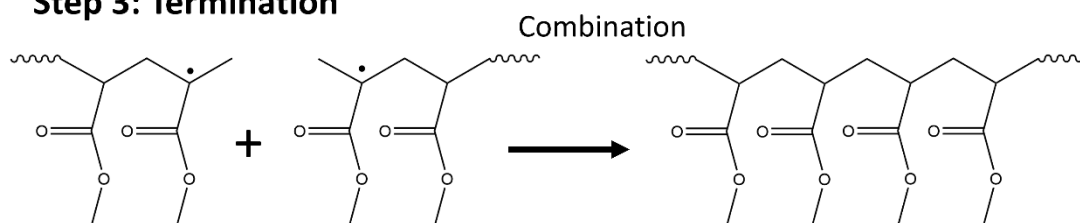
An illustration of these polymerization steps is provided below in Figure 2.1, with BPO as an example initiator and methyl methacrylate as an example monomer.

Step 1: Decomposition/Initiation

$$r_i = 2fk_d[I]$$

**Step 2: Propagation**

$$r_p = k_p[M][P \cdot]$$

Step 3: Termination

$$r_t = 2k_t[P \cdot]^2$$

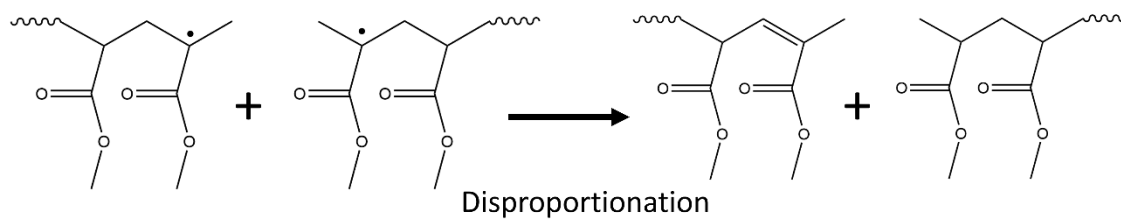


Figure 2.1 Three steps of polymerization, with associated rate equations

One can note that as each of these steps represent a chemical reaction, they can also have a rate equation associated with them. In the first equation denoting the initiation rate, we have $[I]$ as the concentration of our initiator BPO and f as the fraction of free radicals generated that go on to react with monomers. In the second equation denoting the propagation rate, we have $[M]$ as the monomer concentration and $[P\cdot]$ as the concentration of polymer chains that are actively propagating. $[P\cdot]$ in the third equation, which denotes termination rate, is the same as in the second equation. In order to calculate the reaction rates, we usually make a steady state assumption that the amount of $[P\cdot]$ generated in our initiation step is the same amount that is terminated. We can then obtain the following form for the propagation rate.

$$r_p = k_p \left(\frac{fk_d}{k_t} \right)^{\frac{1}{2}} [I]^{\frac{1}{2}} [M]$$

From this, we can calculate some properties of the polymer system, such as the number average length of a polymer chain. One simple way to obtain this is to calculate the kinetic chain length, v , or the number of monomers added on average to an initiator. This is simply

$$v = \frac{r_p}{r_i} = \frac{k_p[M]}{2(fk_d k_t)^{\frac{1}{2}} [I]^{\frac{1}{2}}}$$

Depending on the method of termination, the number average length of a polymer is either $\bar{x}_n = v$ for the case of only disproportionation or $\bar{x}_n = 2v$ for only combination. An intermediate value is obtained if both reactions occur.

We can also calculate the distribution of chain length. We can start by obtaining the probability of chain propagation, q

$$q = \frac{r_p}{r_p + r_t} = \frac{k_p[M]}{k_p[M] + 2(fk_d k_t [I])^{\frac{1}{2}}}$$

We can note that as the rate of propagation is usually quite high compared to the other rates, so the value of q is usually a little under 1. The probability of finding a chain of length n that has undergone $n-1$ propagation steps and one termination step is

$$P(n) = q^{n-1}(1 - q)$$

This distribution is known as a most probable distribution. While the expression may be a little informative, it is possible to arrive at an alternate form involving our number average chain length.

$$P(n) \approx \frac{4n}{\bar{x}_n} \exp\left(-\frac{2n}{\bar{x}_n}\right)$$

We can see that, as a statistical process, there is a broad in chain length of polymers of polymer produced by free radical polymerization. There have been various polymerization techniques developed to control and narrow this dispersity, known as controlled radical polymerization.^{39,40} Three main methods of controlled radical polymerization are atom transfer radical polymerization (ATRP), reversible addition/fragmentation transfer polymerization (RAFT), and nitroxide mediation polymerization (NMP). The key principle of controlled radical polymerization is the suppression of permanent termination of growing polymer chains, and instead have reversible end cap that periodically dissociates to allow propagation. In effect, the polymer stays “alive,” and will continue to grow as long as reaction conditions are sustained. The end result is that all the polymers chains in the system will be growing for approximately the same amount of time at approximately the same rate, leading to a very narrow distribution in molecular weight.

Sub-subsection: Step growth polymerization

Step-growth polymerization follows slightly different statistics, arising from the fact that it requires two monomers with different functional groups to react with one another. Many different situations can be analyzed from this basic premise, and one of the simplest would be starting with a stoichiometric balance of difunctional monomers AA and BB. An example could be the synthesis route for polyethylene terephthalate, whose monomers could be ethylene glycol and terephthalic acid, with hydroxyl and carboxylic acid functional groups. This is shown in Figure 2.2 below.

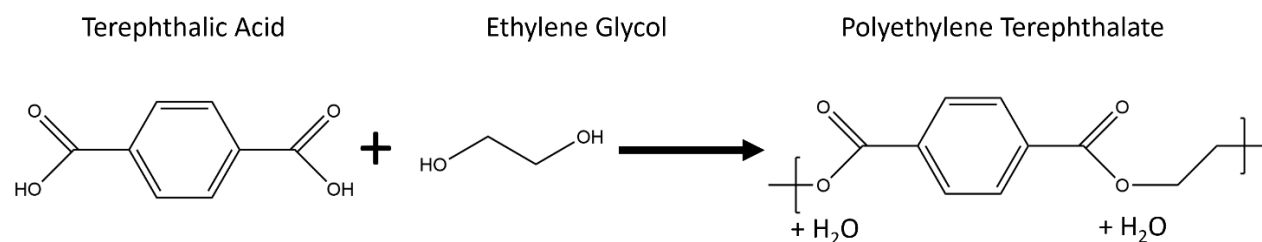


Figure 2.2 Step Growth polymerization of polyethylene terephthalate.

The classical approach is to look at the fraction of functional groups A that have undergone a condensation reaction (which in this case is equivalent to the number of functional groups B reacted). We can denote this fraction f , and this represents the extent that the polymerization reaction has proceeded. Based on this fraction, we can calculate the degree of polymerization. We can then obtain a distribution of degrees of polymerization another the most probable distribution.

$$P(n) = f^{n-1}(1 - f)$$

We can calculate the average of the most probable distribution, but we can also reason that, since each polymer has on average one unreacted A functional group, the number of polymers present in the system is $N(1-f)$, where N is the initial number of monomers in the system. We then divide the number of initial monomers between the number of polymers to get the number average of monomers per polymer. This is also known as the Carothers's equation.

$$\bar{x} = \frac{N}{N(1-f)} = \frac{1}{1-f}$$

We can take the analysis one step further and take a look at the weight-average distribution of the polymer chains as well. We can do this by taking the weighted average as defined below.

$$W(n) = \frac{n}{\bar{x}_n} P(n) = nf^{n-1}(1-f)^2$$

We can observe that at sufficient conversion, a very small fraction of the monomers remain unreacted. This fact is relevant when considering the mechanism by which monomer contaminants may leach out of a plastic material, such as BPA. It turns out that the main mechanism by which this occurs is through the hydrolysis of the polycarbonate chains, in which the reverse reaction of polymerization occurs and a water molecule can come in to break apart a polymer chain.¹⁵

Subsection: Copolymers and Composition

Regardless of the type of polymerization, in many cases polymers have more than one type of monomer, and the distribution and sequences of these monomers are worth considering. Polymers with more than one monomer are known as copolymers, and are important because combining monomers with different characteristics can lead to polymers with a diverse set of characteristics

that can strongly depend on the monomer sequence. There is a bit of technical distinction with step-polymerized polymers with two different bifunctional monomers, as shown in Figure X. One could view this as an alternating sequence of two distinct monomers, otherwise known as an alternating copolymer. However, in many cases, they are still considered homopolymers with the base monomer unit being the combination of the A monomer and B monomer.

Other types of copolymers include block copolymers, in which the polymer sequence is composed of long blocks of a type of monomer. Block copolymers tend to have interesting phase separation properties as polymer chains made of different monomers do not mix well. Another type of copolymer are gradient copolymers, in which the sequence of a chain is primarily composed of one type of monomer, and gradually transitions into another type of monomer. Both block and gradient copolymers are typically made through controlled radical polymerization processes, as the controlled nature of the propagation step of polymerization allows one to change the composition of monomers as they are added onto the polymer.⁴¹⁻⁴⁴

Random and statistical copolymers are another type of copolymer and will be discussed in more detail as the principles are very relevant to this thesis. As the name suggests, the sequences of random and statistical copolymers are determined by chance; for a two-monomer system with monomer A and monomer B, each monomer in the sequence will have some probability of either being A or B. This situation is quite common in most cases of polymerization that occur in mixtures of two monomers. As a polymer chain is growing, there will be a certain chance that a monomer A or monomer B is added, depending on factors such as the fraction of the mixture that is A or B and the chemical details of how an A monomer will react with another A monomer, a B monomer, and vice versa. In general, we treat these statistical rules for adding monomers to a

polymer sequence as Markovian, that the probability of adding a monomer depends on what monomer is currently at the end of the chain.⁴⁵ In the case that the probability of adding a monomer is independent of the previous monomer in the sequence, these copolymers are technically referred to as random copolymers. An illustration is shown below in Figure 2.3.

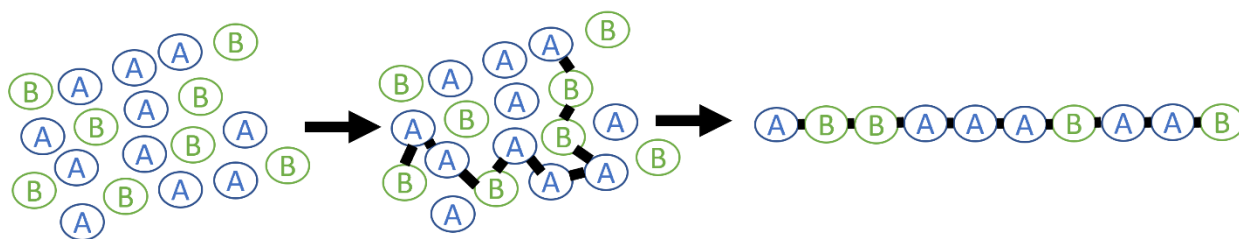


Figure 2.3 An illustration of random copolymerization in a mixture of A and B monomers.

Starting off with the case of random copolymers, we can derive some simple statistics on the properties of the polymer sequence. We only have $P[A]$ and $P[B]$, which denotes the probability of a monomer being A or B respectively. We can then calculate what fraction of the polymer is a particular sequence, such as AAB or ABA. Because the probabilities are independent, we can multiply the probabilities of finding each individual monomer. Some examples of calculating the probabilities of sequences are shown below,

$$P[AAAAA] = (P[A])^5, \quad P[ABABA] = P[AAABB] = (P[A])^3(P[B])^2$$

We can note that the fraction of monomers in the mixture matches the probability of monomer addition, making for a simple way to control polymer composition.

For the more general case with our first-order Markovian probabilities, we have four probabilities to consider, $P[A/A]$, $P[B/A]$, $P[A/B]$, and $P[B/B]$. These are conditional probabilities, such that $P[A/B]$ denotes the probability of adding an A monomer to an B monomer and the end of a polymer

chain. The calculation of sequence probability becomes a little more involved, but still follows basic statistical rules and some examples are shown below.

$$P[AAAAA] = P[A](P[A/A])^4$$

$$P[ABABA] = P[A]P[B/A]P[A/B]P[B/A]P[A/B]$$

$$\{P[AAABB] = P[A]P[A/A]P[A/A]P[B/A]P[B/B]$$

We can use these methods to then calculate relevant quantities of particular polymer sequences. One such quantity is the number fraction of sequences of A (or B) units, or given a sequence of only A units, what is the probability of it being n units long. This can be expressed as

$$F_A(n) = \frac{P[BA_nB]}{\sum_i P[BA_iB]}$$

We can note that the denominator can be simplified greatly as all of these sequences must end in AB, and all other possible preceding sequences are enumerated. Thus we have

$$F_A(n) = \frac{P[BA_nB]}{P[AB]}$$

We can expand upon this result and calculate the average length of A or B run sequences.

$$\overline{N_A} = \frac{\sum_n nF_A(n)}{\sum_n F_A(n)} = \frac{P[A]}{P[AB]} \quad , \quad \overline{N_B} = \frac{P[B]}{P[BA]}$$

(See appendix for derivation)

One thing we can notice is that these quantities can vary significantly depending on whether the polymer sequence is truly random (zero-order Markovian process) or if there is a dependence on

the terminal monomer of a growing chain. One common measure of this departure from randomness is defined as

$$\chi = \frac{P[AB]}{P[A]P[B]}$$

We can note that for random statistics, we get $\chi = 1$. If $\chi = 2$, then we have an alternating copolymer, and if $\chi = 0$, we have a block copolymer.

We can connect these probabilities described above to the kinetics of polymerization, as described in the previous section. We start off with rate equations for the addition of monomers, illustrated in Figure 2.4 below.

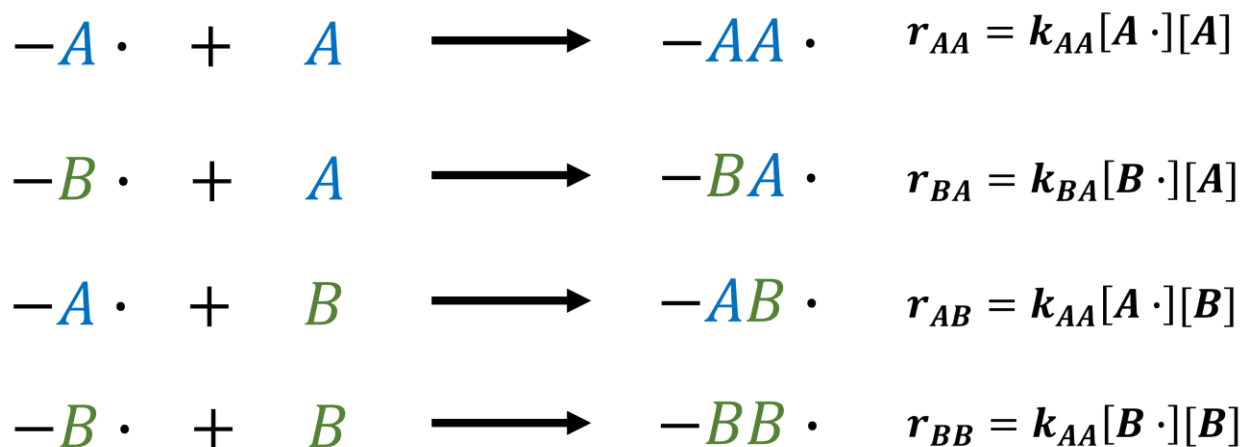


Figure 2.4 Four possible reactions in a two-monomer copolymerization

The conditional probabilities laid out previously can be written in terms of these rate equations.

For example,

$$P[A/A] = \frac{r_{AA}}{r_{AA} + r_{AB}} = \frac{k_{AA}[A \cdot][A]}{k_{AA}[A \cdot][A] + k_{AB}[A \cdot][B]}$$

These relations can be simplified by using reactivity ratios, which tell us the ratio at which one monomer is added over another. We can also define a feed ratio, which described how much more of one monomer is present in the reaction mixture when polymerization occurs.

$$r_A = \frac{k_{AA}}{k_{AB}} \quad r_B = \frac{k_{BB}}{k_{BA}} \quad x = \frac{[A]}{[B]}$$

We can then obtain simplified forms for these conditional probabilities.

$$P[A/A] = \frac{r_A x}{1 + r_A x} \quad P[A/B] = \frac{x}{x + r_B} \quad P[B/A] = \frac{1}{1 + r_A x} \quad P[B/B] = \frac{r_B}{r_B + x}$$

This allows us to calculate quantities such as the amount of monomer A relative to monomer B in a copolymer, based on the initial reaction conditions.

$$y = \frac{P[A]}{P[B]} = \frac{P[A/B]}{P[B/A]} = \frac{1 + r_A x}{1 + \frac{r_B}{x}}$$

This is otherwise known as the Lewis-Mayo equation governing statistical copolymers. We can simply note that if the reactivity ratios are not 1, the composition of the copolymer will be different than the feed ratio of monomers. There are a few main factors that affect this reactivity ratio, all depending on the chemical details of the monomers. Monomers that have the same backbone structure, such as the different methacrylate or acrylate monomers, tend to have reactivity ratios close to one, as the conditions for the reaction of the carbon double bond and a free radical would be very similar. Monomers with different backbone structures and different stabilizing forces for free radicals, such as in aromatic rings can have very different reactivity ratios. Steric and electrostatic forces may also apply.

Understanding the conditions which govern these sequences can be helpful in developing new functions for random and statistical copolymer materials. As noted in the case of proteins, a polymer sequence can be of great consequence to the function and behavior of the polymer. The consequence of polymer sequence for random and statistical polymers is less precise, and often overlooked. In many cases, random copolymers are used in cases where a mixture of properties of different monomers are desired. For example, in the case of the commonly used plastic ABS, acrylonitrile, butadiene, and styrene monomers are polymerized together. Acrylonitrile, being a polar monomer, serves to provide additional cohesive energy between chains and increases the strength and thermal resistance of the material. Butadiene is a softer, rubbery component and increases the toughness of the copolymer. Styrene is a more rigid component and provides the structural stability for the material.⁴⁶ In such a case, the sequence matters less than the overall composition and ratios of the components.

However, there is research that explores how polymer sequences themselves in these statistical polymers can impart unique properties and functions. Some of the earliest work on this topic from Shakanovich, Chakraborty, and other related authors in the 1990's, who theoretically analyzed the statistical mechanics and phase behavior of random copolymers.^{47,48} One functionality they emphasized was that random copolymers, which they refer to as disordered or random heteropolymers, could exhibit a transition from weak to strong adsorption onto multifunctional or heterogenous surfaces based on the statistical correlation of the polymer sequence. In other words, random or statistical copolymers can exhibit a sort of statistical pattern matching onto surfaces. In a summary of their main results, they examine a situation in which a random copolymer is composed of two different types of monomers, which for example could be hydrophilic or

hydrophobic, interacts with a surface that is similarly partitioned into hydrophilic and hydrophobic regions. Figure 2.5 reproduces an illustration from Chakraborty.

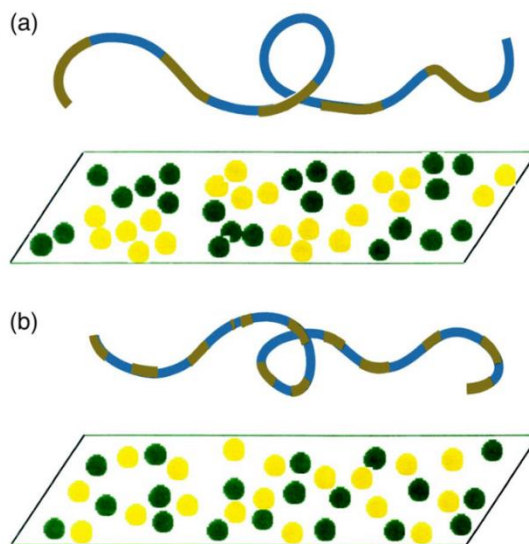


Figure 2.5 An illustration of random copolymers that optimally adsorb onto a patterned surface. Reproduced from Reference 38

From an energetic standpoint, there is a large penalty for hydrophilic and hydrophobic monomers and regions to interact, so hydrophilic monomers tend to interact with hydrophilic surface regions, and vice versa. This seemingly simple concept is the basis for statistical pattern matching, in that for a heterogeneous surface, there will be regions of hydrophilicity and hydrophobicity that can differ in length scale, and either be more “patchy” or “striated” in nature. For any of these surface regions, there are copolymer sequences that are ideal or nearly ideal for interacting and adsorbing onto that region, depending on how well the lengths of the hydrophobic and hydrophilic polymer sequences match the sizes of the surface domains. From the statistical rules we derived earlier in the section, we can see that there is a finite probability the optimal sequence, or any sequence, being present on a polymer chain, depending on factors such as polymer composition and reactivity

ratios. In general, random copolymers as a class of materials could be well suited for interacting with these sorts of heterogeneous surfaces, in part due to the ease of tuning the statistical properties of the polymers to find optimal adsorption conditions.

Chakraborty and others propose that this sort of statistical pattern matching can be useful in understanding a wide variety of biological processes, from cellular recognition to protein folding, and even be the basis of new applications for disordered heteropolymers.⁴⁸ One example they bring up is the case of cellular receptors and transmembrane proteins. While this sort of biological pattern matching is usually quite specific, there are times when many different substrates, sometimes unintended, when a response can be triggered such as in the case of viral infection of a cell. Random heteropolymers can potentially be used to recognize viral protein surfaces and adsorb onto them, then preventing viral entry into the cell. Some experimental results following this premise demonstrate that there are certain copolymer compositions that optimally inhibit influenza viral activity.⁴⁹ Another example is the separation of proteins using disordered surfaces in a chromatographic process. Here they note that protein sequences tend to be either more block or alternating when viewed by a coarse grained model of hydrophobic, hydrophilic, or charged sequences.⁵⁰ Thus the random functionalization of a polymeric surface could be sufficient to recognize and discriminate between various type of proteins.

In recent years, work by Olvera suggests that random copolymers can effectively encapsulate proteins, with the heterogeneity of the random copolymers being a key part to this process.⁵¹ While proteins are nanosized objects, they still present a heterogenous surface with hydrophobic, hydrophilic, and charged regions, and it is thought that these surface properties are important in determining how proteins interact with each other and other molecules. Simulations performed on

the interactions of the random copolymers of hydrophilic and hydrophobic monomers and coarse-grained proteins showed that the same or similar sequences preferred to interact with particular regions of the protein surface. The rationale for this behavior is similar to those presented by Chakraborty and Shakanovich, in that hydrophilic and hydrophobic surface regions prefer to interact with hydrophilic or hydrophobic copolymer sequences. Experimental results were also obtained that demonstrate random copolymers indeed have this sort of recognition ability. In collaboration with Ting Xu, random copolymers based on methacrylate monomers were designed to interact favorably with proteins.⁵² The monomers are shown below in Figure 2.6, which include a hydrophilic polyethylene glycol methacrylate (PEGMA), hydrophobic ethyl hexyl methacrylate (EHMA), hydrophobic methyl methacrylate (MMA), and negatively charged sulfopropyl methacrylate (SPMA).

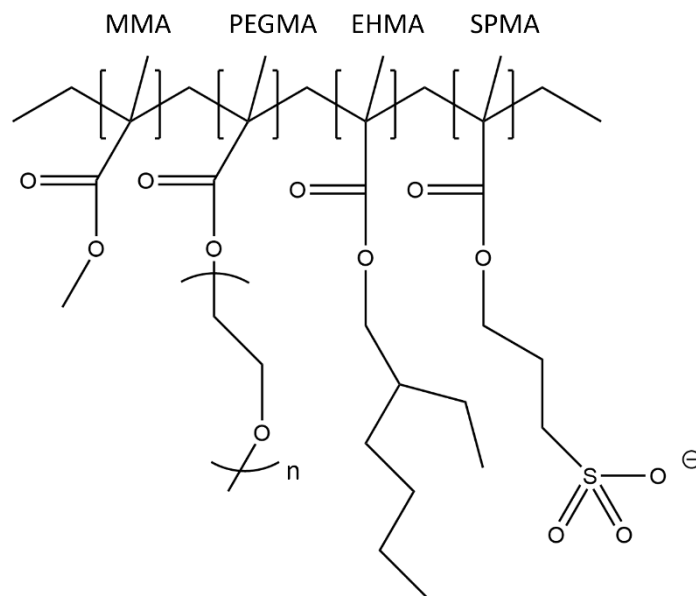


Figure 2.6 Chemical structure of random copolymer used in Reference 42

This random copolymer was shown to form nano-sized aggregate with protein such as organophosphate hydrolase when freeze-dried from water. Additionally, the aggregates protected OPH activity after they were exposed to toluene, an organic solvent condition that would have otherwise denatured the enzyme. This feat demonstrated that the random copolymer could function as a protective layer, preserving enzyme activity in an otherwise unfavorable environment.

Section: Polyelectrolytes and Polyelectrolyte complexes

Polyelectrolytes are polymers with a significant fraction of charged monomers.⁵³ There are some varying definitions of what fraction is considered significant, with some putting the threshold at around 10% charged, below which the polymer could be considered an ionomer. Charged polymers in general are an interesting object of study as the addition of charge can impart more complex behaviors than is observed in neutral polymer systems.⁵³⁻⁵⁵ Proteins, which very frequently contain charge, can be considered natural polyelectrolytes, albeit with a very specific sequence design. In general, the presence of charges can significantly affect the collective behavior of a polymer system, as charges are known to be a long-range force and present non-local effects, affecting other parts of the polymer and other polymer chains as well.

One key aspect in which charge can modify polymer behavior is with interactions with water. As water is a very polar molecule, it has very favorable energetic interactions with charges. Thus polyelectrolytes tend to be very hydrophilic. This effect can be observed in the use of water-absorbent gels, which are cross-linked networks of polyelectrolytes and used in products such as diapers that can absorb many times its own weight in water. Even polymers with very hydrophobic

structures such as polystyrene can become water-soluble if functionalized with charge to a great enough extent (~30% charge fraction).⁵⁶ In fact, much of the context in which polyelectrolytes are used and studied involve being dissolved in the aqueous phase.

The attractive and repulsive coulomb forces between charges also contribute significantly to polyelectrolyte properties and applications. As a general trend, polyelectrolytes tend to have elongated and extended polymer conformations due to repulsion between charges on the polymer chain. This can lead to enhanced and anomalous viscosity-modifying properties for polyelectrolytes dissolved in aqueous solution. The interaction of polyelectrolytes with oppositely charged molecules and surfaces also play quite an important role. Polyelectrolytes easily adsorb onto surfaces with opposite charge, and in doing so can alter the surface charge. In the case of adsorbing onto the surface of colloids, polyelectrolytes can either stabilize particles and prevent them aggregating, or destabilize them and cause aggregation and segregation of the particles from the liquid medium. This latter case is also known as flocculation, and is widely used in water treatment plant to remove colloidal particles such as dust and organic matter from incoming water. One important facet to these charged interactions is that they are quite sensitive to salt and ion concentrations, which screen the effects of electrostatic interactions. In fact, the collapse of polyelectrolyte conformations from extended to more coiled shapes when salt concentration increases is sometimes called the polyelectrolyte effect.

Polyelectrolyte complexation is another key phenomenon that depends on the interactions of oppositely charged polyelectrolytes. Normally, polyelectrolytes are well soluble in aqueous solution. However, when oppositely charged polyelectrolytes are mixed, the polyelectrolytes will form complexes and potentially phase separate from solution. The thermodynamics of this process

depends on the enthalpy and entropy changes due to complexation.⁵⁷ In terms of enthalpy, the charges on polyelectrolyte are initially neutralized by counterions. Thus when complexation occurs and counterions are swapped for charges on another polyelectrolyte chain, enthalpy changes due to the electrostatic interaction tend not to be a dominating factor. However, other factors such as hydrophobic interactions and hydrogen bonding could be significant. In terms of entropy, once polyelectrolytes form complexes, the counterions that were previously bound to the polyelectrolytes are released, which significantly increases the entropy of the system. In general, polyelectrolyte complexes tend to form in salt-free or low salt conditions, which maximizes the entropy gain from counterion release.

Several experiments confirm this general perspective on polyelectrolyte complexation. One such experiment is looking at the phase behavior of polyelectrolyte complex systems as a function of salt. Phase diagrams such as the one in Figure 2.7 are obtained.⁵⁸

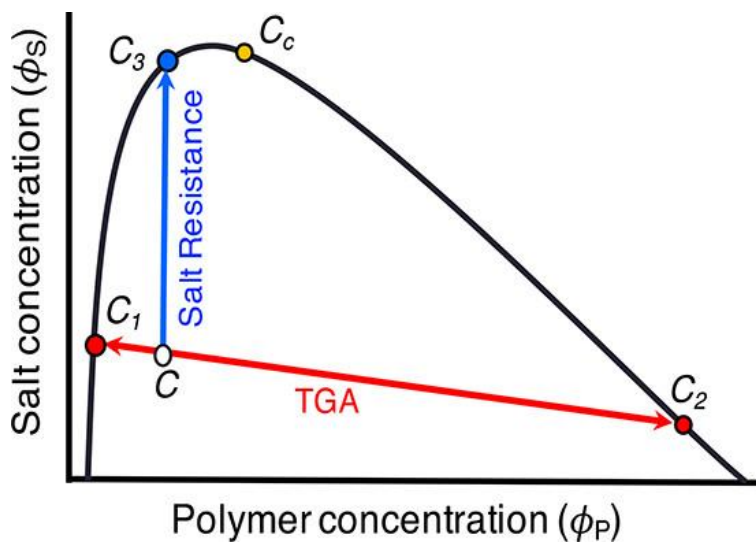


Figure 2.7 A phase diagram of polyelectrolyte complex formation with respect to salt concentration and polyelectrolyte concentration.

We can see that with increasing salt concentration, we arrive in the 1-phase region of the phase diagram. The entropy gained from counterion released is significantly reduced with increasing salt concentration, and thus there is no thermodynamic driving force for phase separation. It should be noted that the thermodynamics of polyelectrolyte complexation is still an active field of study as there remain unresolved questions on how the free energy of complexation is affected by parameters such as charge sequence, solution conditions, chemical identity of ions and monomers, and fine structure of the complexes.

The applications and usage of polyelectrolyte complexes is a similarly expanding field of study. Many applications take inspiration from nature, such as sandcastle worms which emit oppositely charged glue proteins to construct structure out of sand. This has led to investigations to use polyelectrolyte complexes as the basis for underwater adhesives.⁵⁹ Polyelectrolyte complexes are also heavily investigated for biomedical applications, as many charged polymers tend to have some degree of biocompatibility. Proteins, as a type of polyelectrolyte, are also relatively easy to incorporate into polyelectrolyte complex systems. Thus there is a fair amount of work designing drug and biomolecule encapsulation and delivery systems assembled with some form of polyelectrolyte complexation.⁶⁰

Section: Protein complexes and membraneless organelles

Proteins are polymers that nature have designed to accomplish specific tasks and functions. Just as amino acid monomers are strung together to form a functional protein, individual proteins can act as building blocks to form even larger structures. As mentioned in the introduction, ribosomes are one such structure, being composed of various proteins in order to form the molecular

machinery that actually produces proteins. The ribosomal proteins in this case must come together very precisely in order to make a functioning complex. However, not all protein complexes need to be precisely ordered and structured in order to perform a function. In fact, there are proteins that do not fold into predetermined structures known as intrinsically disordered proteins.⁶¹ These proteins can either be entirely disordered, with a random coil structure, or partially disordered, with some common structures and motifs but also segments with conformational flexibility. In part due to this disorder, intrinsically disordered proteins are well suited for having non-specific, multivalent interactions, as opposed to traditional proteins with their more tailored interactions with specific substrates and ligands. This contributes to the role that intrinsically disordered proteins play in cell signaling processes. It is believed that the flexibility of IDP's enable their ability to bind to both a receptor and enzyme that may be crucial to a signaling pathway. The wide range of conformations may also be important in certain cases of allosteric regulation, in which a significant change in conformation arises from a particular interaction and alters the function of the protein.

One interesting case of a protein complex made of intrinsically disordered proteins are known as the membraneless organelles. These complexes help in regulating enzyme activity by sequestering enzymes and/or their substrates into locally defined compartments.⁶² Unlike traditional organelles, whose bilayer membranes impart a degree of permanence, these membraneless organelles do not have membrane walls and can spontaneously form and dissolve as needed. In the case that the enzyme and substrate are both sequestered inside the membrane, enzyme activity is enhanced due to the increase in local concentration of both quantities. However, if only the enzyme or substrate

is sequestered and the other component excluded, the reaction that the enzyme catalyzed is essentially suppressed.

Several types of membraneless organelles have been discovered so far. In the nucleus, RNA-protein condensates such as Cajal bodies or nucleoli have been observed, while in the cytoplasm bodies such as stress granules have been observed. The membraneless organelles inside the nucleus are intimately related to the transcription and translation process of protein and nucleic acid synthesis, and are known to modify certain RNA sequences or nuclear proteins.⁶³ Stress granules spontaneously form in cells when they are stressed, and can function in a myriad of ways. One established function is to sequester RNA that is unused, which can happen when the cell stops protein synthesis when under unfavorable conditions.⁶⁴

The conditions of when these membraneless organelles form and the process of their formation are an active field of research. Many membraneless organelles are composed of oppositely charged intrinsically ordered proteins, or combinations of intrinsically disordered proteins and other biopolymers such as RNA and DNA. It is thought that the multivalent interactions of the disordered proteins contribute greatly to the properties of the membraneless organelles, as opposed to strong, specific binding that is common in biological contexts. They tend to form liquid compartments that are phase separated from the ambient cellular background. A disruption in this liquid-like property to more solid-like behavior, presumably due to changes in inter-protein interactions, has been associated with certain neurodegenerative and other diseases.⁶⁵

The parallels between random copolymers and intrinsically disordered proteins can be quite intriguing. Both random copolymers and intrinsically disordered proteins have conformational

freedom and heterogeneous interactions depending on the properties of their monomers and sequences. When oppositely charged, random copolymers (and polymers in general) can form polyelectrolyte complexes, while intrinsically disordered proteins form membraneless organelles. The liquid-liquid phase separation of membraneless organelles is very reminiscent of polyelectrolyte coacervation, and it is thought that similar physics may be at play. It is then interesting to ask whether complexes of random copolymers can also mimic some of the properties of complexes of disordered proteins, such as molecule sequestration or the enhancement of enzyme activity. It is this question that informs many of the studies pursued in this thesis.

Chapter 3: Polyelectrolyte Complexes of Random Copolymers for Removing Organic Contaminants from Water

Nature harnesses the disorder of intrinsically disordered proteins to organize enzymes and biopolymers into membraneless organelles. The heterogeneous nature of synthetic random copolymers with charged, polar and hydrophobic groups has been exploited to mimic intrinsically disordered proteins, forming complexes with enzymatically active proteins and delivering them into nonbiological environments. In this thesis chapter, the properties of polyelectrolyte complexes composed of two random copolymer polyelectrolytes are studied experimentally and via simulation with the aim of exploiting such complexes for segregating organic molecules from water. The anionic polyelectrolyte contains hydrophilic and hydrophobic side chains and forms self-assembled hydrophobic domains. The cationic polymer is a high molecular weight copolymer of hydrophilic and charged side groups and acts as a flocculant. We find that the polyelectrolyte complexes obtained with this anionic and cationic random copolymer system are capable of absorbing small cationic, anionic, and hydrophobic organic molecules, including perfluorooctanoic acid, a compound of great environmental and toxicologic concern. Importantly, these macroscopic complexes can be easily removed from water, thereby providing a simple approach for organic contaminant removal in aqueous media. MARTINI and coarse-grained molecular dynamics simulations explore how the microscale heterogeneity of these random copolymer complexes relate to their segregation functionality.

It should be noted that colleague Curt Waltmann performed the molecular dynamics simulations along with the accompanying analysis. The work described in this thesis has been published in

ACS Central Science, see reference 54.³²

Introduction

Random copolymers have a statistical distribution of two or more types of monomers, leading to spatial heterogeneity in local composition as different regions of a copolymer chain may have different average composition. This type of heterogeneity from disordered polymer sequences is thought to be important in achieving biomimetic functions such as molecular-scale pattern-matching.^{48,66–68} Membraneless organelles, which are spatio-temporal aggregates of nucleic acids, enzymes and their substrates, and oppositely charged, intrinsically disordered proteins with rather random sequences of amino acid monomers,⁶² likely utilize such concepts of disorder and heterogeneity. Because these membraneless organelles are analogous to polyelectrolyte complexes of oppositely charged random copolymers, the behavior of such complexes could provide insight into the behavior of membraneless organelles. This analogy has inspired research into the use of synthetic random copolymers to interact with enzymes, forming what can be considered to be a type of polyelectrolyte complex.^{52,69} Concentrating small-molecule substrates is also a crucial function of membraneless organelles. Here, we explore the possibility of using polyelectrolyte complexes of random copolymers as mimics of disordered proteins in membraneless organelles with an aim to segregate small organic molecules from aqueous solution.

Polyelectrolyte complexes are generally formed when oppositely charged polymers are mixed in aqueous solution.^{70,71} Depending on factors including charge ratio, degree of polymerization, monomer sequence,^{72,73} ionic solution conditions,^{74–77} or solvent quality,⁷⁸ a wide range of phase behaviors for the polyelectrolyte complex can be observed, including the formation of colloidal

suspensions, liquid coacervates, and solid precipitates.^{60,79–81} Colloidal suspensions of polyelectrolyte complexes have been investigated for their ability to encapsulate bioactive molecules and deliver such molecules in a biological environment.^{82–84} Liquid coacervates of polyelectrolyte complexes have been shown to encapsulate and concentrate enzymes from solution,^{85–87} similar to the capabilities of membraneless organelles.

The formation of solid precipitates with polyelectrolyte complexes can be particularly useful in separating particles from aqueous solution and removing contaminants from water through a flocculation process.^{88,89} Traditionally, flocculation is used to remove negatively charged colloids such as fine clay particles from water via the addition of a single species of high-molecular-weight cationic polymer, which neutralizes the surface charge of the particles, acts as a bridge between them, and coagulates the particles into macroscopic flocs.^{90,91} However, polyelectrolyte complexes have also been used for flocculation purposes,⁸⁸ and solid polyelectrolyte complexes can also be effective at removing ionic compounds such as metal ions or charged organic compounds from water.⁹²

This flocculation behavior provides a relatively simple experimental approach to measure the segregation of organic molecules into polyelectrolyte complexes. There have been studies demonstrating the ability of polyelectrolyte complex coacervates to partition and segregate small organic molecules,^{93–96} and separating the coacervates from the supernatant generally requires centrifugation techniques. In contrast, solid polyelectrolyte complexes that segregate organic molecules can be removed from solution through simple filtration. Segregation efficiencies can then be obtained by measuring the concentration of organic molecules in the filtered solution.

Building upon a rational design principle outlined in earlier work involving complexes of random copolymers and enzymes,⁵² we hypothesize that a random anionic copolymer with hydrophilic, hydrophobic, and anionic monomers will form micellar-like structures in aqueous solution and flocculate with a random cationic copolymer, with the heterogeneity of the resulting complex providing favorable interactions with a wide range of organic molecules. Previously, others have shown that random copolymers with hydrophilic and hydrophobic groups exhibit protein-like folding and form single-chain micelles while segregating dye molecules in aqueous solution.⁹⁷ It is reasonable to expect that the addition of an anionic component would allow the three-component copolymer to form similar structures and encapsulate organic molecules, with the additional benefit of being able to remove the copolymer and dye in a flocculation-like process which may enable applications in industrial water remediation.

Here, we develop a method to segregate and remove organic molecules from water using two oppositely charged random copolymers through experiments, simulations, and analysis. The anionic copolymer is comprised of hydrophilic, hydrophobic, and anionic methacrylate groups. (Figure 3.1a) The cationic copolymer is composed of hydrophilic and cationic methacrylate groups. (Figure 3.1b) These random copolymer polyelectrolytes were synthesized using free radical polymerization and form macroscopic complexes when mixed, (Figure 3.1c) successfully encapsulating several organic dyes with varying degrees of effectiveness. Three dyes, crystal violet, methyl orange, and phenolphthalein, were chosen as model molecules for their respective cationic, anionic, and hydrophobic natures as well as ease of quantification via UV-Vis spectroscopy. Perfluorooctanoic acid was also chosen to demonstrate the relevance of this system in filtering difficult-to-remove chemicals from aqueous systems. (Figure 3.1d)

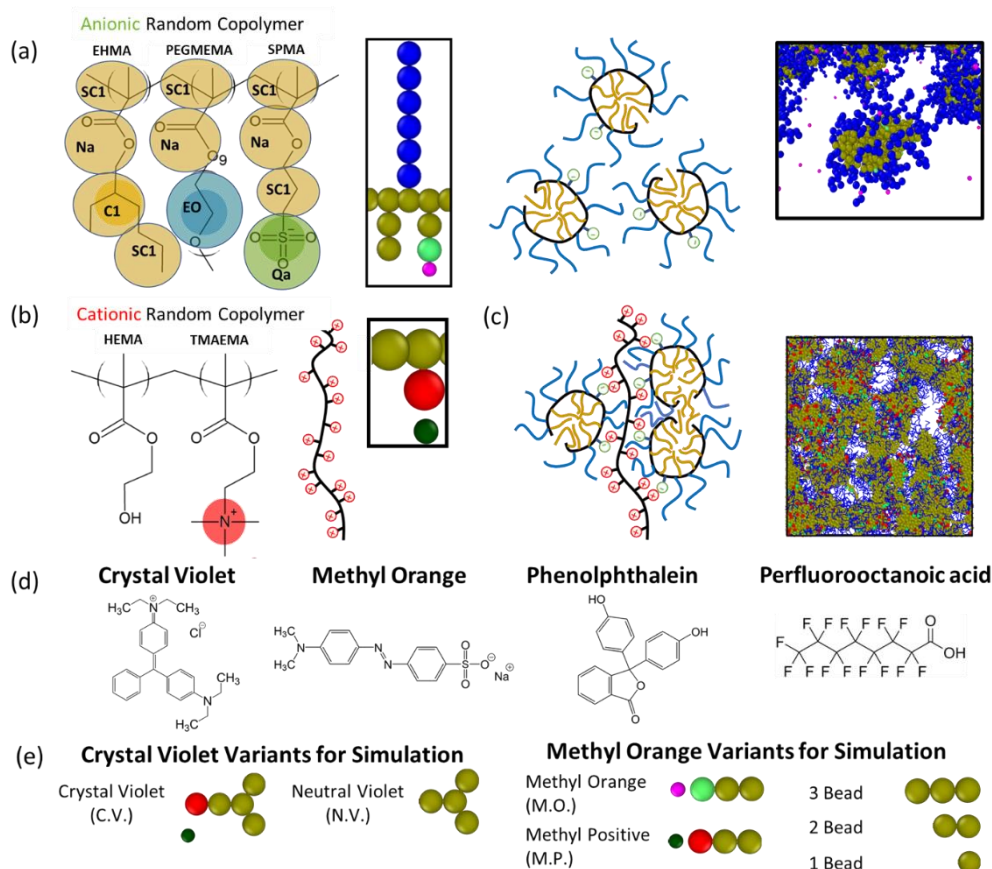


Figure 3.1 Schematic of random copolymer and contaminants with simulation models. (a) Chemical structure, MARTINI parameterization, coarse grain model, illustration, and simulation snapshot of the anionic random copolymer (b) Chemical structure, illustration, and coarse grain model of the cationic random copolymer. (c) Illustration and simulation snapshot of complexation between the anionic random copolymer and the cationic random copolymer. (d) Chemical structure of organic molecules used in experiments. (e) Coarse grain model of organic molecules used in simulations. Red and green beads correspond to positive and negative charges respectively, while tan beads are hydrophobic and blue beads are hydrophilic.

We use coarse-grained molecular dynamics at two different length scales to study how the heterogeneous nature of these random polyelectrolyte complexes affects their ability to flocculate dyes. The simulations show complexes that are highly heterogeneous in composition with hydrophobic domains as well as heterogeneities in the charge distribution throughout the

complexes. We explain the origin of these heterogeneities using statistical analysis that has been used previously to explain compositional heterogeneities observed in strongly incompatible random copolymers⁹⁸ and in random ionomers which are molten state (dry) systems.^{99,100} Models of the dyes are also included in the simulations (Figure 3.1e), and we analyze the roles that hydrophobicity and charge play in the removal of the dyes.

Results and Discussion

Polymerization and Characterization of Random Copolymers.

We synthesized the anionic and cationic copolymers via free radical polymerization. Aqueous size exclusion chromatography was used to determine apparent weight-average molecular weight (M_w), apparent number-average molecular weight (M_n), and apparent dispersity (M_w/M_n) values. (Table 3.1) The values are apparent as polymers which form hydrophobic domains can exhibit intermolecular aggregation in aqueous media via hydrophobic interactions.¹⁰¹ This aggregation behavior can be confirmed for the anionic copolymer as we obtained higher apparent M_w values with higher concentrations of polymer solution. This interpolymer aggregation behavior likely explains the low measured dispersity of 1.1, which is significantly different from the dispersity of roughly 2 that we would expect for polymers produced by free radical polymerization of methacrylate monomers.¹⁰² We note that such a very low apparent dispersity has also been observed in another charged polymer system with inter-chain aggregates that was synthesized by free radical polymerization.¹⁰³

The cationic polymer also shows an anomalously high M_w value for a polymer synthesized by free radical polymerization which is likely due to the fact that the hydroxyethyl methacrylate (HEMA) monomer used in the cationic polymer is susceptible to effects of chain transfer to polymer and

monomer and may act as a branching unit.¹⁰⁴ Thus, it is likely that the cationic polymer is highly branched in structure. This branching may be beneficial in the complexation process, as some studies suggest that highly branched flocculants exhibit better flocculation performance.⁹¹ However, quantifying the degree of branching in polymers is not a simple process,¹⁰⁵ and is not explored further in this study. We note that the dispersity of this polymer was measured to be 2.3, which is in line with expected values.

We analyzed the copolymer compositions via ¹H NMR spectroscopy. (Peak assignments are shown in methodology, Figure S3 and S4.) The anionic polymer has a molar composition of 51% polyethylene glycol methyl ether methacrylate (PEGMEMA), 44% (ethylhexyl methacrylate) (EHMA), and 5% sulfopropyl methacrylate (SPMA). From this information and the apparent M_w , we can calculate an apparent weight-average degree of polymerization (DP_w) of 820. The peak assignments for the cationic copolymer cannot be exactly determined without knowing the branching ratio of the polymer, but upper and lower bounds can be determined for the strictly linear case and strictly branched case (one branch per HEMA monomer). Thus, a reasonable estimate for the molar composition of the cationic polymer is 54-60% HEMA and 40-46% TMAEMA, with an apparent DP_w between 60000 and 62000. From this analysis, we can conclude that the cationic copolymer has a substantial charge fraction and is much longer than the anionic copolymer, potentially making it an effective flocculant. The anionic copolymer has a significant hydrophobic composition while being slightly charged. See Table 3.1 for a summary of copolymer characterization.

Table 3.1 Copolymer Characterization. Mole fractions, apparent average molecular weights, apparent dispersity, and apparent average degrees of polymerization.

	Anionic Random Copolymer	Cationic Random Copolymer
Component 1 mole fraction	PEGMEMMA: 0.51	HEMA: 0.54 - 0.60
Component 2 mole fraction	EHMA: 0.44	TMAEMA: 0.40 - 0.46
Component 3 mole fraction	SPMA: 0.05	N/A
Apparent M_w (g/mol)	290 000	10 000 000
Apparent M_n (g/mol)	260 000	4 300 000
Apparent dispersity (M_w/M_n)	1.1	2.3
Apparent DP_w	820	60 000 – 62 000
Apparent DP_n	770	26 000 – 27 000

Polyelectrolyte complex formation and dye filtration.

We formed solid polyelectrolyte complexes by mixing 300 μL of 66 +/- 2 mg/mL aqueous anionic copolymer solutions and 220 μL of 15.0 +/- 1.5 mg/mL aqueous cationic copolymer solution in 10 mL of distilled water, which leads to a 6 to 1 ratio by weight of anionic copolymer to cationic

copolymer. Initially, the mixture of copolymer solutions turns turbid and cloudy, indicating that polyelectrolyte complexes have grown to a size comparable to the wavelength of visible light. In less than a minute, macroscopic flocs can be observed, indicating the complexes have favorable interactions and a strong tendency to aggregate and coalesce into larger and larger structures. However, we also observe that the solution tends to be slightly turbid after macroscopic flocculation, indicating that there are colloidal polyelectrolyte complexes remain in solution. These are likely charge-stabilized colloids as there is an excess of positive charge in the complexes. At this point, we add 20 μL of a 50 mg/mL magnesium sulfate solution and this addition appears to coagulate the remaining polyelectrolyte complexes within a few minutes and leaves the solution clear. We believe this coagulation process is analogous to how multivalent cations are used to coagulate anionic colloids from solution.¹⁰⁶ The final aggregate sizes are usually on the order of millimeters and are robust to mechanical perturbation. When the mixture is stirred with a magnetic stir bar, the aggregates do not break apart even at stirring speeds exceeding 1000 rpm. After filtration through a 0.22 μm membrane filter, the measured solid concentration in the filtered solution is 0.17 \pm 0.02 mg/mL. This concentration corresponds to a polyelectrolyte complexation efficiency of \sim 92%.

The amounts of copolymer solution that we mixed in the above description are determined by using a titration procedure. Starting with an initial mixture of distilled water and anionic copolymer solution, corresponding to a 10.3 mL solution containing 1.90 \pm 0.05 mg/mL anionic copolymer, we add the 15.0 \pm 1.5 mg/mL cationic polymer solution in 20 μL increments. We consistently find that macroscopic flocculation occurs at 220 μL cationic solution added, which may correspond to a sort of equivalence point. However, this is not a traditional equivalence point

for polyelectrolyte complexes, as the molar ratio of positive charges to negative charges of the complexes are not 1:1 but has a significant excess of positive charge with a ratio of 2.9 - 3.3 : 1. This amount of copolymer solution added to form macroscopic complexes does not change when adding dyes or contaminants at a concentration of 2 $\mu\text{g/mL}$, except for the case of phenolphthalein, where 240 μL of cationic solution was needed for flocculation. This difference is likely due to a slight salt concentration of about 1 mM NaCl from the preparation procedure and suggests that there is a salt concentration dependence on the formation of these complexes, which is normally observed in systems of aggregating polyelectrolyte complexes.¹⁰⁷ This effect may be explored further in a future study.

The removal efficiency for the dyes is determined by comparing the peak visible light absorption of the filtered samples with complexes removed to a calibration curve from stock solutions of the dye. We find that the removal of crystal violet, the cationic dye, is quantitative with a single filtration removing over 99.5% of the dye, reaching the detection limit of the instrument used. We obtain similar results for phenolphthalein, a hydrophobic dye, with a removal efficiency of >98%. It should be noted that filtration experiments for phenolphthalein were performed in its colorless, neutral form, whereas quantification experiments were performed in its colored, charged form. The removal efficiency with a single filtration of methyl orange, the anionic dye, is 65 +/- 5%. We determine the removal efficiency of PFOA in a manner similar to the dyes, except using liquid chromatography with mass spectrometry using electrospray ionization. A value of 63.0 +/- 0.5% is obtained for a single filtration. We also perform repeated filtrations for a sample of perfluorooctanoic acid, with the process of adding anionic copolymer solution, then cationic copolymer solution and magnesium sulfate being repeated twice for a total of three filtrations.

89.0 +/- 0.5% of the perfluorooctanoic acid was removed in this experiment, demonstrating that this system can significantly reduce the concentration of environmentally relevant contaminants from aqueous systems. These results are shown in Figure 3.2(a).

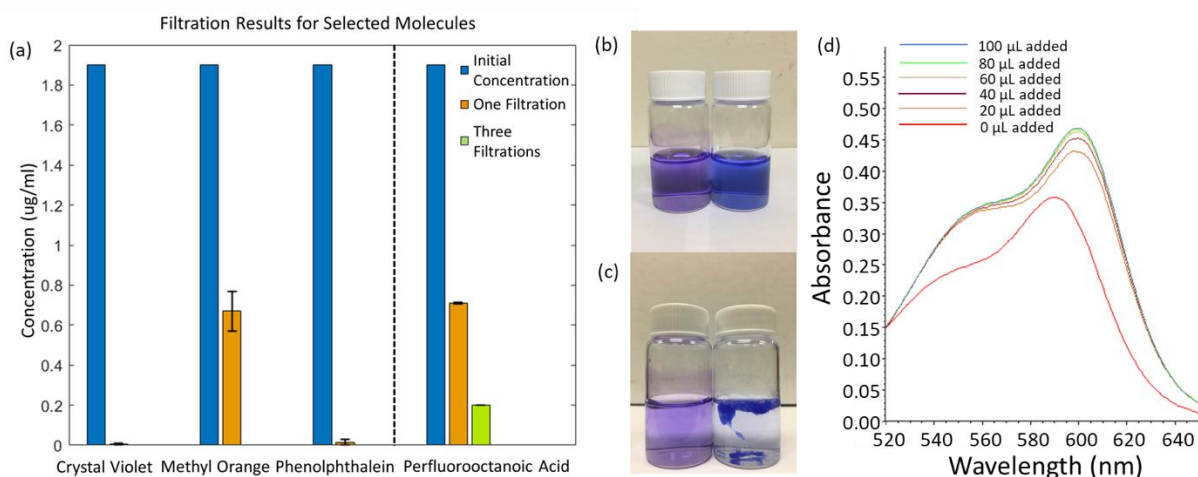


Figure 3.2 Filtration and absorbance results. (a) Filtration results. For each of the three dyes, the results are averages from three separate filtration samples. Crystal violet and phenolphthalein are quantitatively removed. For perfluorooctanoic acid, results for one and three filtrations on a sample of perfluorooctanoic acid are shown. Error bars are standard deviations from three runs of a single sample. (b) Images of 2 $\mu\text{g/mL}$ aqueous solutions of crystal violet before (left vial) and after (right vial) addition of 100 μL of anionic copolymer solution (66 mg/ml). (c) Images of 2 $\mu\text{g/mL}$ aqueous solutions of crystal violet before (left vial) and after (right vial) encapsulation in a polyelectrolyte complex of anionic and cationic copolymer. (d) Visible absorbance spectra of a 2 $\mu\text{g/mL}$ solution of crystal violet in water as a function added anionic copolymer solution (66 mg/ml). A significant solvatochromic shift is observed upon addition of trace levels copolymer solution.

Confirmation of dye encapsulation and micelle formation in anionic copolymer.

Crystal violet and methyl orange are solvatochromic dyes, exhibiting visible absorbance spectral shifts with changes in the hydrophobicity of the local environment.¹⁰⁸ We leverage this behavior to obtain information on the interactions of the dyes with the copolymer and resulting complex.

Figures 2(b) and 2(d) show that solutions of crystal violet exhibit a solvatochromic red shift when

mixed with small amounts of anionic copolymer solution, with a peak absorbance shift from 593 nm to 598 nm. As the small amount of copolymer added does not change the overall polarity of the solvent, the crystal violet must be interacting strongly with the local hydrophobic domains of the anionic copolymer. This spectral shift is similar to the shift shown when anionic micelles of sodium dodecyl sulfate are formed in solution with crystal violet.¹⁰⁹ This shift is retained when complexes of the anionic and cationic copolymers are formed as shown in Figure 2(c), indicating that crystal violet is located near the hydrophobic pockets that exist within the polyelectrolyte complex. No solvatochromic shift is observed in absorbance spectrum when anionic copolymer is added to a solution of methyl orange nor does the resulting complex exhibit a visual color shift. These results indicate that methyl orange does not interact strongly with the hydrophobic domains of the polyelectrolyte complex, possibly due to a weaker hydrophobic character and/or the same charge repulsion from the anionic copolymer. This may explain the lower removal efficiency of methyl orange compared to crystal violet. We turn to molecular dynamics simulations in order to differentiate more clearly the effects that charge or hydrophobicity have in the segregation and removal of these organic molecules and their molecular scale interactions with the polyelectrolyte complexes.

Simulations of Polymers and Dyes.

We use coarse-grained molecular dynamics at two different length scales to study the interactions of crystal violet, methyl orange, and variations of these molecules with the polymer complexes. The MARTINI model provides information on the conformation of the anionic random copolymer while a more coarse, implicit solvent model is developed to study the formation of complexes and interactions with the dyes. Using the MARTINI model, we first perform simulations of only the

anionic copolymers and their counterions without cationic copolymers or dyes. The monomer fractions for the anionic copolymers match the fractions used in experiments (EHMA: 0.44, PEGMA: 0.51, SPMA: 0.05) and each copolymer has a degree of polymerization (DP) of 100. We observe that the anionic copolymers form micelles with both models, and the distribution of hydrophobic, hydrophilic, and negatively charged beads from the micelle center of mass for the MARTINI model can be found in the SI (Figure S2). These distributions are also shown for the two different states we observe using the coarse-grained model when the cationic copolymers are also included in the simulations. Like the anionic copolymers, we use monomer fractions that correspond to experiments (0.54 HEMA, 0.46 TMAEMA). In this case, $DP = 200$ is chosen in order to represent the larger molecular weight of the cationic polymer used in experiment. In both models, the anionic copolymers that are not interacting with the cationic copolymers take on micellar configurations due to the hydrophobic side chains and backbone. When interacting with the cationic polymers, the anionic copolymers take on much more stretched conformations that still feature hydrophobic domains.

The two models confirm that the anionic copolymer forms a hydrophobic core with a hydrophilic corona and charges sitting at the edge of the hydrophobic core. This demonstrates the ability of the coarse-grained model to capture the conformation of the methacrylate-based, random, charged copolymers.

As was noted above, the experimental polymer charge ratio, i.e., the total ratio of positive charges on all of the copolymers to the total number of negative charges on all of the copolymers, was 2.9 - 3.3. (As in the simulations, counterions make the system charge neutral overall). Earlier experimental work done of complex coacervation has suggested that only polymer charge neutral

systems form macroscopic phases whereas non-charge neutral systems should form smaller dispersions.¹¹⁰ Some studies even presuppose that this condition should be met.¹¹¹ Even when studies have extended the modeling to include charge anisotropy and short range attractions, the models include only fluctuations via linear response theory (or Random Phase Approximation) and when ionic correlations are included, they are assumed to be local using a binding energy of ions to the chain backbone.^{78,112}

The distribution of charge on the polymers, along with the formation of hydrophobic domains for the anionic copolymer, likely plays a role in the non-stoichiometric polymer charge ratio of the complexes. The polymer used in this study are nearly ideal random copolymers, as the reactivity ratios of the methacrylate monomers are nearly one.⁵² Thus, the charges are randomly distributed and we can calculate the number fraction or probability of finding a sequence of N charged units on the polymer:¹¹³

$$P(N) = f_c^N (1 - f_c) \quad \text{eq. 1}$$

where f_c is the charge fraction of the polymer. The cationic copolymer has a much higher charge fraction of 0.46, compared to the anionic copolymer charge fraction of 0.05. We can conclude that on average that the cationic copolymer has considerably longer and more frequent positive charge sequences than the anionic copolymer has negative charge sequences. We also note that the average distance between charge sequences is the reciprocal of the charge fraction, being 20 for the anionic copolymer and 2.2 for the cationic copolymer. Compounded with the fact that anionic charges are spread out over the surface of hydrophobic domains, regions of the cationic copolymer with longer charge sequences will require interactions with multiple hydrophobic domains to effectively compensate the charge. Steric effects will limit the number of hydrophobic domains

that can aggregate in a local area, at times leading to uncompensated positive charges.

The coarse-grained simulations support this hypothesis, and a polymer charge ratio near 3 was required to create a percolated structure, in reasonable agreement with the experimental polymer charge ratio (2.9 - 3.3). In Figure 3.3, we explore the percolation (counting only the hydrophobic beads) of the system as more cationic polymer is added by examining the probability of finding a polymer in a cluster of a certain size as a function of polymer charge ratio.

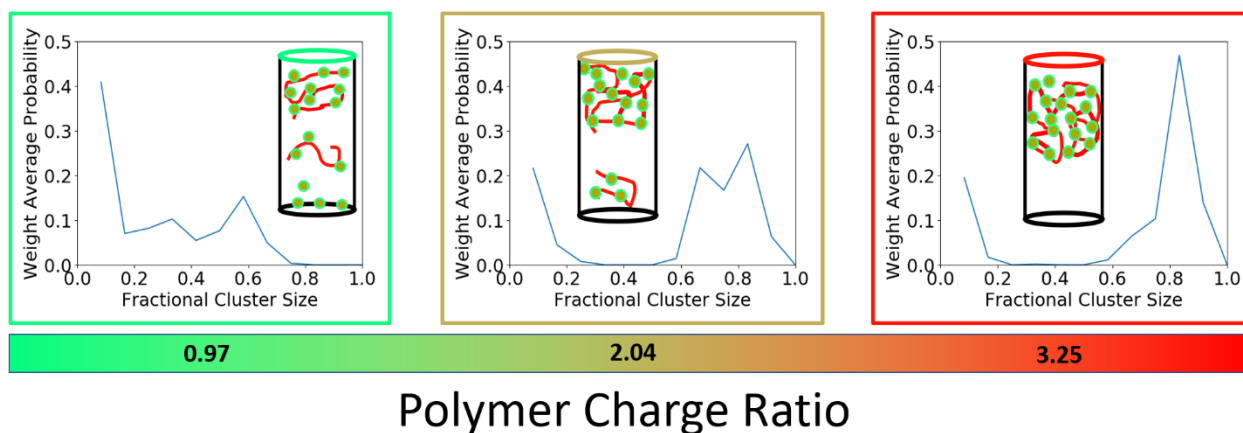


Figure 3.3 Probability of a chain being in a certain sized cluster. The cluster size is measured as a fraction of the finite sized simulation, as a function of polymer charge ratio, which is defined as the ratio of the number of positive charges to the number of negative charges in polymer clusters (the system is electrically neutral due to counterions). At low charge ratio, free micelles, small clusters, medium sized clusters, and large clusters comprised of nearly every chain are observed (left). As the polymer charge ratio is increased above 1, there is an electrostatic driving force for the free micelles to enter the dense phase the free micelles should be incorporated in the dense phase even if it is not connected through hydrophobic interactions (center). As the charge ratio is further increased to 2 and above, the medium sized clusters effectively disappear, leaving the polymers in one dense phase (red test tube). This agrees well with experiments where a polymer charge ratio above 3 is necessary to drive all the polymers into a macroscopic phase.

This probability is a weight average probability, as opposed to a number average probability, meaning that the probabilities are normalized by the total number of polymers in a cluster of a certain size as opposed to the total number of clusters of a certain size. Thus, a delta function for

a cluster size of 1 signifies a single cluster of all the components. At polymer charge ratios below 1, large clusters constituting up to 60% of all polymers are observed. In these clusters, cationic copolymers serve as high valency cross-linkers, forming hydrophobic connections with on average 8 anionic copolymers in a “pearl necklace”-like structure.¹¹⁴ The ratio of charges on the average cationic polymer to the average anionic polymer is 9.2, meaning that the charge on the average cationic polymer is incompletely compensated by the 8 anionic copolymers on average to which it is connected. Consequently, free micelles and smaller clusters containing both cationic and anionic polymers are also observed. For the same reason, these smaller clusters always have a net positive charge even though the system is net negatively charged. As the charge ratio is increased above 1, more cationic polymer is added and there is an electrostatic driving force for the free micelles to enter the densely connected phase. However, smaller dispersions are still observed, and only when the charge ratio continues to increase to the observed experimental ratio of ~3 do we see the smaller dispersion completely incorporated into one large cluster.

The use of positively and negatively charged polymers combined with the statistical nature of copolymerization creates a system where individual polymers have a range of compositions in terms of charge sign, fraction, and hydrophobicity. It has been shown that amphiphilic copolymers with a distribution of compositions should phase separate into many phases with different compositions.^{98,115} However, we do not observe this in simulation or experiment due to the addition of the charged monomers and the energetic cost of creating many interfaces. Instead, we observe local charge heterogeneity as shown in Figure 3.4.

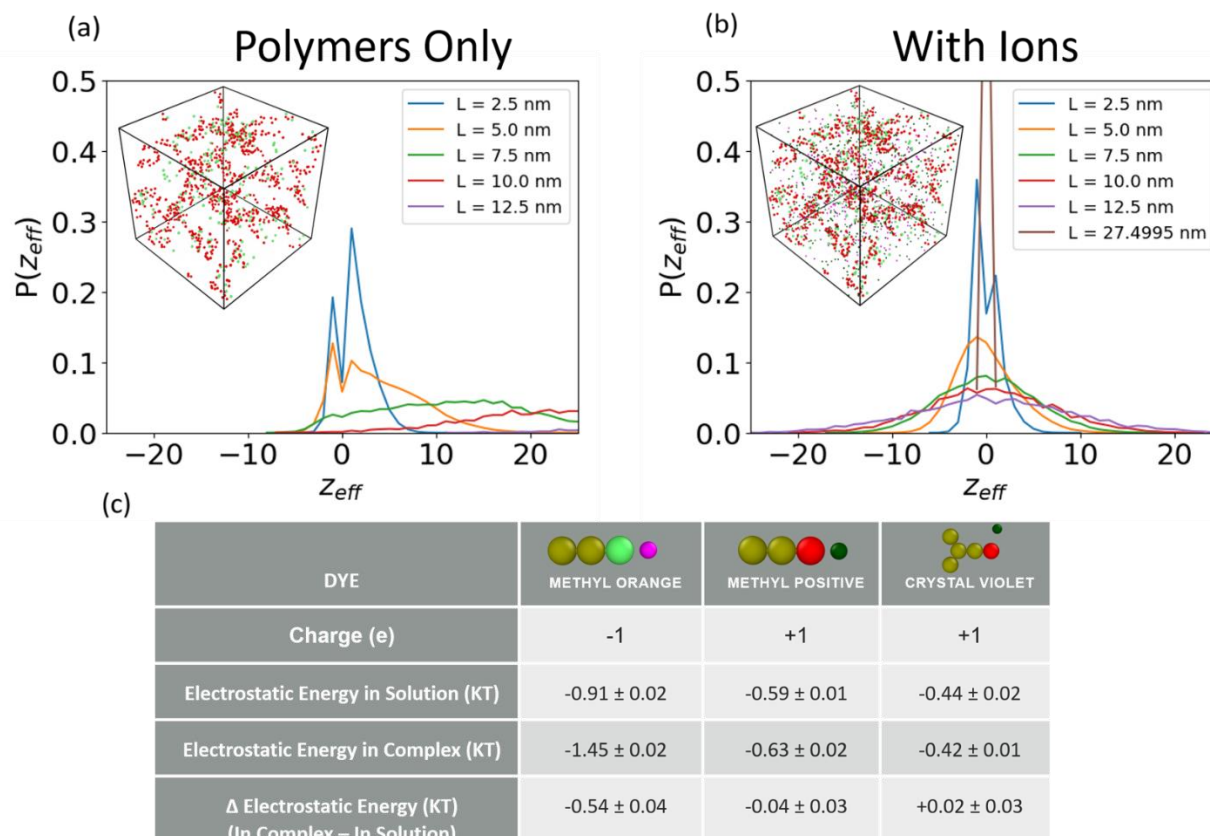


Figure 3.4 Simulation results on copolymer complex charge distribution. (a) Calculations of charge heterogeneity for charges on polymers. The simulation box is split into smaller cells of different lengths, L , and then the effective charge from the polymers in these boxes is calculated according to Eq. 2. Box sizes of 2.5nm and 5nm shows two peaks where the effective charge is ± 1 . This shows how the hydrophobic energy of the polymers leads to local charge segregation in these polyelectrolyte complexes. (b) Calculations of charge heterogeneity for charges on polymers and counterions. The same calculation is performed as described above. Free counterions help to negate some of this charge segregation, but at small length scales the two peaks are still observed. At larger length scales a Gaussian distribution centered at 0 effective charge is observed. (c) Electrostatic driving force for dye segregation. The electrostatic energy of different dyes when they are free in solution, segregated in the complexes, and the energy difference between the states.

This is shown by splitting the simulation box into many smaller cells of a certain size, L , and calculating the effective charge in those cells, Z_{eff} :

$$Z_{\text{eff}} = N^+ - N^- \quad \text{eq. 2}$$

where N^+ is the number of positive charges in the cell and N^- is the number of negative charges in the box. In Figure 4(a), N^+ and N^- are restricted to be charges on the polymers; in Figure 3.4(b), they can be any charge including those from the counterions. At small cell sizes, we observe two peaks at ± 1 with and without the inclusion of counterions in the effective charge of the box. That is, the system develops domains with different fractions of charge. The energy penalty, F_c , associated with this charge heterogeneity is proportional to the square of the effective charge, divided by the cell size, L , in terms of the Bjerrum length, $l_B = e^2 / (4\pi\epsilon_0\epsilon K_B T)$, with ϵ_0 being the permittivity of vacuum, ϵ the relative permittivity of the media, e the elementary charge, K_B is Boltzmann's constant, and T is absolute temperature. Here, we use the Bjerrum length in water, 0.7 nm, which comes from its bulk dielectric constant, $\epsilon = 80$.

As the cell size increases, the effective charge scales with the number of charges, which scales with the volume of the cell or the cell size cubed. Thus, the overall charge energy scales with the cell size to the fifth power.

$$F_c / K_B T \propto \frac{Z_{eff}^2 l_B}{L} \propto l_B L^5 \quad \text{eq. 3}$$

The compensation for this charge heterogeneity must come from the hydrophobic interactions of the anionic and cationic copolymers. The energy of these hydrophobic interactions, F_H , come from the interface between the solvent and hydrophobic domains. It scales with the surface tension, γ , and, by dimensional analysis, the cell size squared.

$$F_H / K_B T \propto \gamma L^2 \quad \text{eq. 4}$$

Thus, the charged term has a much stronger scaling with the cell size and as a result, the two peaks at ± 1 are observed only at small length scales, obtained by minimizing the sum of eqs. 3 and 4 giving $L_{hetero} \sim (\gamma/l_B)^{1/3}$. Free counterions help to compensate the charge on the polymers, decreasing this length scale in Figure 4 (b). Above this length scale, the population of cells with different numbers of charges tends towards a Gaussian distribution with zero average net charge, while the distribution width becomes broader as L increases. This is due to the stretched conformations of the copolymers in complexes as described in Figure S2. We note that when L increases beyond a critical value, the width of the charge distribution should shrink again because there is no system with macroscopic excess charge. Finally, when L approaches the system box size, we observe a delta function at zero given the electroneutrality condition imposed in the simulations.

The charge heterogeneity also impacts the absorption of the dyes. In order to explore the generality of the method to segregate different molecules, we used seven variations of crystal violet and methyl orange coarse grain dyes shown in Figure 3.2. These molecules were added into the simulations with a polymer charge ratio of 3.25 at a ratio of 1 dye molecule: 130 polymer monomers. A dye is considered segregated if any of its hydrophobic beads is within a certain distance of a hydrophobic bead belonging to a polymer. Following experimental trends in removal rate, the crystal violet has a higher condensation rate than methyl orange. This makes sense given the additional hydrophobic benzene ring in the crystal violet that effectively increase its hydrophobic interaction with the complex. Overall, for purely hydrophobic dyes, the more hydrophobic beads it contains, the higher the percentage of segregated contaminants in the sample.

This dependence of segregation to hydrophobicity is in line with experimental results in related polymer-micelle complexes.⁹⁶ We also see that adding a charged bead to a given hydrophobic structure decreases the percentage of molecules segregated. These segregation results are shown in Figure 3.5(a).

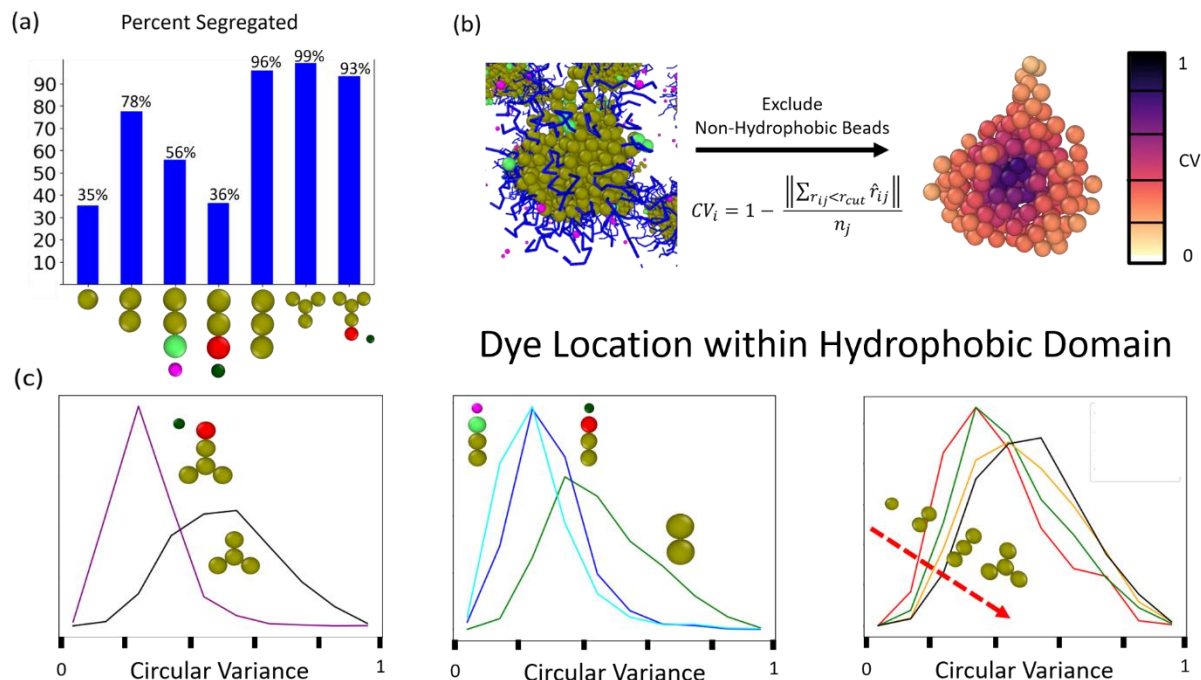


Figure 3.5 Simulation results of molecular encapsulation. (a) Calculations of charge heterogeneity for charges on polymers. The simulation box is split into smaller cells of different lengths, L , and then the effective charge from the polymers in these boxes is calculated according to Eq. 2. Box sizes of 2.5nm and 5nm shows two peaks where the effective charge is ± 1 . This shows how the hydrophobic energy of the polymers leads to local charge segregation in these polyelectrolyte complexes. (b) Calculations of charge heterogeneity for charges on polymers and counterions. The same calculation is performed as described above. Free counterions help to negate some of this charge segregation, but at small length scales the two peaks are still observed. At larger length scales a Gaussian distribution centered at 0 effective charge is observed. (c) Electrostatic driving force for dye segregation. The electrostatic energy of different dyes when they are free in solution, segregated in the complexes, and the energy difference between the states.

As expected for the net positively charged polymer complex, the negative methyl orange dye is more readily segregated than its positive counterpart. This is supported by Figure 4(c), which

shows that the electrostatic driving force is stronger for methyl orange than its positive counterpart. That is, for the negative dye, the electrostatic energy decreases upon condensation into the polymer complex, whereas for the positive dyes, there is almost no difference in electrostatic energy despite the polymer charge ratio of 3.25. Figure 3.4(c) also shows that, due to the charge heterogeneity demonstrated in Figure 3.4(a), the absorption of the positive dyes is not adversely impacted by the net positive charge on the complexes. The heterogeneity of the charges in the complex makes it possible for both negative dyes to reduce their energy upon condensation. In contrast, the positive dyes are relatively unaffected because there are areas of net positive and net negative charge in the polymer complex, which is net positive. This encouraging generality of the method is not anticipated by simple intuition, which shows the importance of the heterogeneities in charge and composition caused by the random copolymers (some domains have positive charge and some negative) as shown in Figure 3.4(a,b).

This generality is explained by examining the location of condensed dyes within the hydrophobic cores present in the polymer complexes. To this end we measure the hydrophobic circular variance. A full explanation of the circular variance is given in Figure 3.5(b), but it is used as a measure of the degree of burial of the dyes. Maximum burial by hydrophobic beads corresponds to a circular variance of 1 and minimum burial to a circular variance of 0. The distribution of circular variances for the different dyes is shown in Figure 3.5(c). There are two basic distribution shapes, one for charged and one for uncharged dyes. The distribution for charged dyes skews to lower values meaning that these dyes are restricted to be closer to the surface of the hydrophobic region due to the charges preferring the ionic solvent environment. However, we notice a difference in the segregation behavior of oppositely charged dyes, with 10% of the segregated anionic methyl

orange condensed to a hydrophobic bead on the cationic copolymer, compared to 1% for the segregated crystal violet. Despite the fact that both dyes reside at the interface of hydrophobic and hydrophilic regions of the polyelectrolyte complex, their hydrophobic interactions can be significantly different given that the methyl orange is more likely to interact with the cationic copolymer than the crystal violet. This discrepancy may help explain why we do not observe a solvatochromic shift in experiments where methyl orange was segregated into complexes.

The distribution for the uncharged dyes tends toward higher values of burial, and the distributions indicate more burial as more hydrophobic beads are added. This burial means a stronger overall interaction between the hydrophobic portion of the dye and the hydrophobic domain of the complex, explaining the trend of lower percent segregated for charged dyes despite no adverse effects observed in the electrostatic potential (see Figure 3.4c). The stretched conformations of the anionic copolymers could be contributing to the removal of the charged dyes because they have a higher surface area to volume ratio than spherical micelles and thus allow more low circular variance sites for the charged dyes to condense.

Conclusion

We developed a method to segregate organic molecules from water into complexes formed by two oppositely charged, random copolymer species. We demonstrated that the heterogeneity of the complex plays an important role in providing favorable interactions to a wide variety of small molecules, as shown by our analysis of positively charged, negatively charged, and hydrophobic molecules. Hydrophobic interactions from hydrophobic cores play a dominant role for segregation into the complexes, and charged molecules undergo relatively favorable electrostatic interactions

due to nanoscale charge segregation in the complexes. There are still many interesting aspects of this system to explore. The sizes and distribution of the hydrophobic domains, and whether such domains are formed primarily through interactions between multiple polymer chains, is another aspect of heterogeneity in our system which likely affects molecule uptake. We also claim that the hydrophobic domains, along with differences in charge distribution of the polyelectrolytes, leads to non-stoichiometric charge ratios for macroscopic complexes. It may then be possible to tune the charge distribution and hydrophobic content to change this charge ratio, which may also affect molecule uptake. Investigating how different copolymer compositions affect these various parameters and molecule uptake could be an active field of research.

Our work has implications for disordered systems such as membraneless organelles to concentrate small molecule substrates necessary for enzymatic biological processes. Combining this result with the ability of synthetic random copolymers to form complexes with enzymes,⁵² we expect that it may be possible to replicate the function of membraneless organelles in optimizing enzymatic activity by co-localizing an enzyme and its substrate, with potential industrial applications.

This method has the potential to provide an economical approach to remove a wide range of dye and contaminants from water on a large scale, as random copolymers can be synthesized inexpensively via free radical polymerization. The basis of favorable interactions between various molecules lies within the statistical distribution of monomers that leads to heterogeneity at the nanoscale, and controlling dispersity or other structural features of the polymer through more expensive techniques such as controlled radical polymerization is not necessary. This technique could be incorporated into existing water remediation processes via addition of a well-designed

anionic random polyelectrolyte during a flocculation step. The flocculation behavior of these polyelectrolyte complexes also has the potential to lead to the removal of hydrophobic particles from water such as enzymes and nanoparticles including nanoplastics,¹¹⁶ something which traditional flocculants may have difficulty accomplishing as they lack a significant hydrophobic interaction. Further studies on interactions between these heterogeneous polyelectrolyte complexes and bulk polymer surfaces are planned to explore such a possibility.

Methodology

Materials

The monomers used for polymerization, polyethylene glycol methyl ether methacrylate ($M_n = 500$ g/mol, PEGMEMA), ethyl hexyl methacrylate (EHMA), 3-sulfopropyl methacrylate salt (SPMA), 2-hydroxyethyl methacrylate (HEMA) and 2-trimethylammonioethyl methacrylate (TMAEMA), were purchased from Sigma, and inhibitors were removed under inhibitor removers from Sigma. The chain transfer agent dodecanethiol, NMR solvent deuterium oxide, thermal initiator benzoyl peroxide, antioxidant hydroquinone, and dyes crystal violet, methyl orange, phenolphthalein, and contaminant perfluorooctanoic acid were also purchased from Sigma. Ethanol, hexane, HPLC-grade water, distilled water, hydrochloric acid, sodium hydroxide, and sodium chloride were purchased from ThermoFisher.

The anionic random copolymer was synthesized as follows. Benzoyl peroxide (0.40 mmol, 96 mg) was added to a 50 mL test tube and was dissolved in 25 mL of ethanol. PEGMEMA (34 mmol, 16 mL) and EHMA (43 mmol, 9.6 mL) were added to the solution, along with SPMA (8.5 mmol, 2.1 g) dissolved in 1.6 mL of water. Dodecanethiol (0.30 mmol, 72 μ L) was added to inhibit side

reactions involving crosslinking of polyethylene glycol side chains.¹ The solution was then heated to 65 °C for 150 min. The polymer was precipitated and washed several times in hexane, followed by drying under vacuum at 40 °C for 30 min. The polymer was then dissolved in a 70-30 vol% deionized water-ethanol mix and dialyzed against 2 L of a 70-30 vol% deionized water-ethanol mix for 1 day, and then dialyzed against 2 L of deionized water for 2 days, changing the dialysis solution each day. The aqueous polymer solution retrieved from dialysis was directly used in experiments.

The cationic random copolymer was synthesized as follows. Benzoyl peroxide (0.21 mmol, 50 mg) was added to a 20 mL test tube and dissolved in 4 mL of methanol and 2 mL of water. HEMA (41 mmol, 5 mL) and TMAEMA (20 mmol, 5 mL of 75 w/w% solution) were added and the solution heated to 65 °C for 165 min. The polymer was precipitated in ethanol. Excess solvent was removed with flowing air, and the polymer was dissolved in deionized water and dialyzed in 2 L of deionized water for 2 days, changing the dialysis solution after 1 day. The aqueous polymer solution retrieved from dialysis was directly used in experiments.

The mass concentration of the two polymer solutions were determined by drying a known volume of solution in an oven and weighing the mass of the remaining polymer. Reported results are an average of three separate measurements.

Previous research has shown that PEGMEMA monomers tend to participate in unwanted radical crosslinking reactions, which causes gelation of the polymer sample at low conversion.¹¹⁷ Additionally, polymers containing PEGMEMA may also gel during handling or storage after precipitation or recovery and are most stable when dissolved in solvent. The addition of chain

transfer agent suppresses gelation during polymerization, and the addition of an antioxidant such as hydroquinone can suppress gelation when in dry form. These precautions were taken in our study.

Copolymer characterization.

Copolymer composition was characterized using ^1H NMR spectroscopy (Bruker X500 NMR spectrometer), with deuterium oxide as solvent. To prepare appropriate solutions for NMR analysis, a small amount of hydroquinone was added to the aqueous copolymer solutions before drying in a vacuum oven and redissolving in deuterium oxide. The final polymer concentrations were ~ 20 mg/mL, and the final concentration of hydroquinone was ~ 2 mg/mL. The addition of an antioxidant inhibits a known gelation effect noted in previous literature for polymers containing polyethylene glycol sidechains.¹¹⁷ It also inhibits a gelation effect observed in the cationic polymer. Full dissolution of the dried anionic random copolymer can require up to 24 h.

^1H NMR peak assignments were done broadly by distinguishing low chemical shift hydrogens next to non-polar carbons, labeled (a), and high chemical shift hydrogens next to polar functional groups and carbons next to polar functional groups, labeled (b). For the anionic copolymer of EHMA, PEGMEMA, and SPMA, a third label (c) is needed, and was determined by comparing to a ^1H NMR spectrum of EHMA and PEGMEMA. For the cationic HEMA-TMAEMA copolymer, the number of hydrogens assigned to the peaks will differ based on the exact structure of the copolymer, which was not determined in this study. Instead, upper and lower bounds were determined by assuming either a strictly linear polymer with no branching, or one branch per

HEMA monomer for a highly branched polymer. The assignments are shown below along with NMR spectra in Figures 3.6 and 3.7.

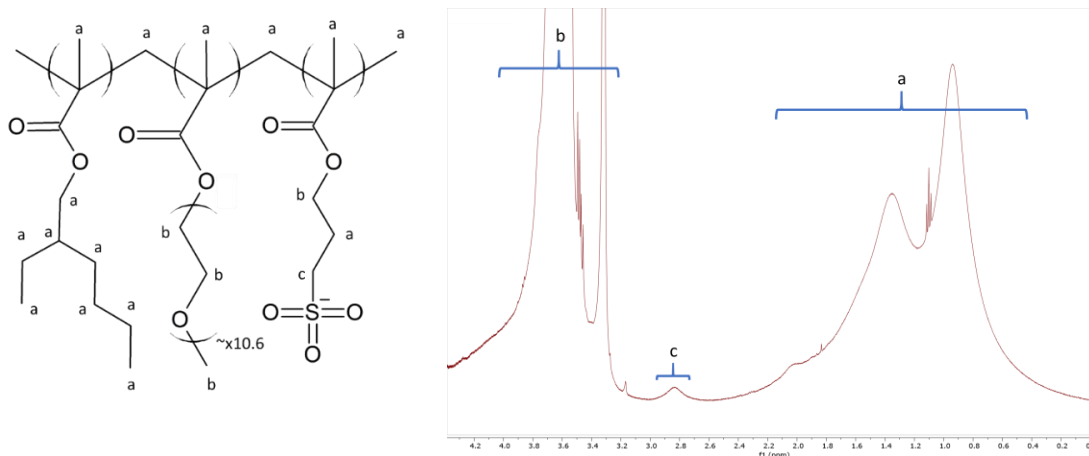


Figure 3.6 NMR assignments for the anionic copolymer of EHMA, PEGMEMA, and SPMA.

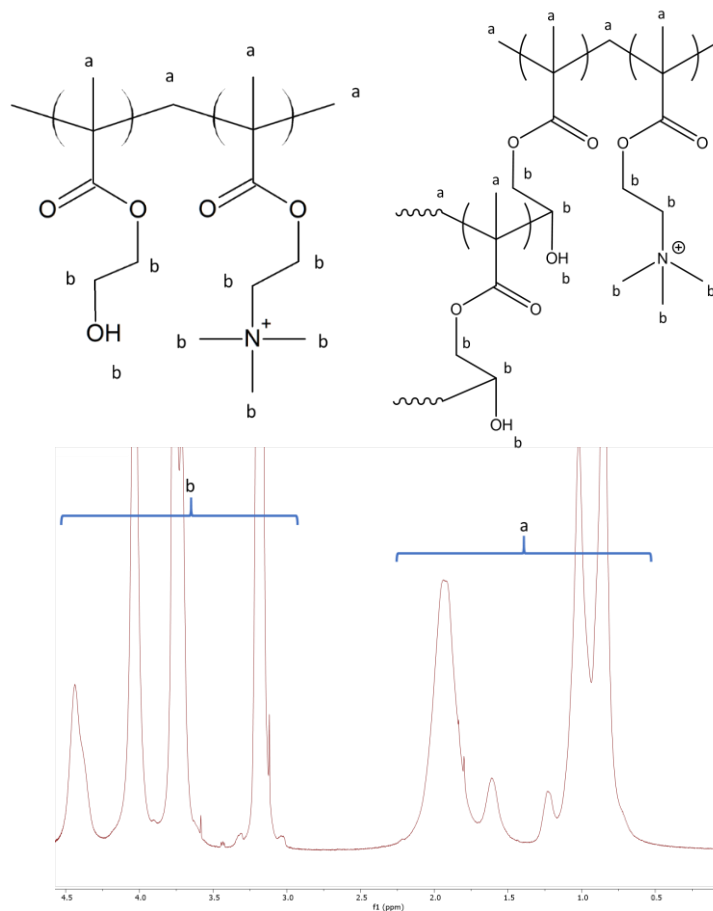


Figure 3.7 NMR assignments for the cationic copolymer of HEMA and TMAEMA. Upper left shows a linear polymer, while upper right shows a highly branched polymer.

Apparent molecular weight was characterized by aqueous gel permeation chromatography (Agilent 1260 series HPLC, Superdex 200 Increase 10/300 GL column) with a multi-angle static light scattering detector (Wyatt DAWN HELEOS II) in 0.1M NaCl aqueous buffer. An approximate refractive index increment (dn/dc) value was measured for each polymer by using an Atago pocket refractometer on a serial dilution of polymer solution. The dn/dc value of the anionic polymer in 0.1 M NaCl buffer was determined to be 0.155 mL/g, and the dn/dc value of the cationic polymer in 0.1 M NaCl buffer was determined to be 0.143 mL/g.

Quantification of dye and contaminant removal.

Crystal violet, methyl orange, and PFOA are water soluble and a 200 ug/mL stock solution was prepared by mixing the appropriate mass of reagent with distilled water. Phenolphthalein was not easily dissolved in water even at concentrations below its solubility limit, and a stock solution of 50 $\mu\text{g}/\text{mL}$ was prepared by dispersing 500 μg of phenolphthalein in 10 mL of water, adding 100 μg of 0.1 M sodium hydroxide solution, and then adding 100 μg of 0.1 M hydrochloric acid. Adding sodium hydroxide to the solution changes phenolphthalein into its charged form, which is readily soluble in water. The hydrochloric acid reverts the solution to its original pH and the phenolphthalein into its neutral form, which is key for the complexation experiments.

Visible absorbance spectra were obtained (Thermo Scientific Evolution 201 Spectrophotometer) for crystal violet, methyl orange, and phenolphthalein solutions at various concentrations, and five-point calibration curves were determined by comparing peak absorbance wavelength of the solution to its concentration. Anionic copolymer was added to crystal violet solutions in order to account for the solvatochromic shift. Visible absorbance spectra for phenolphthalein were obtained

under basic conditions, as solutions of phenolphthalein are colorless under neutral or slightly acidic conditions. The concentration of dyes after filtration was determined by comparing the peak absorbance of the absorbance spectrum to the calibration curve. Reported results were obtained by measurements on three separate samples.

For PFOA solutions, concentrations were measured by liquid chromatography-mass spectrometry with electrospray ionization (Bruker Amazon-X) in negative polarity mode using a reverse phase column (Acentis Express C18, 5 cm, 2.1 mm I.D., 5 μm). A flow rate of 0.3 mL/min was used with a 60/40 vol% acetonitrile/water solvent mixture. Chromatogram peaks with m/z of 368.9 g/mol and 412.9 g/mol, corresponding to counts of ionized fragments of PFOA, were integrated with a peak elution time of 160 s. A five-point calibration curve was constructed, and the concentration of PFOA in filtered solution was determined by comparing the integrated peak values to the calibration curve. Reported results were obtained from three measurements on the same sample.

Coarse Grain Simulations.

Molecular dynamic simulations were run at two different length scales. The finer simulations use the MARTINI forcefield with polarizable water.¹¹⁸ In these simulations, we study the distribution of different groups in micelles formed by the anionic copolymers. The model parameters used in these simulations were taken from a combination of sources studying similar polymers.¹¹⁹ The beads used are shown in Figure 3.1 and a full description of the forcefield can be found in Supporting Information. The coarse grain molecular dynamics simulations were performed using the HOOMD-blue package.¹²⁰ An implicit water forcefield comprised of hydrophobic,

hydrophilic, and charged beads was used to model both types of polymers and many different dyes (full forcefield parameters can be found in Supporting Information). As shown in yellow in Figure 1, the backbone of all methacrylate polymers is composed of one hydrophobic bead per monomer, which is bonded to the next monomer via a harmonic bond. The side chains are unique to each monomer. The side chain of EHMA is modeled with two more hydrophobic monomers, PEGMEMA is composed of 6 hydrophilic beads (blue), and SPMA is a hydrophobic, followed by a negatively charged bead (green), which is accompanied by a positive counterion (pink). The cationic polymers are made of TMAEMA, which is modeled a positive bead (red) and accompanying counterion (green), and HEMA, which has no side chain. Crystal violet, methyl orange, and variants of these dyes were also modeled using the same hydrophobic and charged beads as described in Figure 2. By utilizing additional angle potentials, their rigid shapes were conserved.

Coarse Grain Model

Bead Types

Our forcefield features 7 types of beads. The “B” beads are used to represent hydrophobic subunits of polymers and contaminants, while the “L” beads represent the hydrophilic subunits. The rest of the beads represent positive and negatively charged subunits and ions. They are “QP”, “QM”, “QP_i”, “QM_i”, and “QM_{small}”. The beads ending in “i” are smaller ion beads. “QM_{small}” is the same size as an ion, but is used to represent the fact that we expect the negative charge on the SPMMA to be less shielded than the METAC.

Potentials

Non-Bonded

Volume excluding and hydrophobic pair interactions are handled by a Lennard-Jones potential

$$V_{LJ}(r) = 4\epsilon \left[\left(\frac{\sigma}{r} \right)^{12} - \left(\frac{\sigma}{r} \right)^6 \right]$$

For all pairs of beads which are not both “B” beads this potential is truncated at $2^{1/6}\sigma$, making it a purely repulsive WCA potential.¹²¹ For pairs of “B” beads the Lennard-Jones potential has a well-depth, ϵ , of 1 KT and is truncated at 3σ . The mixing rule for σ is arithmetic

$$\sigma = \sigma_{ij} = (\sigma_i + \sigma_j)/2$$

Charged

Explicit coulomb interactions are calculated using the PPPM method.¹²² All bead types beginning with “Q” have a charge of $1.609 * 10^{-19}$ c. We use the bulk dielectric constant of water, 80. The charge, q , and diameter, σ , of each bead type is shown below in Table 3.2.

Table 3.2 Non-Bonded Parameters for the Coarse-Grain forcefield.

Type	σ (nm)	q (e)
B	0.5	0
L	0.5	0
QP	0.5	+
QM	0.5	-
QP _i	0.3	+

QM _i	0.3	-
QM _{small}	0.3	-

Bonds

All bonds use a harmonic spring potential of the form

$$V_{Bond}(r) = \frac{1}{2} k_{bond} (r - r_0)^2$$

where $k_{bond} = 120 \text{ KT/nm}^2$ and $r_0 = 0.5 \text{ nm}$.

Angles

All angles used are harmonic angle potentials of the form

$$V_{Angle}(r) = \frac{1}{2} k_{angle} (\theta - \theta_0)^2$$

Angle potentials used in contaminants use $k_{angle} = 120 \text{ KT/rad}^2$ and $\theta_0 = 120^\circ$ or 180° depending on the chemical shape of the contaminant. Angle potentials in the backbones of the polymers use $k_{angle} = 1 \text{ KT/rad}^2$ and $\theta_0 = 180^\circ$. These values were calibrated to observe the gelation of the system.

MARTINI Model

We use Martini version 2.2 with polarizable water.^{118,123} The parameters for the random anionic copolymers come from a combination of sources.^{119,124} A parameterization is shown below in Figure 3.8.

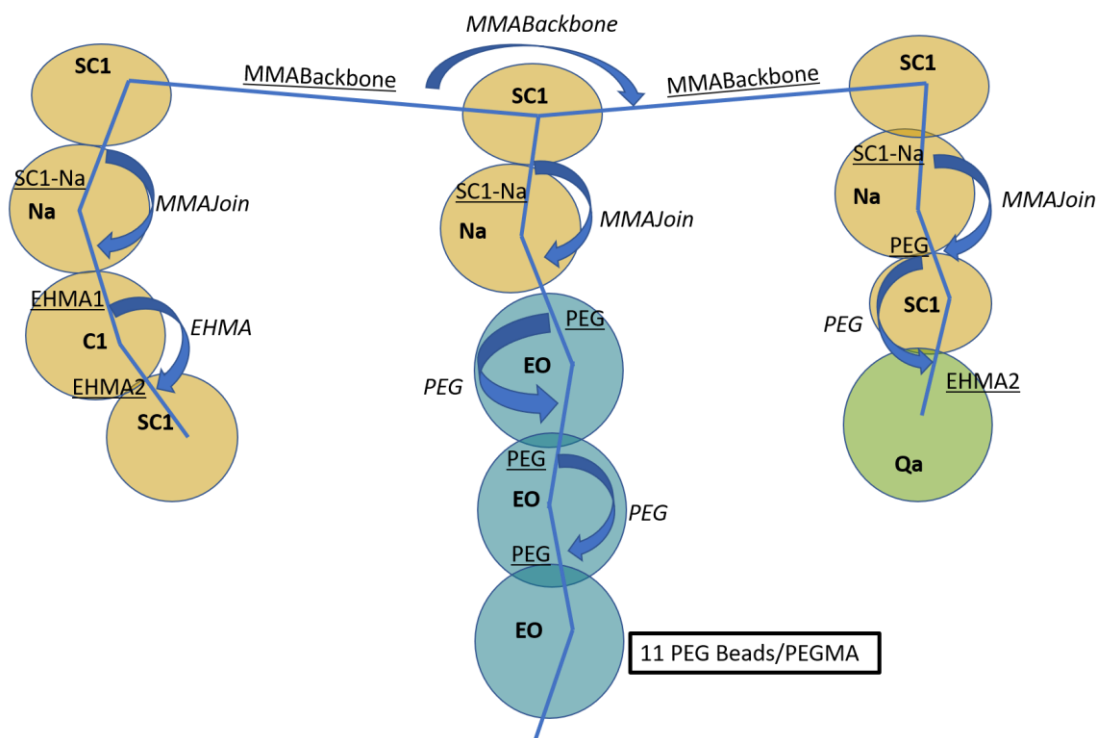


Figure 3.6 MARTINI parameters for the random anionic copolymers. Angle names (see Table 3.4) are italicized, and bond names (see Table 3.3) are underlined. Bead names which control the Lennard-Jones parameters all come from the standard MARTINI forcefield.

Bead Types

All beads come from the

Potentials

Bonds

All bonds use a harmonic spring potential of the form

$$V_{Bond}(r) = \frac{1}{2}k_{bond}(r - r_0)^2$$

And the parameters are detailed in Table 3.3.

Table 3.3 Bond Parameters for the MARTINI Forcefield

Type	k_{bond} (kJ/mol/nm ²)	r_0 (nm)
MMABackbone	21,100	0.289
PEG	7,000	0.32
SC1-Na	17,000	0.282
EHMA1	17,000	0.54
EHMA2	1250	0.425

Angles

All angles used are harmonic angle potentials of the form

$$V_{Angle}(r) = \frac{1}{2} k_{angle} (\theta - \theta_0)^2$$

And the parameters are detailed in Table 3.4.

Table 3.4 Angle Parameters for the MARTINI Forcefield

Type	k_{angle} (kJ/mol/rad ²)	θ_0
MMABackbone	13	175
MMAJoin	67	144
PEG	400	122
EHMA	25	180

Chapter 4: Tailoring Interactions of Random Copolymer Polyelectrolyte Complexes to Remove Nanoplastic Contaminants from Water

We investigate the usage of polyelectrolyte complex materials for water remediation purposes, specifically their ability to remove nanoplastics from water, on which there is currently little to no prior research. We demonstrate that oppositely charged random copolymers are effective at quantitatively removing nanoplastic contamination from aqueous solution. The mechanisms underlying this remediation ability are explored through computational simulations, with corroborating quartz crystal microbalance adsorption experiments. We find that hydrophobic nanostructures and interactions likely play an important role.

It should be noted that colleague Curt Waltmann performed the computational simulations, colleague Qifeng Wang performed the quartz crystal microbalance experiments, and colleagues Benjamin Shindel, Jack Hegarty, and Caroline Harms performed fluorescence measurements and microscopy work.

Introduction

Microplastic, and more recently, nanoplastic pollution are issues of emerging concern. A bulk of microplastics come from larger pieces of plastics exposed to the environment. The combination of UV light, which makes plastic particles brittle, and the constant abrasion of wave motion from bodies of water cause erosion of the macroplastics and the release of smaller particles.^{125–127} Over

time, these particles can become even smaller through other degradation processes which can be chemical or biological.^{12,128}

While the plastic particles themselves are thought to be relatively inert, they can still have adverse effects on environmental and human health. Microplastics can concentrate toxic chemicals or heavy metals already present in the environment.¹⁰ Due to the hydrophobic nature of microplastics, hydrophobic chemicals such as bisphenols or other molecules of concern easily partition onto their surface,¹²⁹ while favorable electrostatic interactions between polymer surfaces and ions contribute to heavy metal adsorption.¹³⁰ Nanoplastics are thought to be considerably more potent at this partitioning and adsorption behavior due to their increased surface area to volume ratio.^{131,132} They also present additional concerns from their small size, as research has shown that these nanoplastics are much more biologically active and can penetrate cell membranes or even be cytotoxic.^{133,134} The combination of these aspects make nanoplastics potentially more hazardous than microplastics.

Currently, there are various techniques being investigated to remove microplastics and nanoplastics from water. Some recent methods include the use of advanced oxidation processes to decompose plastics through catalytic means.^{135,136} Others involve the electrocoagulation of the plastic particles from water using charged electrodes.^{137,138} However, microplastics and nanoplastics tend to be quite dilute in bodies of water, leaving large volumes of water to be treated.¹²⁵ Thus, there is a need for economical and scalable processes to remove microplastics and nanoplastics from water. Industrial treatment processes such as sand filtration, activated carbon filters, and membrane filtration have been shown to be relatively effective at removing microplastics and nanoplastics, either by preventing particulate contaminants above a certain size

from passing through the filter or by adsorption of the particles onto the filtration medium.^{12,131,139}

However, these techniques run into the issues of membrane fouling, pore clogging and adsorption capacity, which reduce the water flow and effectiveness of the filters over time.^{12,131}

The technique of flocculation, where negatively charged colloidal particles are aggregated through the use of oppositely charged flocculants, such as cationic polymers, has also been explored.^{88,90} Flocculation has particular advantages, as it is relatively simple to perform and is a widely adopted form of water treatment. It can also help reduce fouling of membranes used in subsequent membrane filtration.¹⁴⁰ Studies on the removal of nanoplastics through flocculation are somewhat sparse and the results can be quite variable, depending on factors such as size, solution pH, and flocculant dosage. Most studies have focused on polystyrene nanoplastics, and removal results typically range from 40% to 90+%,¹⁴¹⁻¹⁴⁴ with one study reporting no removal.¹³⁹ One study used a methacrylic acid polymer as a surrogate for polyethylene terephthalate and found a removal rate of 88%.¹⁴⁵ Developing reliable and effective flocculation techniques to remove nanoplastics could go a long way in addressing nanoplastic pollution with established and accessible techniques.

In the previous thesis chapter, we used a flocculation-like technique to remove chemical contaminants from water. By combining a negatively charged random copolymer with a positively charged random copolymer, we were able to create macroscopic, solid complexes that could be removed from water through a simple filtration process. These polyelectrolyte complexes (PECs) have the ability to absorb various molecules due to favorable hydrophobic and charged interactions. In general, PECs are formed due to the presence of oppositely charged groups, but their interactions, properties, and phase behavior are highly tunable by a number of

different factors. These can include solvent quality,⁷⁸ ionic solution conditions,^{74,77,146–148} polymer rigidity,¹¹¹ and monomer sequence (blockiness).^{73,149} One can even include other components in PECs including micelles⁹⁶ and bioactive proteins containing both positive and negative charges into these complexes.^{150–153}

The usage of random copolymers can provide additional tunability through the polymer composition, with the statistical distribution of the monomer sequence potentially enhancing polymer-surface interactions through a form of pattern recognition.^{48,66,68,154} Correlations in monomer sequence increase the affinity of polymer adsorption onto surfaces, particularly for heterogeneous surfaces. This concept was utilized to form nanoscale aggregates of oppositely charged random heteropolymers and single proteins, which have a heterogeneous surface, in organic solvents and polymer melts.^{52,155} We have demonstrated in the next thesis chapter the complexation of random copolymers and the enzyme PETase in an aqueous solution, which increased the activity of the PET-degrading enzyme on PET films. One potential mechanism for this enhancement is the ability of the copolymer-enzyme complex to stick and adsorb onto a PET surface due to a hydrophobic surface affinity between the polymer and PET surface.⁴⁸ Here, we hypothesize that favorable interactions between macroscopic random copolymer PECs and PET can be utilized in flocculation to remove PET nanoplastics from solution.

In this study, we investigate the ability of random copolymer polyelectrolyte complexes to remove PET nanoplastics through a flocculation technique. As in our previous work, we use random methacrylate copolymers synthesized via free radical polymerization. The anionic copolymer is composed of hydrophobic ethyl-hexyl methacrylate (EHMA), hydrophilic polyethylene glycol methyl ether methacrylate (PEGMEMA)(500 Mn), and negatively charged sulfopropyl

methacrylate (SPMA); the cationic copolymer is composed of the hydrophilic hydroxyethyl methacrylate (HEMA) and the positively charged trimethylaminoethyl methacrylate (TMAEMA). PET nanoplastics were prepared through nanoprecipitation techniques and loaded with Nile red fluorescent dye to enable the quantification of removal via fluorescence measurements. We observe that increasing the content of hydrophobic monomer EHMA in the anionic copolymer increases the amount of nanoplastics removed from solution, with the most hydrophobic polymer showing quantitative removal. Our hypothesis is that these PECs can adsorb and stick onto PET nanoplastics, encapsulating them into macroscopic flocs which can be removed relatively easily through coarse filtration. We investigate these polymer-surface interactions using quartz crystal microbalance (QCM) experiments to gauge the adsorption behavior of the anionic random copolymers on PET, along with corresponding MARTINI¹¹⁸ coarse-grained molecular dynamics simulations. We show that hydrophobicity can non-monotonically impact polymer-surface interactions due to changes in polymer conformation. Finally, implicit solvent coarse-grained molecular dynamics simulations of the copolymer complexes are used to understand how the nanostructure of the complexes may play a role in adsorption, again due to the arrangement of hydrophobic and hydrophilic groups within the complex.

An illustration of the encapsulation of nanoplastics (Figure 4.1(a)), diagrams of monomer structures (Figure 4.1(b)), simulation snapshot of copolymer adsorption (Figure 4.1(c)), and image of the polyelectrolyte complexes (Figure 4.1(d)) are shown below.

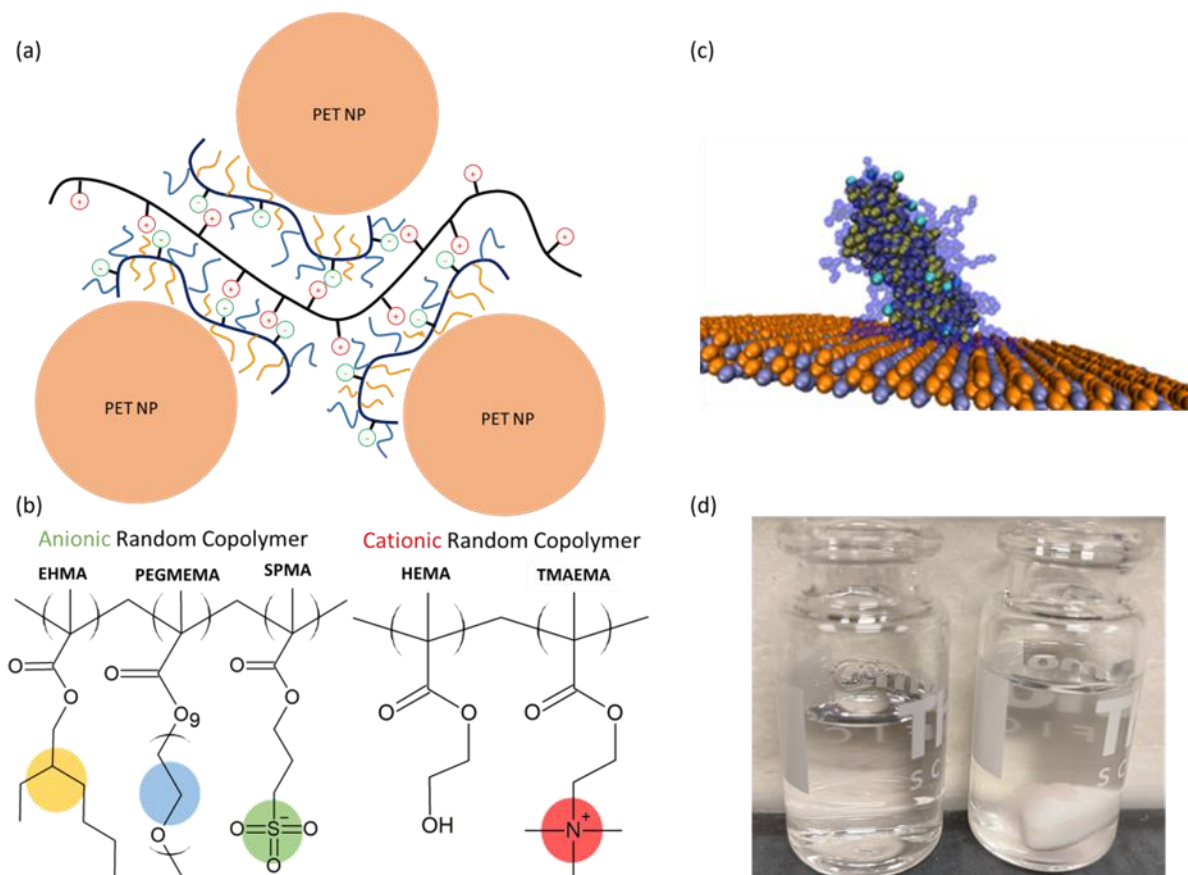


Figure 4.1 Schematic of polymer complexes and polymer adsorption onto PET. (a) Diagram of polyelectrolyte complex of random copolymers with adsorption of PET nanoparticles. (b) Chemical composition of the anionic and cationic copolymers. (c) Coarse-grained molecular dynamics simulation of anionic copolymer adsorbing onto PET. (d) Picture of nanoplastic spiked solution (left) and the polyelectrolyte complex formed after addition of random copolymer solutions, which has accumulated on a stir bar. (right)

Experimental results

Copolymer characterization

Table 4.1 shows the various compositions of the anionic copolymers used in the study, which were chosen to investigate how relative hydrophobicity and charge fraction affect nanoplastic uptake. Samples 1-4 are in descending hydrophobic content, with Sample 1 being the most

hydrophobic. Samples 5 and 6 are hydrophobic polymer compositions but with increased charge content. The cationic polymer was characterized with a 28% charge fraction (mol % TMAEMA) and an apparent number average molecular weight of 4.3 million g/mol.

Table 4.1 Anionic Copolymer Compositions

Samples	EHMA mol%	PEGMEMA mol%	SPMA mol%	M_n (g/mol)
Sample 1	54	36	10	268 000
Sample 2	49	42	9	183 000
Sample 3	33	59	8	248 000
Sample 4	25	67	8	304 000
Sample 5	51	33	16	274 000
Sample 6	39	26	35	201 000

Nanoplastic Remediation

The nanoplastic removal procedure is similar to that described in the previous thesis chapter. In short, anionic copolymer is added to an initial aqueous solution with our nanoplastic contamination. Under stirring, the cationic copolymer is then added until flocculation occurs and the solution becomes clear. A small amount of magnesium sulfate is then added to help coagulate the remaining flocs. The remaining solution is then filtered through a coarse 1 μm syringe filter, and fluorescence measurements are performed on the filtrate to determine the amount of nanoplastic removed.

The nanoplastics (Figure 4.2(a)) were characterized to have a number average size of 80 nm with a dispersity of 1.3. We find that we remove significant quantities of nanoplastics from our solution, with the complexes formed with our most hydrophobic sample (Sample 1) quantitatively removing nanoplastics below the detection limit of our fluorescence plate reader. We see in Figure 4.2(b) that there is a correlation between the hydrophobicity of the polymer composition and amount of nanoplastics removed. This would indicate that hydrophobic interactions play a significant role in the removal process. We find that charge does not have nearly as significant an impact on removal rate when comparing results of Samples 1, 5 and 6 in Figure 4.2(c), all with removal rates exceeding 90%.

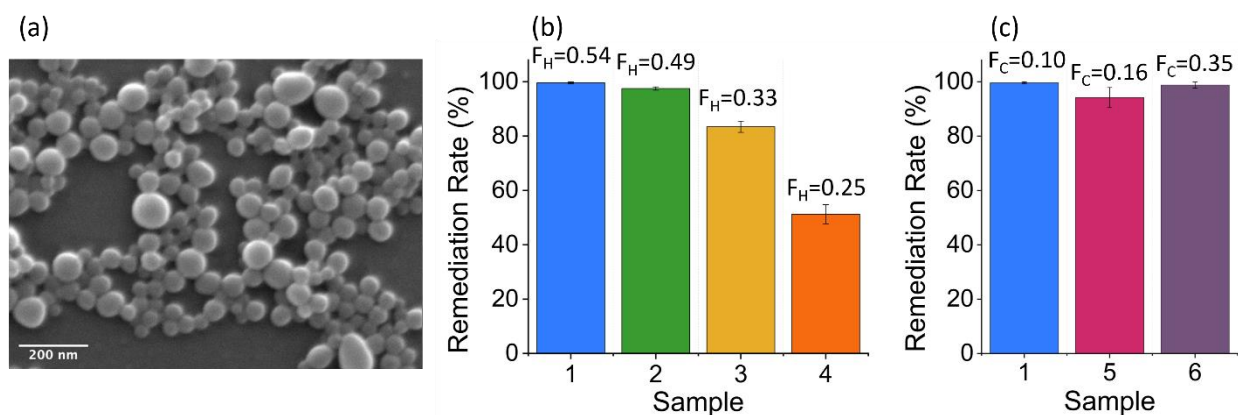


Figure 4.2 Image of PET nanoplastics and remediation rates from water. (a) SEM image of PET nanoplastics synthesized through a nanoprecipitation technique. (b) Remediation rates of nanoplastics for complexes that include polymer samples 1-4, which have a similar charge fraction. F_H denotes the fraction of hydrophobic monomer of the polymer sample. (c) Remediation rates of nanoplastics for complexes that include polymer samples 1, 5, and 6, which have roughly 50% more hydrophobic monomer than hydrophilic monomer. F_C denotes the fraction of charged monomer of the polymer sample.

Copolymer adsorption

To understand better the adsorption behavior of the polymers and the role it plays in nanoplastic removal, we perform quartz crystal microbalance experiments to measure directly the amount of anionic polymer adsorption on a PET surface.¹⁵⁶ We report the mass of polymer adsorbed in Figure 4.3(a) as obtained by the Sauerbrey equation. Our results indicate that the adsorption is non-monotonic with hydrophobicity, with high adsorption for the most hydrophilic and most hydrophobic samples. These results appear to be counter-intuitive, especially given our nanoplastic removal results.

A similar trend is observed in Martini simulations (see methodology for details) of the anionic random copolymers on a PET surface in Figure 4.3. Hydrophobic interactions are quantified by counting the number of contacts between hydrophobic beads of the anionic copolymer and the PET surface, and we find that polymers with the lowest and highest hydrophobic monomer fractions, F_H , have highest numbers of hydrophobic contacts (see Figure 4.3).

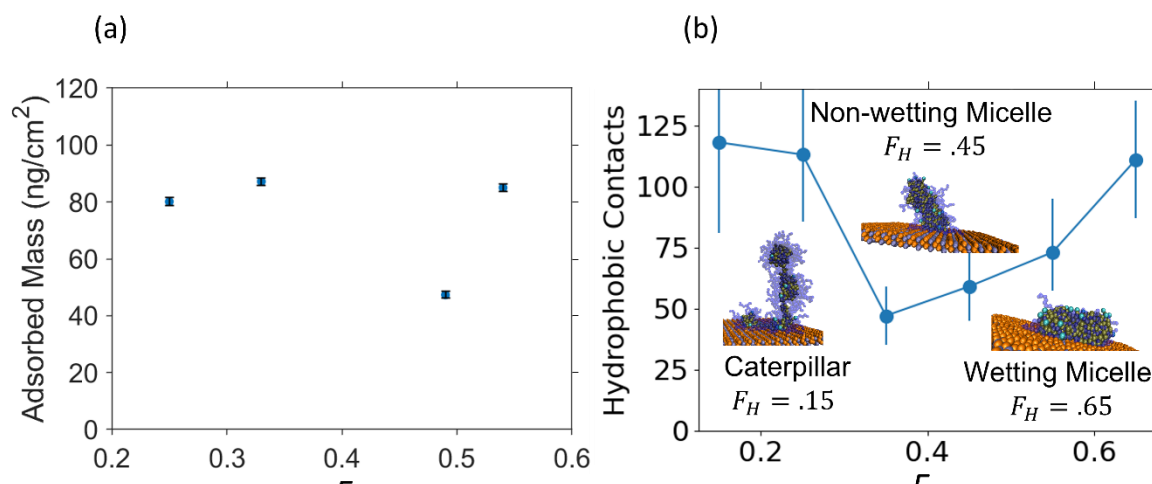


Figure 4.3 Polymer adsorption onto PET vs hydrophobic fraction F_H with experiments and simulation. (a) Mass of polymer adsorbed by samples 1-4 onto a film of PET as measured by QCM. The error bars are approximately the size of the markers used in the plot. (b) Simulation results of hydrophobic contacts between anionic copolymers and PET surface.

The simulations reveal a potential explanation for this behavior through polymer conformation. The highly hydrophilic copolymers form more caterpillar/train-like structures which can lie flat on the polymer surface. However, with increasing hydrophobic content, the polymers take more of a micellar conformation, with the formation of hydrophobic cores. This can lead to lower surface area of interaction between the polymers and the PET surface. At the highest hydrophobic monomer fraction, there is an insufficient amount of hydrophilic monomer to cover the core of the micelle, and as a result the polymer will wet the surface and create more hydrophobic contacts.

The discrepancy between the anionic polymer adsorption and the ability of the complex to remove nanoplastic particles is likely due to conformational and structural differences between the single polymers and polymer complexes. We used an implicit solvent, coarse grained model to perform simulations of the polymer complexes with variable hydrophobic fractions of the anionic copolymer, $F_{H,anionic}$. We examined the local hydrophobic distribution of the complexes at length scales smaller than the interdomain spacing of the complexes as calculated using the scattering function⁹⁹ (Figure 4.4a). This is done by splitting the simulation box into many cells of size, L , and then measuring the fraction of hydrophobic monomers from both polymer species, F_H . The least hydrophobic complexes ($F_{H,anionic} = 0.25$) show a strong peak to the left of the mean composition suggesting many cells are more hydrophilic than the mean (Figure 4.4(c)). In Figure 4.4(e), there is also a weaker peak to the right of the mean, which suggests some local separation is present. For the most hydrophobic complexes, we instead see one peak near the mean, although the distribution is skewed hydrophilic in Figure 4.4(e). When the cell size, L , is greater than the interdomain spacing, Gaussian distributions around the mean are observed for all $F_{H,anionic}$ as expected. Snapshots of the complexes show much stronger segregation of polymer components

into hydrophobic domains in Figure 4.4(d) than in Figure 4.4(b) due to the higher fraction of hydrophobic monomers, in agreement with the peak heights in Figure 4.4(a).

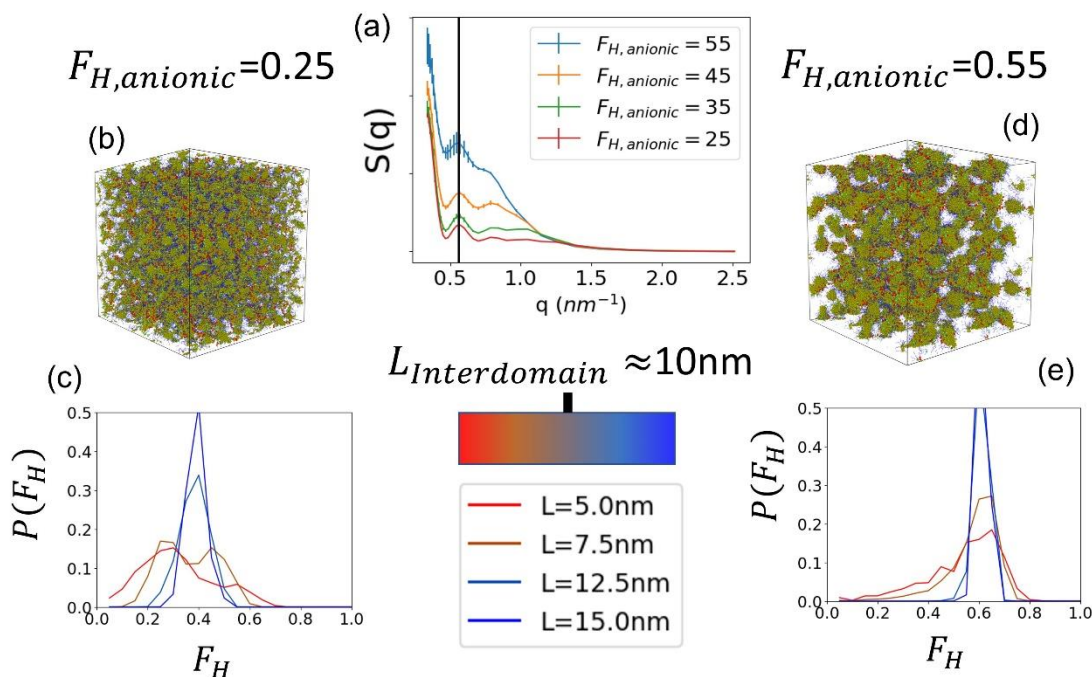


Figure 4.4 Simulation results for polyelectrolyte complexes with varying hydrophobic fraction of the anionic copolymer, $F_{H,anionic}$. (a) Scattering functions for $F_{H,anionic} = 25, 35, 45,$ and 55 all show peaks at $q = 0.56 \text{ nm}^{-1}$ and some show a smaller peak at $q = 0.78 \text{ nm}^{-1}$. These peaks correspond to the spacing between domains, which $\approx 10 \text{ nm}$. (b, d) Snapshots of the most and least hydrophobic complexes. (c,e) Local hydrophobic monomer density distributions show multiple peaks for the least hydrophobic complexes at length scales smaller than the interdomain spacing.

These domains may be similar to the "wetting micelle" conformations that were able to create more hydrophobic contacts with the surface in the single polymer simulations.^{157,158} In the single polymer simulations we also observed high absorption with the low hydrophobicity polymers due to their ability to lie flat on the surface in "caterpillar" conformations. However, in the complex they likely lack the necessary degrees of freedom for this to occur. Taken together, these results suggest that the properties and functions of these random copolymer polyelectrolyte complexes depend greatly on the nanoscopic details of polymer composition and conformation. For the

particular case of removing nanoplastics, hydrophobicity appears to play a key role but is intertwined with the interactions between the two polymers in the complex system. The distribution of hydrophobic regions in the polyelectrolyte complex, as well as the PET surface, could be important.¹⁵⁹ This could be similar to the significance of charge distribution and the ability to encapsulate molecular contaminants in aqueous solution, as discussed in Chapter 4.

Conclusion

The ability to tune the interactions of the random copolymer polyelectrolyte complexes by adjusting hydrophobicity and charge clearly lends great utility and versatility to this remediation technique. While we have focused on the removal of PET nanoplastics in relatively pristine condition in this study and found hydrophobicity to be the dominating factor, the potential still remains to expand the type of contaminants that can be removed. Nanoplastics composed of different polymeric materials will likely have different surface properties and interactions, with a different composition that may be tailored to optimally remove said material. Environmental conditions can also potentially alter nanoplastic surface characteristics through the adsorption of biomolecules and the formation of a corona layer.¹⁶⁰ The removal of microplastic contamination may have entirely different considerations. Biofilms, which tend to be a layer of naturally growing bacteria or other microorganism, readily accumulate onto microplastic surfaces and can present drastically altered surface properties.¹⁵² The type of random copolymers that we used in this study have already been shown to interact well with biological molecules such as proteins,⁵² and thus may be well suited for interacting with such biological surfaces.

Thus, these random copolymer polyelectrolyte complexes may prove to be a potent water remediation technique due to the wide range of potential favorable interactions they can provide, with a simple mechanism of tuning these interactions through the adjustment of the polymer compositions. This in turn can provide a level of robustness in operating conditions and use cases that may very well extend beyond the case of addressing nanoplastic pollution. For example, in a preliminary experiment, we were able to quantitatively remove lead contaminated nanoplastics and lead ions from a sample solution with our flocculation technique (see methodology for details). The results are shown below in Figure 4.5.

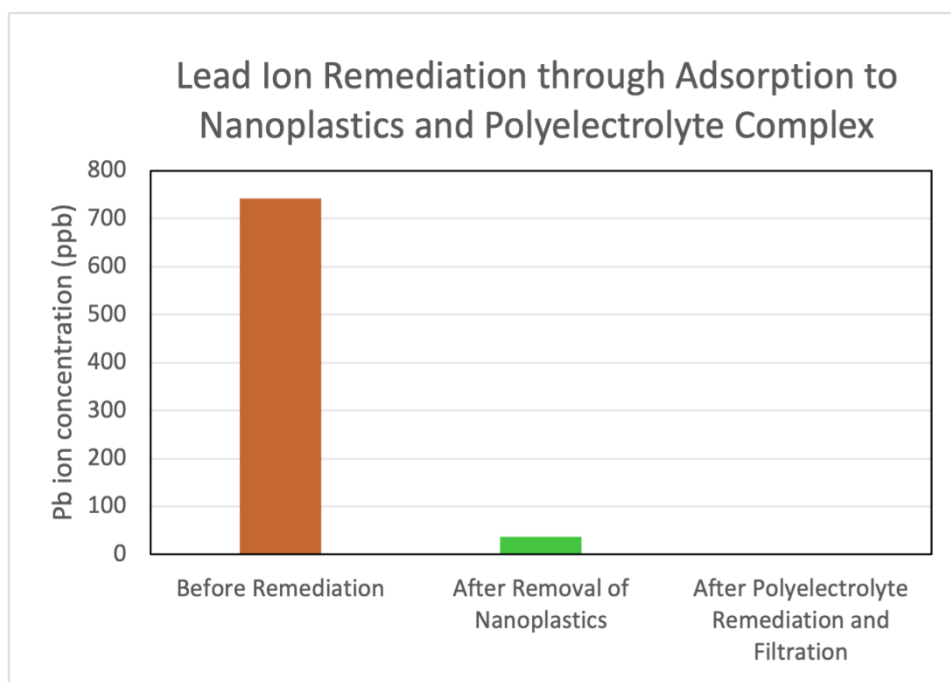


Figure 4.5 Lead ion removal results with remediation technique. The left column represents the initial lead ion concentration. The middle column represents lead ions adsorbed onto the nanoplastics and removed through fine filtration. Some lead ions remain in solution. The right column demonstrates that the polyelectrolyte complex remediation technique with coarse filtration quantitatively removes both nanoplastics with lead ions adsorbed and residual lead ion in solution.

The abundance of electrostatic interactions in the polyelectrolyte complexes likely promote heavy ion adsorption, which has been demonstrated in other cases.^{88,92} While further understanding of the nanoscale interactions of these materials is needed to improve these functionalities, it is clear there is great potential in using this class of materials to address relevant issues in water remediation.

Methodology

Materials

The monomers polyethylene glycol methyl ether methacrylate ($M_n = 500$ g/mol, PEGMEMA), ethyl hexyl methacrylate (EHMA), 3-sulfopropyl methacrylate potassium salt (SPMA), 2-hydroxyethyl methacrylate (HEMA), and 2-trimethylammonioethyl methacrylate (TMAEMA) were purchased from Sigma-Aldrich and deinhibited using monomethyl ether hydroquinone inhibitor remover (Sigma-Aldrich). The chain transfer agent dodecanethiol, ^1H NMR solvent deuterium oxide, thermal initiator benzoyl peroxide (BPO), antioxidant hydroquinone, PET solvent 1,1,1,3,3,3-hexafluoro-2-propanol, and Nile red dye were also purchased from Sigma-Aldrich. PET samples were purchased from Sigma-Aldrich and manufactured by Goodfellow. Ethanol, hexane, HPLC-grade water, and distilled water were purchased from Fisher.

Polymer synthesis

Anionic random copolymers were synthesized by free radical polymerization at $65\text{ }^\circ\text{C}$ using BPO as initiator. Monomer mixtures with different compositions were used to generate copolymers with various hydrophilic/hydrophobic and charge ratios. See Table S1 for detailed mole fractions of monomers in the feed. In a typical synthesis of an anionic random copolymer

with a final composition of 67 mol % PEGMEMA, 25 mol% EHMA, and 8 mol% SPMA, 30 mg BPO (0.12 mmol) was dissolved with 12 mL ethanol in a 20 mL test tube. Then, 1.5 mL EHMA (6.7 mmol), 8.0 mL PEGMEMA (17 mmol), and 650 mg SPMA (2.6 mmol) dissolved in 1 mL deionized water were added into the test tube. Dodecanethiol (30 μ L, 0.125 mmol) was added to prevent side reactions associated with cross-linking of polyethylene glycol side chains.¹¹⁷ The test tube containing the reaction mixture was transferred to a water bath that was pre-heated to 65 °C for 150 min. After polymerization, the polymer was precipitated in hexane and dissolved in ethanol, and this step was repeated two additional times. Deionized water was added, and the ethanol and residual hexane were removed by rotatory evaporator. The resulting aqueous polymer solution was then dialyzed against 2 L deionized water for 2 days. Dialysis water was changed every day. The composition of the aqueous polymer solution retrieved from dialysis was determined with ¹H NMR spectroscopy. The polymer was further diluted with deionized water to 10 mg/mL for complexation experiments.

In a typical synthesis of cationic random copolymer with a final composition of 28 mol% TMAEMA/72 mol% HEMA, 50 mg benzoyl peroxide (0.21 mmol) was added to a 20 mL test tube and dissolved in 4 mL of methanol and 2 mL of water. Then, 5 mL HEMA (41 mmol) and 5 mL TMAEMA (20 mmol, 75 wt% aqueous solution) were added to the test tube. The test tube containing the reaction mixture was transferred to a water bath that was pre-heated to 65 °C for 150 min. After polymerization, the polymer was precipitated in ethanol once. The polymer was then dissolved in a small amount of deionized water and dialyzed against 2 L deionized water for 2 days. Dialysis water was replaced every day. The composition of the aqueous polymer solution retrieved from dialysis was determined with ¹H NMR spectroscopy.

The polymer was further diluted with deionized water to 5 mg/mL for complexation experiments.

Polymer NMR characterization

Copolymer compositions were characterized using ^1H NMR spectroscopy (Bruker X500 NMR spectrometer), using deuterium oxide as the solvent. Aqueous polymer samples were dried in a vacuum oven before redissolving in deuterated solvent to a concentration of 15 mg/mL. 1 mg of hydroquinone was added before drying to suppress potential cross-linking reactions from occurring. ^1H NMR peak assignments were done broadly by distinguishing low chemical shift hydrogens next to non-polar carbons, labeled (a), and high chemical shift hydrogens next to polar functional groups and carbons next to polar functional groups, labeled (b). A third label (c) was assigned to distinct hydrogens on the SPMA group to solve for the molar ratios of the anionic copolymer. Diagrams of the assignments are shown in Figure 4.6 for the anionic copolymer and Figure 4.7 for the cationic copolymer.

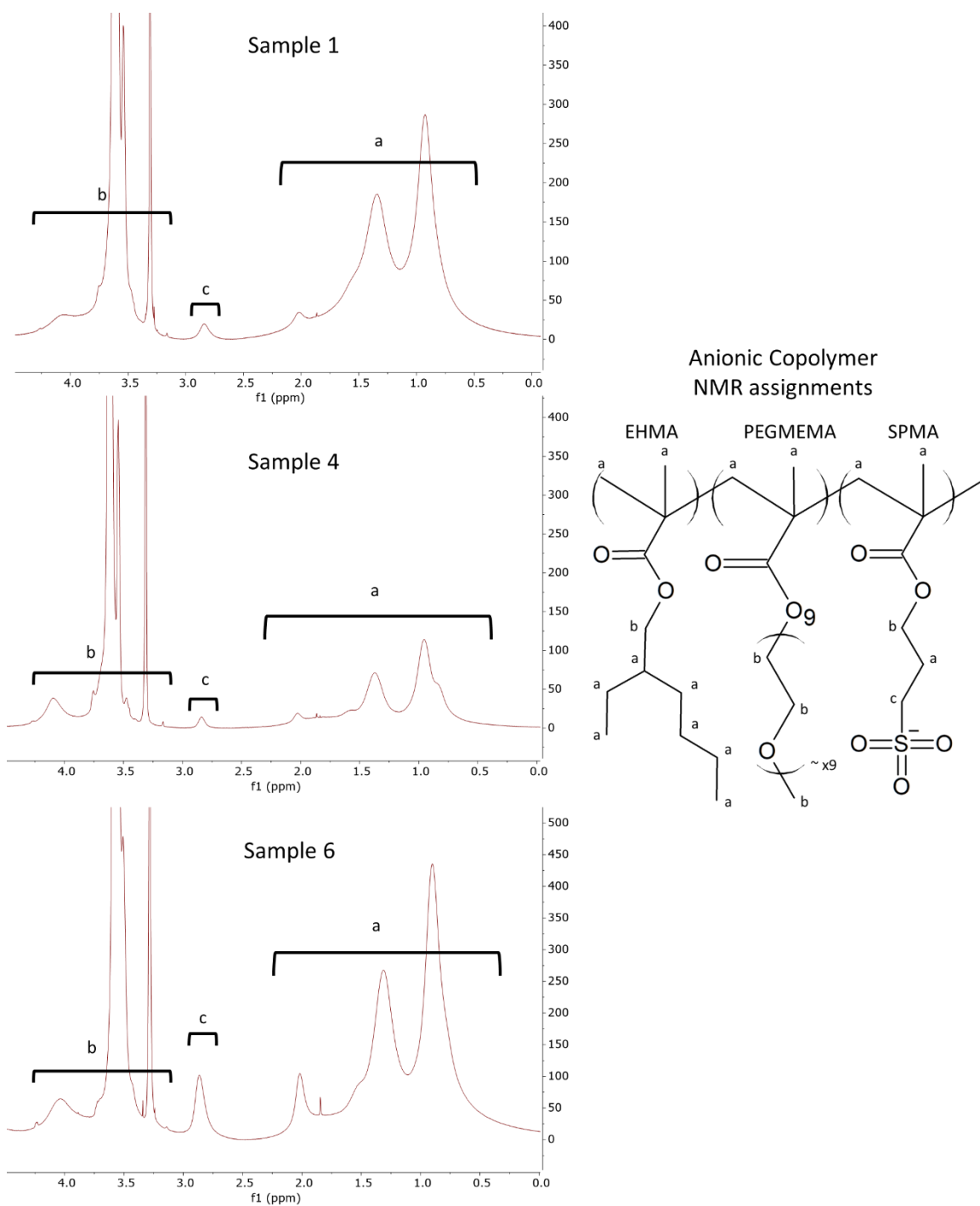
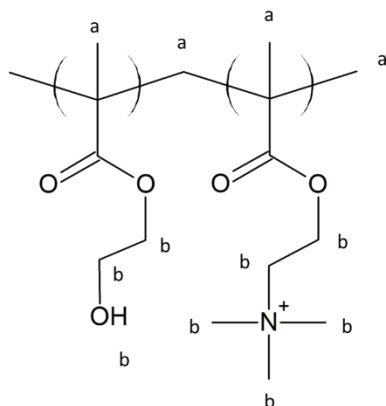


Figure 4.6 Anionic copolymer NMR spectrum and peak assignments. NMR spectra for samples 1, 4, and 6 are shown of the left. The assignments of low chemical shift hydrogens (a), high chemical shift hydrogens (b), and and SPMA specific-assignment (c) are shown on the right.

Unbranched cationic copolymer
NMR assignments



Fully branched cationic copolymer
NMR assignments

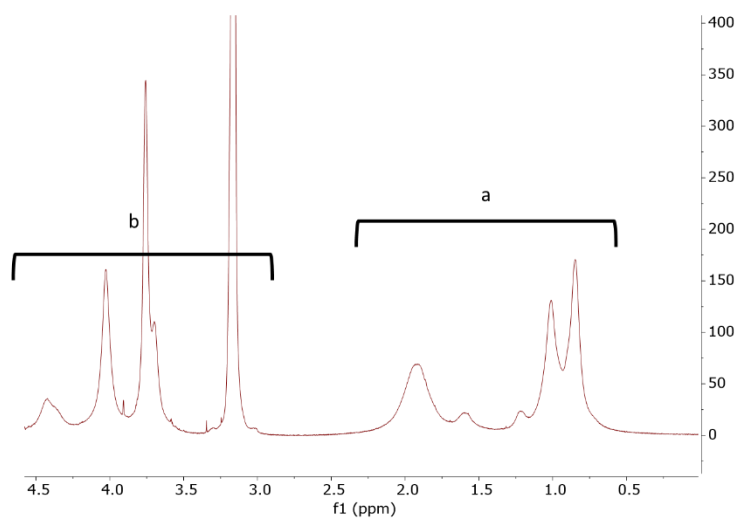
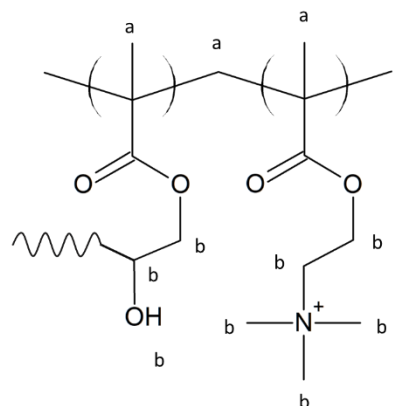


Figure 4.7 Cationic copolymer NMR spectrum and peak assignments. The assignments of low chemical shift hydrogens (a) and high chemical shift hydrogens (b) are shown for a linear polymer and a fully branched polymer.(top) The NMR spectrum of the cationic is also shown. (bottom)

Some interpretation is needed for the analysis of the cationic copolymer. It has been shown that polar monomers such as TMAEMA may be susceptible to branching reactions.¹⁰⁴ Our cationic copolymer is likely branched, which affects the NMR assignments and calculations. Assuming no branching, a polymer composition of 76% HEMA and 24% TMAEMA is obtained, while an assumption of 100% branching leads to a composition of 68% HEMA and 32 % TMAEMA. We report the average of these two extreme cases to obtain an intermediate composition value which corresponds to a branching fraction of approximately 50%.

Polymer molecular weight characterization

Molecular weight was characterized by aqueous gel permeation chromatography on an Agilent 1260 series high performance liquid chromatography (HPLC) instrument using a Superdex 75 increase 10/300 GL column. Detection was performed with a multi-angle static light scattering detector (Wyatt DAWN HELEOS II). 50 mM sodium phosphate buffer at pH 7.4 was used as the mobile phase. 0.3 mL of polymer solution at 0.8 mg/mL was injected at a flow rate of 0.4 mL/min, except for sample 6, where 0.5 mL of polymer solution was injected. The molecular weights and dispersity are shown in Table 4.2. The cationic polymer could not be characterized under these conditions, and no elution peak was observed. However, the cationic polymer was previously successfully characterized under different solvent conditions in the previous thesis chapter, with a number average molecular weight of 4.3 million g/mol and a weight average molecular weight of 10 million g/mol.

Table 4.2 Anionic copolymer Molecular Weights

Samples	M_n (g/mol)	M_w (g/mol)	PDI
Sample 1	268 000	304 000	1.13
Sample 2	183 000	270 000	1.48
Sample 3	248 000	466 000	1.88
Sample 4	304 000	537 000	1.77
Sample 5	274 000	376 000	1.38
Sample 6	201 000	270 000	1.34

An approximate refractive index increment (dn/dc) value was measured using an Atago pocket refractometer with a serial dilution series for each polymer sample in 50 mM 7.4 pH sodium phosphate buffer. Calculated dn/dc values are shown in Table 4.3. A sample serial dilution plot is shown in Figure 4.8.

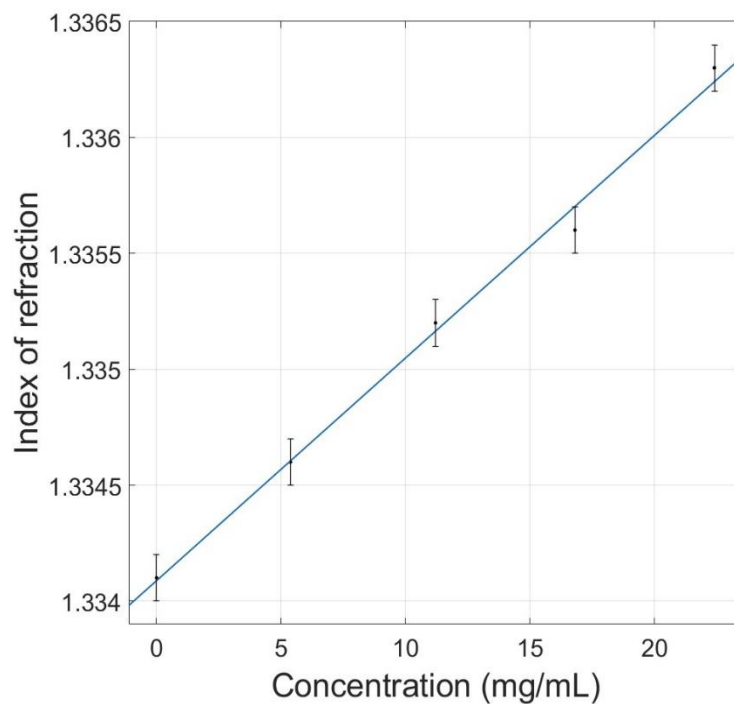


Figure 4.8 Serial dilution plot for Sample 3. The index of refraction is plotted as a function of polymer concentration, leading to a fit for the dn/dc value of 0.096.

Table 4.3 Anionic Copolymer dn/dc values

Samples	dn/dc (mL/g)
Sample 1	0.103
Sample 2	0.106
Sample 3	0.096
Sample 4	0.101
Sample 5	0.137
Sample 6	0.143

Nanoplastic Synthesis and Characterization

10 mg of PET cut from an amorphous film was dissolved in 2 mL of hexafluoroisopropanol with 1 mg of Nile Red. The solution was slowly precipitated in 40 mL of deionized water with constant vigorous stirring, and was dispensed through a syringe fitted with a Luerlocked PTFE tube with an 18 gauge inner diameter. The PET nanoplastic solution was then dialyzed against deionized water for 2 days to remove excess solvent and dye, changing the dialysis solution each day. After dialysis, the solution was filtered through a 0.45 μm nylon syringe filter, and a concentration of 0.23 mg/mL was measured by drying 10 mL of solution and measuring the dried mass. The size of the PET nanoplastics was characterized using dynamic light scattering on a PUNK DLS system, yielding a number average size of 75 nm with a dispersity of 1.3. (Figure 4.9) The stock solutions used in experiments were made by diluting the original solution by 100x in deionized water, with an approximate concentration of 2.3 $\mu\text{g/mL}$.

SEM image preparation

Scanning electron microscopy (SEM) images of nanoplastic samples were captured using JEOL JSM-7900FLV operating at 15 kV. Aqueous samples were drop-cast onto the surface of plasma-cleaned silicon wafers and coated with Os (8 nm) to avoid charging effects.

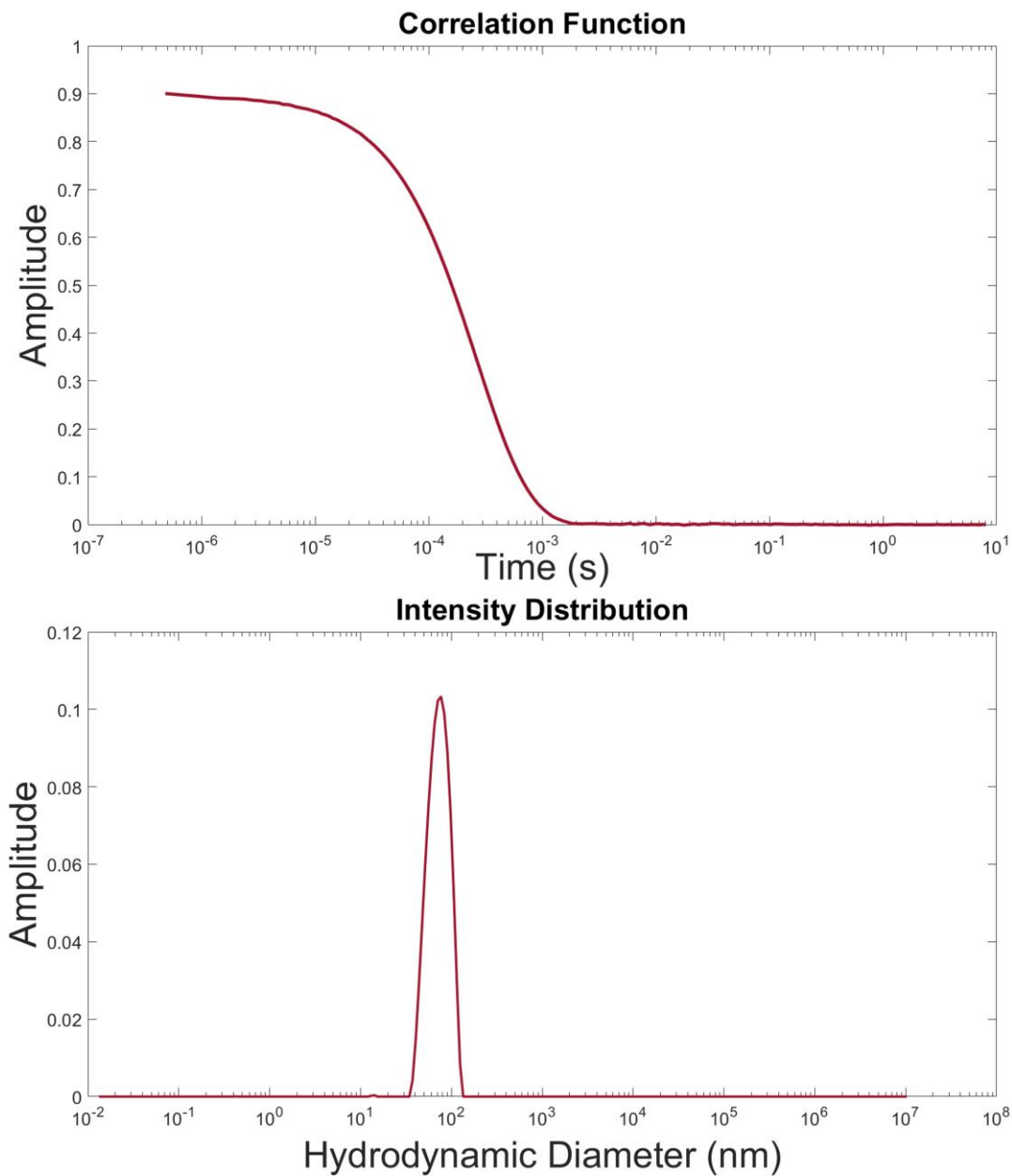


Figure 4.9 Correlation function (above) and Intensity distribution (below) from DLS measurements of PET nanoplastics.

Remediation procedure

5 mL PET stock solution and 2 mL anionic polymer (10 mg/mL) were added into a 20 mL glass vial and stirred vigorously at 500 rpm with a stir bar. Solid polyelectrolyte complexes were formed by adding small aliquots (25 μ L increments) of cationic polymer (5 mg/mL) into the vial until the mixture of copolymer solutions flocculates, forming macroscopic aggregates and becoming clear. (See Table 4.4 for the amount of each anionic polymer required for complex formation.) Before this point, the addition of cationic copolymer makes the solution progressively turbid and cloudy, indicating the formation of colloidal structures with sizes comparable to the wavelength of light. After flocculation, 20 μ L of a 50 mg/mL magnesium sulfate solution was added into the vial to help aggregate any remaining flocs and colloidal particles. The final aggregate sizes are usually on the order of millimeters and are robust to mechanical perturbation. The polyelectrolyte complex was removed by filtration through a 1 μ m glass fiber membrane filter, leaving a clear filtrate.

Table 4.4 Cationic polymer solution added for flocculation

Samples	Cationic Polymer Added (mL)
Sample 1	0.875
Sample 2	0.650
Sample 3	0.575
Sample 4	0.475
Sample 5	1.450
Sample 6	2.225

Fluorescence measurements of nanoplastic concentration

Stimulated fluorescence of the Nile Red-dyed nanoplastic solutions was measured using a BioTek Synergy Neo2 multimode microplate reader with a xenon flash light source. The optimal excitation and emission bands for these samples were determined to be 585/10 nm and 638/20 nm respectively. These parameters were used for all plate reader measurements. Corning® 96 well black polystyrene microplates with clear flat bottoms were used to minimize well-to-well crosstalk. A working volume of 200 μL was used in each well. The background fluorescence was measured for wells filled with deionized water and subtracted from sample measurements. To measure the nanoplastic remediation percentage of each polymer complex sample, calibration curves were created relating fluorescence intensity to plastic concentration. Serial dilutions of the stock solutions of nanoplastics were made to obtain solutions of known nanoplastic concentration. Two equivalent stock solutions were used—one for trials 1-4 and one for trials 5 and 6—thus two calibration curves were made to account for any differences in fluorescence yield (Figure 4.10). Controls were run to account for any impact on fluorescence from the polymer complexes or the syringe filtration.

It was determined that the polymer complexes had no fluorescence intensity contribution. The syringe filtration step with 1 μm glass fiber syringe filters resulted in a 63% decrease in fluorescence, which was taken into account in the determination of the actual nanoplastic concentration of the samples reported in the main text.

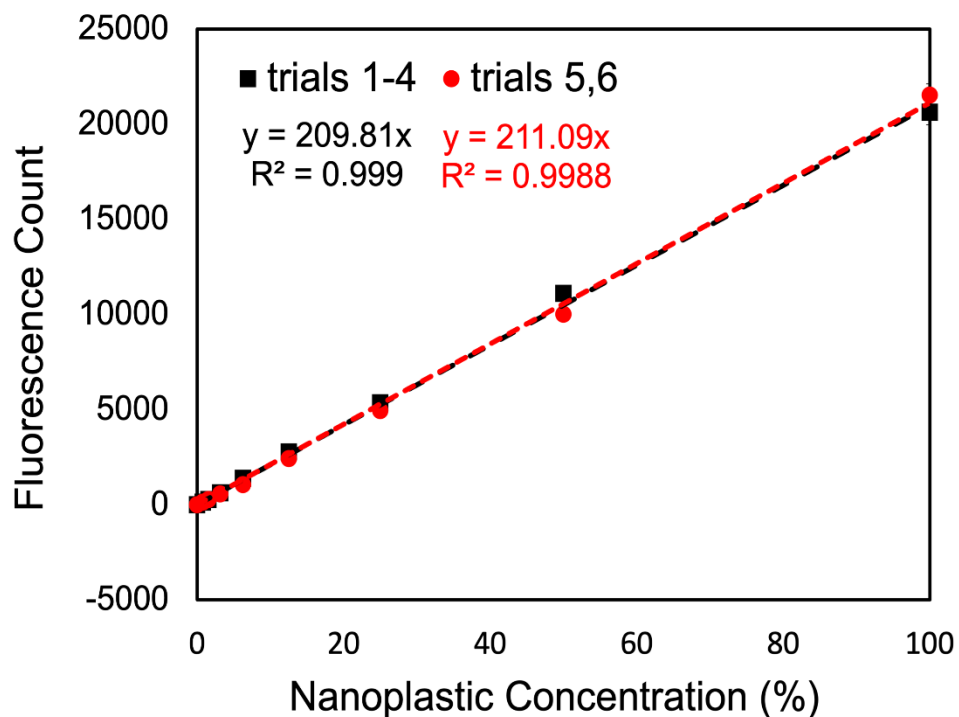


Figure 4.10 Calibration curves for PET nanoplastic solutions as a function of percentage of stock solution. Two stock solutions were made for different sets of experiments.

Lead ion adsorption and removal

Simultaneous dilutions of nanoplastics and lead ion in deionized water were prepared from a stock solution of 1000 ppm lead ion in water, which was in turn prepared from the dissolution of lead (II) nitrate powder. Samples were created at lead ion concentrations between 10 ppb and 1 ppm, and these were sampled before and after remediation by polyelectrolyte complex, as well as by direct filtration of the nanoplastics, using 0.02 μm Anotop 25mm inorganic membrane filters produced by Whatman International Ltd. Comparing the lead ion concentration with and without removal of the nanoplastics through fine filtration, it was found that high percentages of the lead ions adsorbed to the surface of the nanoplastics. The

polyelectrolyte complex remediation experiments demonstrated a quantitative removal of lead ions from solution to the detection limit of our instrument, which implies that both nanoplastics with lead adsorbed and residual lead ions were effectively removed. Lead ion concentrations were determined using inductively plasma mass spectrometry (ICP-MS), performed on a Thermo iCapQ instrument. Samples were acidified by adding 3% by volume concentrated nitric acid, necessary to digest any remaining plastic particulates and to generate standard results with ICP-MS. Calibration solutions of lead ion solutions were created and used to generate a calibration curve containing the range of all samples tested.

Quartz Crystal Microbalance (QCM) tests

QCM tests were carried out on a customized setup. Au covered (Au/Ti) quartz crystal resonators (Renlux, Shenzhen, China) with a fundamental resonance frequency of 5 MHz were used. The crystal was mounted in a cell (AWSensors, Paterna, Spain) which was connected with a N2PK impedance analyzer (Makarov Instruments, Thornhill, ON, Canada). A lab developed open source program, rheoQCM,¹⁵⁶ written in Python was used for both the data collection and analysis. The electrical conductance and susceptance of the quartz crystal near each odd harmonics (n) up to the 9th were collected and Lorentz curves were fitted to each resonant peak from which the resonant frequencies (f_n) and dissipation ($D_n = 2\Gamma/f_n$, Γ is the half width at half max of the peak) were recorded. For the polymer adsorption tests, 3 mL distilled water was added on top of the QCM crystal coated with 200 nm thick amorphous PET film at $30.0 \pm 0.1^\circ\text{C}$, and stabilized until the frequency and dissipation become constant. Then, 12 μL of 10 mg/mL polymer solution was introduced into the water to a final concentration of 40 $\mu\text{g/mL}$ and the shifts of frequencies (Δf_n) and dissipation (ΔD_n) were recorded. The real mass

of from the adsorption was calculated from the Sauerbrey equation. Reported values in the manuscript are calculated from the 5th harmonic results. The QCM data is shown below in Figure 4.11.

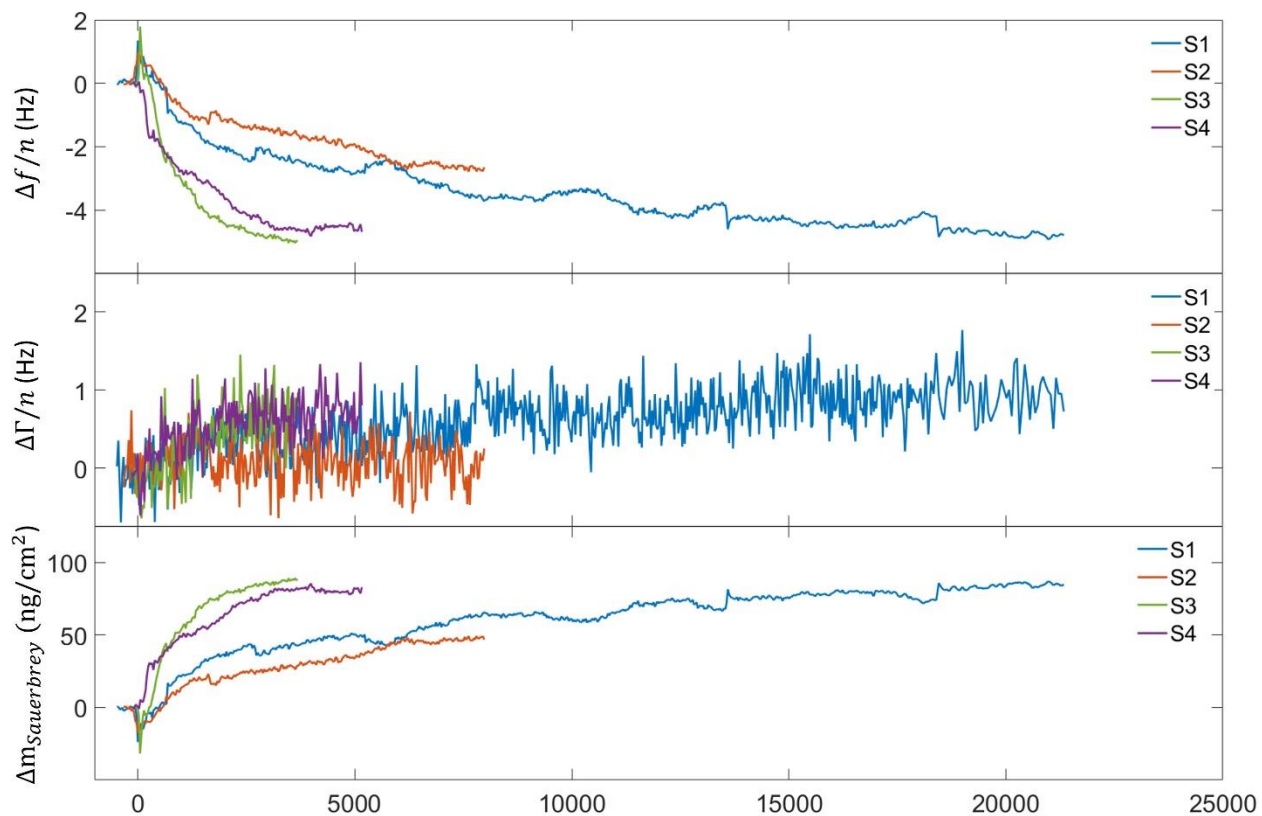


Figure 4.11 QCM data for polymer adsorption experiments of samples 1-4. The top plot shows measured the frequency change. The middle plot shows the measured change in dissipation. The bottom plot shows the calculated Sauerbrey mass of adsorbed polymer.

Martini Simulations of Random Copolymer Adsorption

Forcefield

We use the Martini 2.2 forcefield with polarizable water. The potentials for the methacrylate-based random copolymers come from a few sources and are fully described in the previous

thesis chapter. For the polyethylene surface, we convert from the atomic crystal structure using 3 STY beads for the benzene ring and 2 more "Na" beads for the ester groups. The "Na" beads are also used in the random copolymer backbone for an equivalently bonded group of 4 atoms. During the simulations the PET surface is held using positional restraints. In the production simulations, we use the following parameters. The short-range Coulomb interactions were calculated up to 1.35 nm with the 3d Ewald summation approach (relative permittivity of 2.5 for Martini with polarizable water) for the long-range electrostatic interactions in order to mimic 2D periodic boundary conditions in the x and y direction. The box length was 20 nm x 20 nm x 20 nm with an extra 60 nm of vacuum in the z direction to avoid errors in the ewald sum coming from the periodic boundary. The LJ 12-6 potential interactions were truncated at 1.35 nm. The NVT ensemble was applied. The temperature was coupled at 300 K using the velocity rescaling method. The leapfrog integration time step of 10 fs was employed.

Protocol

For each hydrophobic fraction the polymer sequence is randomly generated under the constraint of the mean composition. The degree of polymerization is 200 monomers in order to sample a large number of different sequences within the chain. The mean composition features 3 different types of monomers. The charged monomer, SPMA, is always present at 10% while the hydrophilic monomer, OEGMA-9, varies based on the given hydrophobic fraction, F_H which determines the amount of the hydrophobic monomer, EHMA. We build the random copolymer with only the 20 positive counterions necessary to ensure electroneutrality. For each composition we run steered and non-steered binding simulations. To avoid the stochasticity of initial binding between the random copolymer and the surface, we start with

a steered MD run to initiate contact and then allow the polymer to react in a longer, completely unsteered simulation. In the steered MD simulations the first bead on the backbone of the polymer is pulled towards the PET monolayer at a rate on 1.0 nm/ns until it is 0.5 nm away from the monolayer surface using a harmonic spring with force constant 1000 kJ/mol. This bead is then held at this distance from the surface for 40 ns using the same spring with a pull rate of 0. For the final 180 ns of the simulation the polymer is completely unrestrained. This entire binding process is repeated 3 times for each composition.

Analysis

Hydrophobic PET-polymer contacts are defined as two hydrophobic beads, one in the polymer and one in the PET surface, within a cutoff of 0.53 nm from one another. This is approximately the lowest energy distance for the largest Martini beads. All bead types in the PET surface (STY and Na) as well as SC1 and C1 are considered hydrophobic according to the Martini forcefield. Error bars on the total number of hydrophobic contacts are the standard error of 3 replicas which are run for each composition.

Simulations of Polyelectrolyte Complexes

Forcefield

Coarse grained molecular dynamics simulations of the polyelectrolyte complexes were performed using HOOMD. We use an implicit solvent model for the polymer chains as described in our previous work. This model differentiates between hydrophobic, hydrophilic, and charged beads allowing use to include the basic chemical properties of the different monomers used in the experiments including the hydrophobic methyl methacrylate backbone

of all monomers. Charged interactions are calculated using a bulk dielectric constant of 80, which corresponds to a Bjerrum length, l_B of 0.7 nm. The calculation is performed using the PPPM method. We use the NVT ensemble and the Langevin thermostat.

Protocol

We initialize the box by randomly placing 60 total polymer chains, 9 cationic and 51 anionic. We attempt to replicate the experimental parameters as all cationic polymers have a degree of polymerization of 200 monomers, and the mean charge fraction of those monomers is 30%, while anionic polymers have a degree of polymerization of 100 and the mean charge fraction is 10%. Counterions are included for all charged monomers, but no additional salt is added. All sequences are randomly generated assuming that all reactivity ratios are 1⁵² and under the constraint that the mean compositions of the anionic and cationic copolymers must be met exactly. Simulations are run with the timestep, $dt=0.001 \tau$ in LJ units which corresponds to $dt \approx 80$ fs in real units using the formula $\tau = \sqrt{\frac{md^2}{\epsilon}}$, where ϵ is the energy unit, 1 KT at 300K, d is the distance unit, 0.5nm and m is the mass unit 100 g/mol. We initially generate the polymers in an 40 nm x 40 nm x 40 nm box. The polymers are then annealed by raising the temperature from $T=1$ to $T=2$ in LJ units over the course of 2 million timesteps, holding there for 2 million timesteps and then going back down to $T=1$ over 2 million timesteps. The box is then compressed to its final dimensions, 27.5 nm x 27.5 nm x 27.5 nm before repeating the annealing cycle. The final simulation is then run for 50 million timesteps which corresponds to ≈ 4 microseconds. This entire process is done 4 times for each composition and data is averaged over many frames per simulation and the 4 independent simulations.

Analysis

The scattering function $S(q)$ is computed according to

$$S(q) = \frac{1}{N_{pairs}} \sum_{pairs} \frac{\sin(qr)}{qr}$$

For computational efficiency we use an equivalent form where we create a histogram for the probability of a certain pair distance, r :

$$p(r_i) = \frac{N(r_i)}{N_{bins}}$$

$$S(q) = \sum_{bins,i} p(r_i) \frac{\sin(qr_i)}{qr_i}$$

This is much faster as it is over the number of bins which is far less than the number of pairs for the large amount of data we use.

$$S(q) = \sum_{bins,i} p(r_i) \frac{\sin(qr_i)}{qr_i} = \frac{1}{N_{bins}} \sum_{bins,i} N(r_i) \frac{\sin(qr_i)}{qr_i} = \frac{1}{N_{bins}} \sum_{pairs} \frac{\sin(qr)}{qr}$$

There is a different normalization factor but the relative peak heights are the same.

We use only the polymer beads ignoring the counterions. We use only the backbone bead of each monomer in computing the location of different monomers when we split the box into smaller boxes and calculate the hydrophobic fraction in each box. Each monomer is classified as hydrophobic if it is EHMA on the anionic copolymer or TMAEMA on the cationic copolymer.

Chapter 5: Random Copolymer Complexes with PETase for Enhanced Enzymatic Degradation of PET

Engineered and native enzymes are poised to solve challenges in medicine, bioremediation, and biotechnology. One important goal is the possibility of upcycling polymers using enzymes. However, enzymes are often inactive in industrial, nonbiological conditions. It is particularly difficult to protect water soluble enzymes at elevated temperatures by methods that preserve their functionality. Through atomistic and coarse-grained molecular dynamics simulations that capture protein conformational change, we show that an enzyme, PETase, can be stabilized at elevated temperatures by complexation with random copolymers into nanoscale aggregates that do not precipitate into macroscopic phases. We demonstrated the efficiency of the method by simulating complexes of random copolymers and the enzyme PETase, which depolymerizes polyethyleneterephthalate (PET), a highly used polymer. We explore the experimental implications of this active site stabilization method and show that PETase-random copolymer complexes have enhanced activity on both small molecule substrates and solid PET films. These results provide guidelines for engineering enzyme-polymer complexes with enhanced enzyme functionality in non-biological environments.

It should be noted that colleague Curt Waltmann performed the simulations of PETase-copolymer complexes, and colleague Carolyn Mills synthesized the PETase enzyme and performed PETase activity experiments on small molecule substrates.

Introduction

Enzymes have the potential to tremendously impact the fields of pharmacology,^{161,162} biotechnology,¹⁶³ and bioremediation.¹⁵⁵ They are especially useful for upcycling plastics,¹⁶⁴ which are currently polluting oceans and freshwater supplies harming both humans and animals.^{165–167} Enzymes such as lipases, cutinases, hydrolases, and cytochrome P450 can catalyze a growing number of reactions due to advances in enzyme engineering.¹⁶⁸ In addition to engineering new catalytic functions, attempts have been made to increase enzyme efficiency by creating multi-enzyme complexes, immobilizing them on two-dimensional surfaces,¹⁶⁹ embedding them in plastics,¹⁵⁵ and modifying the amino acid composition of enzymes to increase their thermal stability.¹⁷⁰ Stabilizing these enzymes is crucial for applications in non-biological conditions such as elevated temperatures and pressures. Here, we investigate how complexation with random copolymers can enhance the high temperature stability of the enzyme PETase, which degrades polyethyleneterephthalate (PET).¹⁷¹ PET is a glassy polymer at room temperature. Therefore, for PETase to function effectively, the temperature should be raised above T_g (70°C), which would normally denature the enzyme.

Preliminary experiments demonstrate that complexes of PETase and our random copolymers suppress aggregation at elevated temperatures and must have some effect on protein behavior. Our simulations demonstrate the relationship between polymer composition and protein-polymer structure as well as the spatial correlations between chemically different monomers and the heterogeneous protein surface. We then show how the structure of the protein-polymer complex can impact the catalytic function of the enzyme, especially at elevated temperatures. Finally, we

provide experimental verification of this enhanced catalytic activity of PETase in the presence of random copolymers.

Charged polymers have been used to encapsulate and stabilize proteins through either macroscopic segregation or microphase separation into nanoscale aggregates that do not precipitate into macroscopic phases.^{151–153} This approach works on a wide variety of proteins including engineered proteins with non-biological functions, because protein-polymer interactions can be altered in many ways to enhance complexation including by modifying the charge of the proteins themselves.^{52,172,173} Phase separation through engineering protein charge distribution has also been demonstrated *in vivo* in cellular bodies known as membraneless organelles (MLOs).⁶² MLOs are composed of proteins, nucleic acids, and small molecule metabolites³⁹ and are often formed from intrinsically disordered proteins (IDPs) or proteins with intrinsically disordered regions (IDRs). IDPs control the MLO composition based on specific interactions that originate from the IDP sequence and this spatial organization helps to regulate the internal biochemistry of cells. Inspired by IDPs, we design a microphase separated protein-polymer complex using random copolymers. These random copolymers contain monomers with a common backbone but different side chains that can be polar, nonpolar, or charged. The monomers, shown in Figure 5.1(d) and (e) are oligo-ethyl glycol methacrylate with a length of nine ethyl glycol units (OEGMA-9), ethyl hexyl methacrylate (EHMA), and sulfo-propyl methacrylate (SPMA). Due to their methyl methacrylate backbone, they are inexpensive to randomly polymerize in large-scale, industrial processes. They have also been used in previous computational and experimental studies of polymer complexes with proteins including horseradish peroxidase, glucose oxidase, and organophosphorus hydrolase as well as small organic molecules. Further, amphiphilic random copolymers are well-suited to

complex with the heterogeneous polar and nonpolar surfaces of proteins. Thus, in addition to the electrostatic attraction between the polymer and protein, the polar and nonpolar groups of the random copolymers can self-optimize, maximizing their interactions with protein surface domains making this complexation quite general.

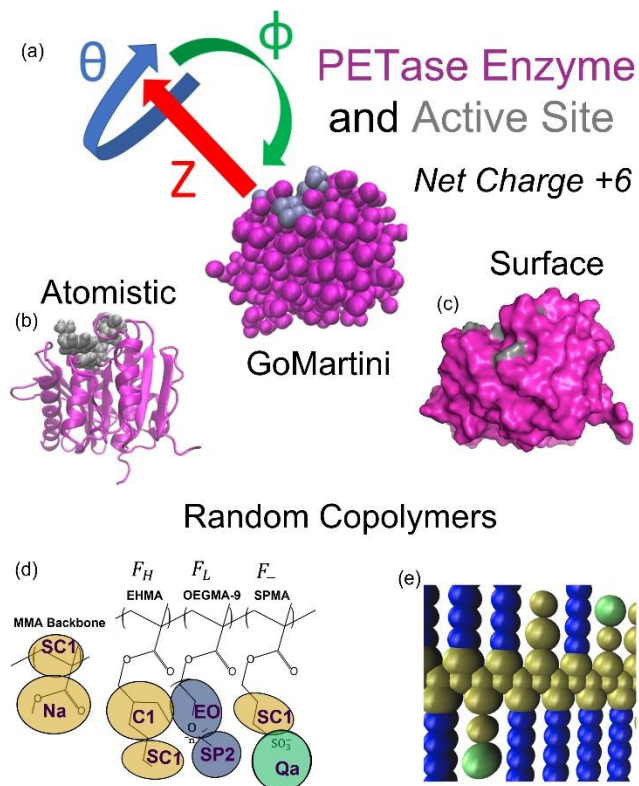


Figure 5.1 Description and models of PETase and the random copolymers. (a) GoMartini model of PETase in magenta with the active site in gray. (b) The secondary structure of PETase is shown with the same color scheme as in (a). The active site is shown using the van der Waals representation to highlight the cleft-like binding pocket for PET. (c) Surface representation of PETase. (d) Chemical and Martini description of the methacrylate-based random copolymers. Hydrophobic beads are tan, while hydrophilic beads are blue, and negatively charged beads are cyan. F_H , F_L , and F_- refer to the percentage of the respective monomer in the random copolymers. (e) Snapshot of the Martini random copolymer model with the colors corresponding to (d).

In the present study, we explore how complexation with random copolymers can affect the conformation, and thus the function, of PETase especially at temperatures the enzyme does not

experience *in vivo*. We achieve this by varying the mean polymer composition, which controls the polymer-protein surface interactions. This, in turn, affects complex formation and the spatial distribution of contacts on the surface of the enzyme. While there have been previous studies of protein-polymer complexation, experimental studies are inherently limited in the direct observation of surface correlations. Previous computational studies have used coarse models that did not include charges or vary the mean composition.^{51,52} Other models were used to study PETase and cytochrome P450 in the context of macroscopic complexes instead of nanoscale complexes and they were also unable to study the effect of the polymers on the conformation of the enzyme active site, which we show is affected by the spatial distribution of protein-polymer contacts both at room and elevated temperatures. Specifically, we demonstrate that when these PETase-random copolymer complexes have an abundance of polymer-active site contacts, they can have less perturbed active sites than the protein by itself and remain stable as the temperature is increased.

Results and Discussion

PETase Structure at Elevated Temperature

PETase denatures as temperature is increased, leading to detectable decreases in activity above room temperature. In Figure 2a, all-atom molecular dynamics simulations demonstrate the deformation of the active site at elevated temperatures. We use protein RMSD to measure the conformation of the protein relative to the energy minimized crystal structure, not including rotational or translational diffusion. We measure the conformation of the whole protein as well as the active site using a previously published definition of the seven active site residues.¹⁷¹ This

provides metrics for the behavior of the whole protein and the active site, whose conformation relative to the crystal structure correlates with enzymatic activity.¹⁷⁴

As shown in Figure 5.2(a), there is an upward trend for both the whole protein and active site RMSD values as the temperature increases and PETase activity decreases. The active site RMSD at 330K is an outlier - despite decreasing from 320K, it is still higher than 298 or 310K. In agreement with studies highlighting the flexibility of the active site, we see that the active site is more perturbed by increases in temperature (especially at the highest temperatures) when compared to the whole protein. In the following sections where random copolymers complex with PETase, we use the GoMartini model of PETase, which agrees reasonably well with the temperature-dependent conformation of atomistic PETase (Figure 5.2(a)).

As shown in Figure 5.2(b), the GoMartini PETase also shows an upward trend for both RMSD values with temperature as well as larger increases for the active site than the whole protein. Although the RMSD values are different between the atomistic and GoMartini models, they are also measured on different time scales, 10 ns for the atomistic results and 300 ns for the GoMartini results (see SI Appendix, Materials and Methods for more details), with longer times potentially leading to further perturbation of the protein structure. The ability to access these longer time scales is a great advantage of the GoMartini model.

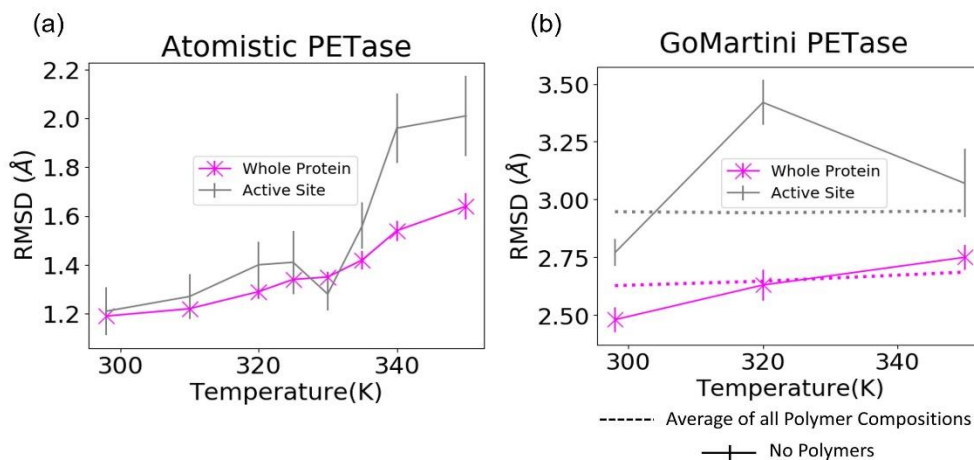


Figure 5.2 Comparison of the GoMartini PETase (b) alone to atomistic simulations (a) and to the GoMartini PETase complexed with random copolymers as the temperature is increased (b). RMSD is used to measure the conformation relative to the crystal structure with higher values signifying more deformation. (a) Results for the atomistic model show a general increase in the RMSD of the protein as well as the active site as is expected based on known decreases in activity with increasing temperature. (b) The GoMartini model shows an increase in RMSD for the whole protein and the active site at 320K, but at 350K the active site RMSD decreases, unlike the entire protein backbone. The active site RMSD may be inaccurate at high temperatures, but can still be used as a baseline to measure the thermal stability of the PETase-polymer complexes. In these complexes, temperature dependence of the whole protein and active site conformation is nearly eliminated.

In agreement with atomistic simulations, the GoMartini model does have a noticeable increase at 320K. However, at 350K, the active site RMSD decreases instead of increasing. Here, the model is failing to accurately predict the active site behavior of PETase, although the whole protein RMSD displays the correct trend. Despite this issue, the GoMartini model still provides a baseline that can be compared to the case of polymer complexation to evaluate the ability of the polymers to stabilize the active site. This issue is also mitigated by restricting our analysis of the active site to 320K in some cases such as Figure 5.6(c).

Enzyme-Polymer Complexation

Since the stabilization of enzymes through microphase complexation depends on the structure of the adsorbed random copolymers, we seek to understand how to control the adsorption through mean composition of the polymer. We measure the adsorption *via* the number of contacts between the polymer and the enzyme at three set temperatures. The results at 298K are shown in Figure 5.3. The trends observed at this temperature continue at higher temperatures.

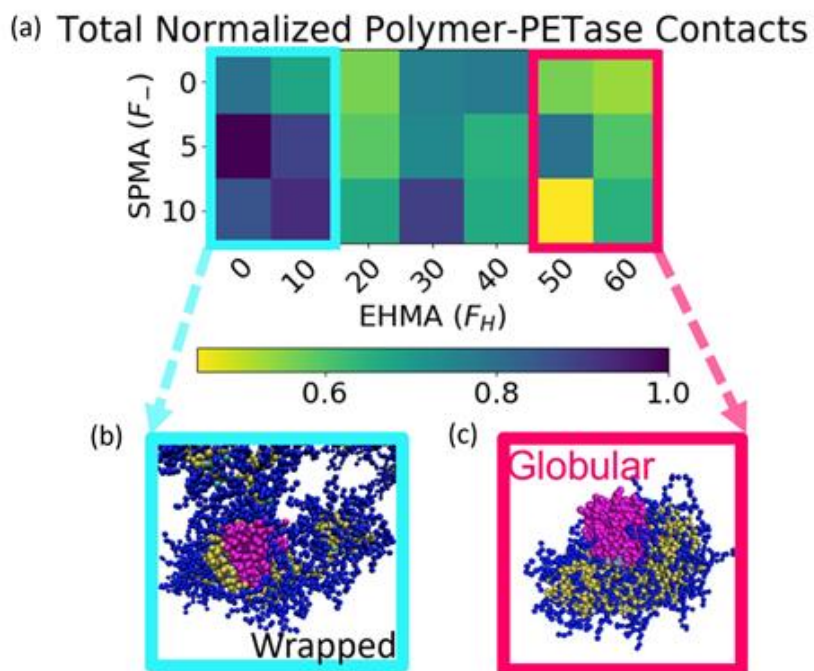


Figure 5.3 Random copolymer complexation with the PETase protein for different mean polymer compositions. F_H is the percentage of hydrophobic EHMA, F_- is the percentage of negatively charged SPMA and F_L is the percentage of hydrophilic OEGMA-9. These percentages sum to 100 and thus F_L , which is not displayed, is $100 - F_H - F_-$. (a) The number of contacts is shown as a function of composition at 298K. A maximum is observed at very low percentages of EHMA and higher percentages of SPMA, while a local minimum is observed at $F_H=20\%$. (b) Simulation snapshot of a wrapped polymer conformation, which occurs at low values of F_H and is characterized by a high percentage of contacts between the enzyme and polymer backbone. (c) Simulation snapshot of a globular polymer conformation, which occurs at high values of F_H and is characterized by micelle-like behavior of the amphiphilic polymers.

As shown in Figure 5.3(a), the mean compositions with the most contacts between polymers and protein tend to be those with a relatively high percentage of negatively charged SPMA, F_- , and a lower percentage of hydrophobic EHMA, F_H . Thus, additional hydrophobic EHMA monomers are unnecessary for the polymer to complex with the hydrophobic domains of the protein surface since the polymer backbone is already hydrophobic.

This is further illustrated in Figure 5.4(a) by the fraction of protein-polymer contacts that involve a hydrophobic polymer bead either from the backbone of the polymer or the side chains. Local maxima of the fraction of hydrophobic contacts occur at both the highest and the lowest values of F_H . These low F_H conformations wrap around the PETase surface (see Figure 5.3(b)), as opposed to higher F_H compositions that lead to globular polymer conformations (see Figure 5.3(c)). Thus, the wrapped conformation of the low F_H random copolymers allow the hydrophobic backbone to more easily access the protein surface leading to more hydrophobic and total protein-polymer contacts. The connectivity of the hydrophobic backbone and hydrophobic globular conformations seems to lead to the creation of contacts with both the polar and hydrophobic parts of the protein as shown by the weaker hydrophobic correlations between polymer and protein (Figure 5.4(b)). The polar correlations are stronger, possibly due to reduced connectivity of the polar side chains and the ability to interact with the aqueous solvent instead of the protein surface. We note this analysis is highly sensitive to how the hydrophobicity of different beads is defined (see methodology).

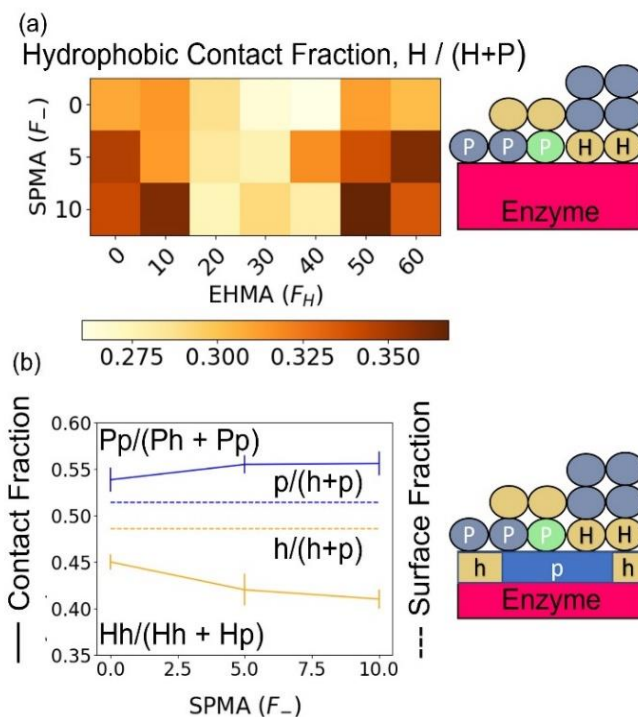


Figure 5.4 Hydrophobic interactions affect PETase-random copolymer complexation. (a) The fraction of contacts that involve hydrophobic polymer beads. There are two local maxima, one at very low F_H where the polymer backbone wraps around the protein surface and one at high F_H where the EHMA increases the baseline hydrophobic fraction of the polymer. (b) The fraction of these hydrophobic contacts that occur on the hydrophobic surface of PETase is lower than the hydrophobic surface fraction of PETase. This struggle to optimize the interaction could be related to ill-defined hydrophobic domains due to partially hydrophobic amino acids in the Martini model. However, polar-polar interactions seem to be optimized and this increases as charge is added, while the opposite occurs for hydrophobic-hydrophobic interactions.

The number of polymer-enzyme contacts grew as F_- increased, especially for wrapped conformations. This increased attraction between the enzyme and the random copolymers is intuitive since PETase has a +6 net charge. The increase in contacts occurs on the positively charged part of the surface as shown in Figure 5. Thus, the charge of the polymer influences the spatial distribution of the polymer on the dipolar PETase surface and the overall number of contacts.

Additional Contacts (ACs) of Negatively Charged Polymers Are Located on Positive Protein Domains

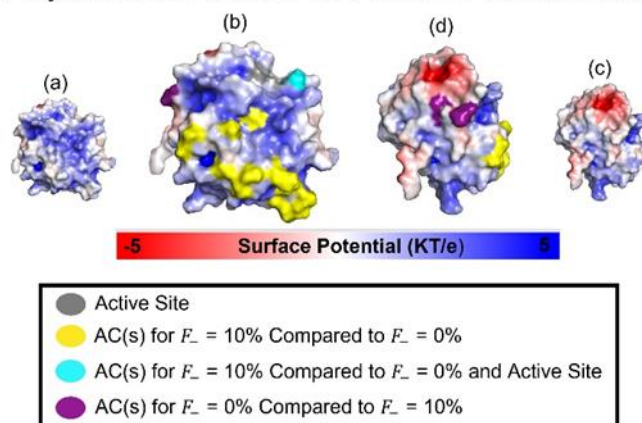


Figure 5.5 Contact of negatively charged monomers with positive surface domains. (a) and (b) show PETase with only the surface potential and with additional contacts (ACs) overlaid respectively. One can see that the yellow and cyan sites preferred when $F_- = 10\%$ are overwhelmingly on the positive part of the protein due to the addition of negative charge to the polymer. (c) and (d) show the a rotated orientation of the protein.

There is also some competition between optimizing charged and hydrophobic interactions as the addition of charge slightly weakens the hydrophobic correlations (Figure 5.4(b)). These contacts were biased to a specific protein domain despite the randomness of the polymer sequence, suggesting that using more controlled polymerization or peptide engineering is not necessary to intentionally contact these charged domains. It also suggests that the inverse can be achieved, i.e., a certain protein domain could be targeted by engineering the surface potential. Experiments have also demonstrated that protein charge domains are crucial in macrophase behavior of protein-polyelectrolyte complexes.¹⁷⁵ This is also true of polymer blockiness,⁶⁹ or the tendency of like monomers to be grouped together in the polymer sequence, in phase separation of polyelectrolyte complexes especially as ionic conditions are varied.⁷⁴

Stability of the Complexed Enzyme

In Figure 5.2(b), we measure how complexation affects the conformation of the protein at room and elevated temperatures, using the RMSD values for the protein and the active site. These RMSD values are a measure of the protein conformation relative to the PETase crystal structure with lower values representing less perturbed active sites and thus a more active enzyme.

We find that the random copolymers are very effective at preventing PETase from deforming as the temperature is increased. This is shown by the RMSD values for the active site and the whole protein averaged over all polymer compositions and comparing with the results for PETase without polymers (Figure 5.2(b)). The RMSD values as a function of temperature with polymers bound is almost flat for the whole protein and the active site; the actual values for the active site and the whole protein are only slightly greater than the protein alone at 298K. The perturbations caused by polymer binding are less than the perturbations seen at elevated temperatures as at 320K. Thus, the stability of the active site is much improved with the addition of polymers. The distribution of active site RMSD values at 320K shows that for nearly every polymer composition the active site RMSD is lower than without polymers.

The RMSD values for the active site also have a much broader range when compared to the values of the whole protein. Further, this range includes some active site RMSD values that are lower at room temperature with polymers than without. This wide range of RMSD values for the active site is not well explained by trends in mean polymer composition. To explain the wide range of active site behavior we look at the location of the contacts for those compositions where active sites are

less perturbed than the PETase alone at room temperature and compare to compositions where active sites are more perturbed than the PETase alone at room temperature (see Figure 5.6).

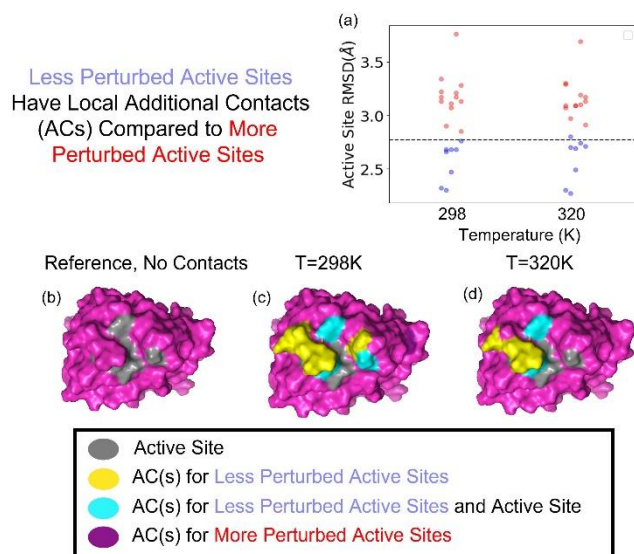


Figure 5.6 Active site stabilization by polymer contacts. (a) The distribution of active site RMSDs at 298K and 320K. The less perturbed active sites are colored in blue while the more perturbed active sites are colored in red. Each point refers to a different polymer composition and the line refers to PETase alone at 298K. These are the groups being compared in (c) and (d). (b) Surface representation of PETase with no excess contacts shown for comparison. (c) Comparison at 298K shows many additional contacts (ACs) around the active sites for less perturbed compositions. These contacts stabilize the active site instead of further perturbing it at 320K (d) as well.

We find that less perturbed compositions have significantly more contacts near or on the active site of the enzyme at both 298K (Figure 5.6(c)) and 320K (Figure 5.6(d)). This suggests that contacts on the active site stabilize instead of perturbing the active site. Thus, although we found a correlation between polymer contacts on the positive section of the enzyme and mean polymer composition in Figure 5.5, these contacts were not concentrated on the active site, which explains the absence of correlation between mean polymer composition and active site conformation. In other words, the composition of the polymers (especially charge) biases the spatial distribution of contacts, but it does not bias these contacts to the active site, where they provide stability. This

does not necessarily have to be the case for PETase or any given enzyme, since previous work has shown that complexation can be influenced by engineering the net charge on various proteins.¹⁷³ A similar strategy could be used to change the charge distribution near the active site. Thus, we suggest that engineering the spatial distribution of charges near the active site could increase the activity of an enzyme-polymer complex by biasing the charged polymers near the active site and stabilizing the active site. While active site stabilization due to local contacts may not be completely general, previous studies have illustrated that the addition of polymers to enzymes can enhance the activity at elevated temperatures in water,¹⁵³ suggesting the phenomenon extends beyond PETase. Moreover, most active sites are partially hydrophobic, suggesting that polymers with hydrophobic groups can stabilize the active site with local contacts as shown here.¹⁷⁶

PETase-copolymer complexes with suppressed aggregation

We performed dynamic light scattering experiments (DLS) on PETase and PETase-copolymer solutions to confirm stabilization effects of the complexes enzyme. PETase at 20 °C has a measured size of around 7 nm. We found that even exposing PETase to 40 °C for ten minutes was enough to observe significant aggregation. (Figure 5.7(a)) The PETase solution became cloudy and aggregates were sized in the hundreds of nanometers. However, for PETase-copolymer solutions, with a mass ratio of 1:9 PETase:copolymer, we did not observe significant aggregation after 10 minutes of heating at 40 °C and the solution remains clear. (Figure 5.7(b)) However, it is interesting to note that there are two peaks observed which correspond well to the size of PETase and the copolymer individually.

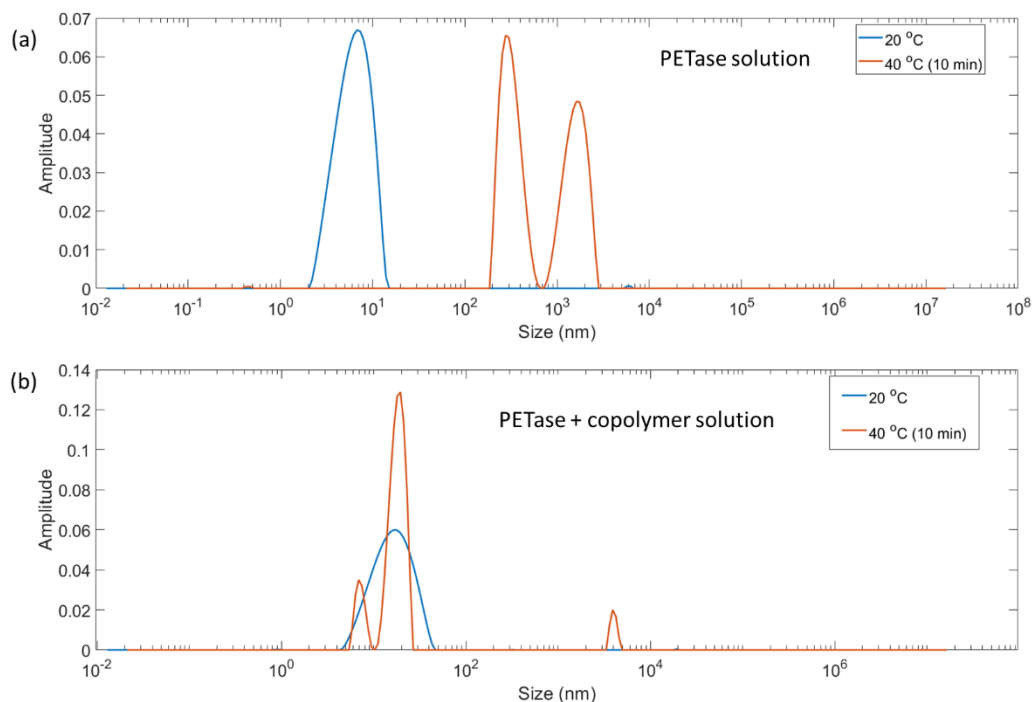


Figure 5.7 DLS measurements of PETase aggregation and copolymer solution behavior. (a) DLS curves for a solution of PETase at 20 °C and then heated to 40 °C for 10 minutes. Significant aggregation is observed. (b) DLS curves for a solution of PETase and copolymer at 20 °C and then heated to 40 °C for 10 minutes. Aggregation is barely observed.

Looking at DLS curves for PETase copolymer solutions when heated at 40 °C for twenty minutes, we can begin to see some signs of aggregation, although the solution remained clear. The DLS measurements indicated that by mass, 99% of the objects in solution retained a size of about 15 nm due to heating after twenty minutes. (Figure 5.8) This is experimental confirmation that copolymer complexes can indeed stabilize enzymes with respect to elevated temperatures.

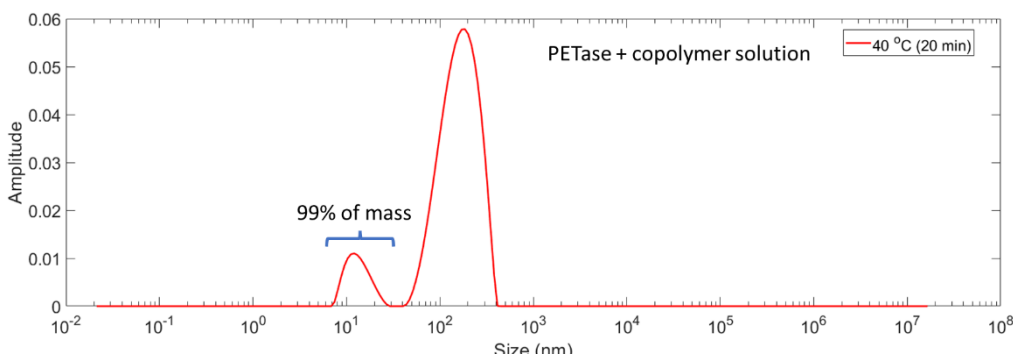


Figure 5.8 DLS curves for PETase copolymer solutions after 20 minutes heating. Two peaks were detected, but due to large objects scattering more light, the smaller peak contains 99% of the mass detected in solution. Thus aggregation is still mostly suppressed.

Activity of Enzyme-Polymer Complexes on Small Molecule and Solid Substrates

We performed experiments to assess the impact of active site stabilization on enzyme activity. We first examined the temperatures at which our PETase/copolymer complexes are stable. We incubated PETase or PETase/copolymer mixtures at a range of temperatures (4-50 °C) for 1 hour, and assayed esterase activity at room temperature against the small molecule substrate, p-nitrophenyl acetate (Figure 5.9a). Here, we used a small molecule substrate to avoid confounding effects of temperature on PETase's PET degrading activity (an established phenomenon^{24,25}). The copolymer used in these studies has a mean composition with $F_H=43\%$ and $F_- = 12\%$, within the normal range of F_H in the simulations and a reasonably similar value of F_- (methodology section for further detail). Interestingly, we found that for all incubation temperatures, the specific esterase activity of PETase was enhanced in the presence of copolymer, and that this activity enhancement increased at higher copolymer concentrations (Figure 5.9a). Our data also indicate that PETase activity in PETase/copolymer complexes is stable at temperatures up to 40 °C. Notably, this is less than the glass transition temperature of PET (70 °C). While the activity enhancement with the

addition of copolymer could improve the utility of the enzyme, further thermal stabilization of the PETase enzyme is likely needed to realize the full potential of this system. For example, polymers with side groups that penetrate PET could be used to decrease its T_g .

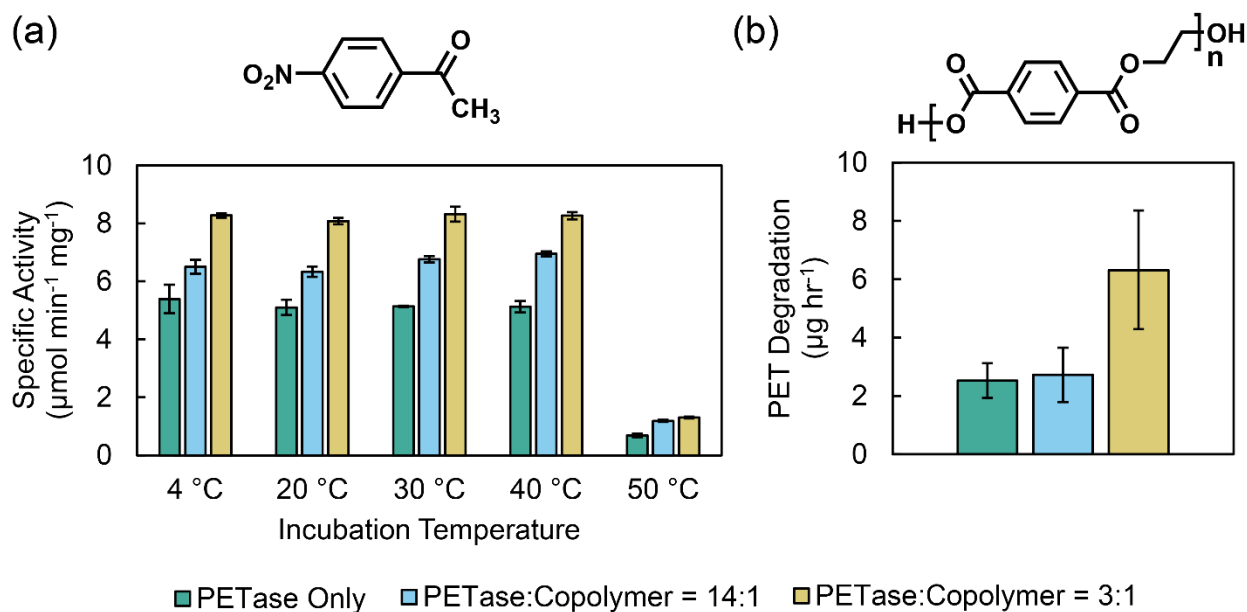


Figure 5.9 Activity of PETase and PETase/copolymer complexes at two different PETase:copolymer molar ratios. (a) Specific activity against small molecule substrate p-nitrophenyl acetate after one hour incubation at various temperatures. Error bars represent standard deviation over 3 replicate experiments (b) PET degradation activity over five hours at 35 °C. Error bars represent the 95% confidence interval on activity values.

Next, we examined the activity of PETase/copolymer complexes on solid PET as a substrate over five hours at 35 °C (Figure 5.9(b)). The presence of copolymer enhances the activity of PETase towards PET, similar to the results obtained with our small molecule activity assay. We confirmed that none of the formulations tested exhibited any decrease in esterase activity after incubation at 35 °C for five hours, suggesting that the enhanced enzyme activity with copolymer is not due to changes in the temporal stability of the enzyme. Thus, our experimental data suggest that PETase activity is improved upon addition of copolymer regardless of the substrate. These results, in

conjunction with our simulation studies, suggest that copolymer binding impacts active site conformation, thus altering PETase activity. We observe a wide distribution of active site conformations in simulations in the presence of copolymer compared to the naked enzyme (Figure 2(c)). While some of these active site conformations may be less active than the native enzyme, we hypothesize that there may be a few active conformations present at any given time that confer substantially higher enzyme activity. An alternative hypothesis is that the random copolymers interact favorably with the substrate leading to an increase in local substrate concentration. Indeed, we showed in Chapter 4 that these random copolymers can bind hydrophobic small molecules, and that IDRs in proteins, similar to the random copolymers in Figure 5.3(b), promote higher order assembly.⁶¹ However, because the increase in PETase activity appears to be independent of substrate (solid PET or aqueous p-nitrophenyl acetate), it is more likely that the interactions responsible for this activity enhancement are between the PETase and the random copolymer rather than the random copolymer and the substrate.

Conclusions and Outlook

The ability to use various types of enzymes in industrial conditions could dramatically impact biotechnology, pharmacology, and bioremediation. Here, we show that PETase is functionally stabilized by complexation with industrially scalable random copolymers. We demonstrate this through simulations of whole protein and active site conformations and using experiments measuring enzyme activity in response to thermal challenge; this effect is further enhanced when random copolymers form more contacts with the enzyme active site; and polymer composition biases the conformation and location of the random copolymers on a protein despite the randomness of the polymer sequences. Thus, engineering the surface potential of the protein, using

standard protein mutation or modification techniques, could bias polymers to bind near the active site, further increasing enzyme activity. This approach may be compatible with a variety of enzymes as long as their surfaces can be engineered without misfolding. However, the use of copolymer complexation to modify active site conformation does not necessitate further protein mutation or modification as the diverse functional groups on the copolymer should permit binding to a variety of protein surfaces. Further, this approach can also be used in the absence of information on the sequence and structure of an enzyme. Thus, this strategy has the potential to be a widely accessible route to increasing enzyme functionality, especially given that it requires only a random polymerization. Future experiments using substrates with various physical properties could elucidate the role of interactions between substrates and random copolymers, opening a new avenue for engineering enzyme activity via complexation with copolymers. These interactions could be controlled by using monomers with specific affinities and promote assembly on solid substrates like PET films.

Complexation with random copolymers is a welcome addition to the enzyme engineering toolbox, offering an orthogonal, versatile strategy for increasing functionality either in conjunction with or independent of other protein engineering techniques.

Methodology

Materials

Hexane, diethylether, and distilled water were purchased from Thermo-Fisher Scientific. Dimethylformamide (DMF) was purchased from Sigma Aldrich. The monomers polyethylene glycol methyl ether methacrylate (OEGMA-9, $M_n = 500$), 2-ethylhexyl methacrylate (EHMA),

and 3-sulfopropyl methacrylate (SPMA), along with chain transfer agent (2(dodecylthiocarbonothioylthio)-2-methylpropionic acid (DDMAT) and initiator 2,2'-azobis(2methylpropionitrile) (AIBN) were purchased from Sigma Aldrich. Monobasic and dibasic sodium phosphate salts were also purchased from Sigma Aldrich. Membrane filters were purchased from DOT Scientific. PET films were purchased from Goodfellow. AIBN was recrystallized from methanol prior to use.

Copolymer synthesis

The copolymer used in this study was synthesized by reversible addition-fragmentation chaintransfer (RAFT) polymerization. 0.47 mmol (135 mg) DDMAT and 0.08 mmol (13.5 mg) AIBN were dissolved in 5 mL DMF and mixed with 10.8 mmol (5.4 g, 5 mL) OEGMA-9 and 13.4 mmol (2.7 g, 3 mL) EHMA. 2.64 mmol (650 mg) SPMA was dissolved in 1 mL of distilled water and added to the monomer mixture. The solution was then purged with nitrogen gas for 30 minutes, and heated at 60 °C for 24 hours. The resulting polymer was then precipitated in diethyl ether and washed several times in hexane, resulting in a yellow precipitate. The precipitate was then redissolved in a 50% v/v solution of water/ethanol, resulting in a cloudy yellow solution. Excess hexane was removed from this solution using a rotary evaporator, resulting in a clear yellow solution. This clear yellow solution was then dialyzed against deionized water for two days, with a replacement of the dialysis solution after 24 hours. The dialyzed product was then filtered through a 0.22 μm polyethersulfone (PES) membrane filter and used in experiments. Concentrations of polymer solutions were determined by drying 1 mL volumes of solution and measuring the mass of the residual solid.

Copolymer molecular weight characterization

Molecular weight was characterized by aqueous gel permeation chromatography on an Agilent 1260 series high performance liquid chromatography (HPLC) instrument using a Superdex 75 increase 10/300 GL column. Detection was performed with a multi-angle static light scattering detector Wyatt DAWN HELEOS II). 50 mM sodium phosphate buffer at pH 7.2 was used as the mobile phase. 0.3 mL of polymer solution at 0.8 mg/mL was injected at a flow rate of 0.4 mL/min. An approximate refractive index increment (dn/dc) value of 0.106 mL/g was measured using an Atago pocket refractometer on a serial dilution series of the same polymer solution.

Copolymer composition characterization

Copolymer composition was characterized using ^1H NMR spectroscopy (Bruker X500 NMR spectrometer), using deuterium oxide (99.9% Cambridge Isotope Labs) as the solvent. Aqueous polymer samples were dried in a vacuum oven before redissolution in deuterated solvent to a concentration of 15 mg/mL. ^1H NMR peak assignments were done broadly by distinguishing low chemical shift hydrogens next to non-polar carbons, labeled (a), and high chemical shift hydrogens next to polar functional groups and carbons next to polar functional groups, labeled (b). A third label (c) was assigned to distinct hydrogens on the SPMA group to solve for the molar ratio of each component (Figure 5.10).

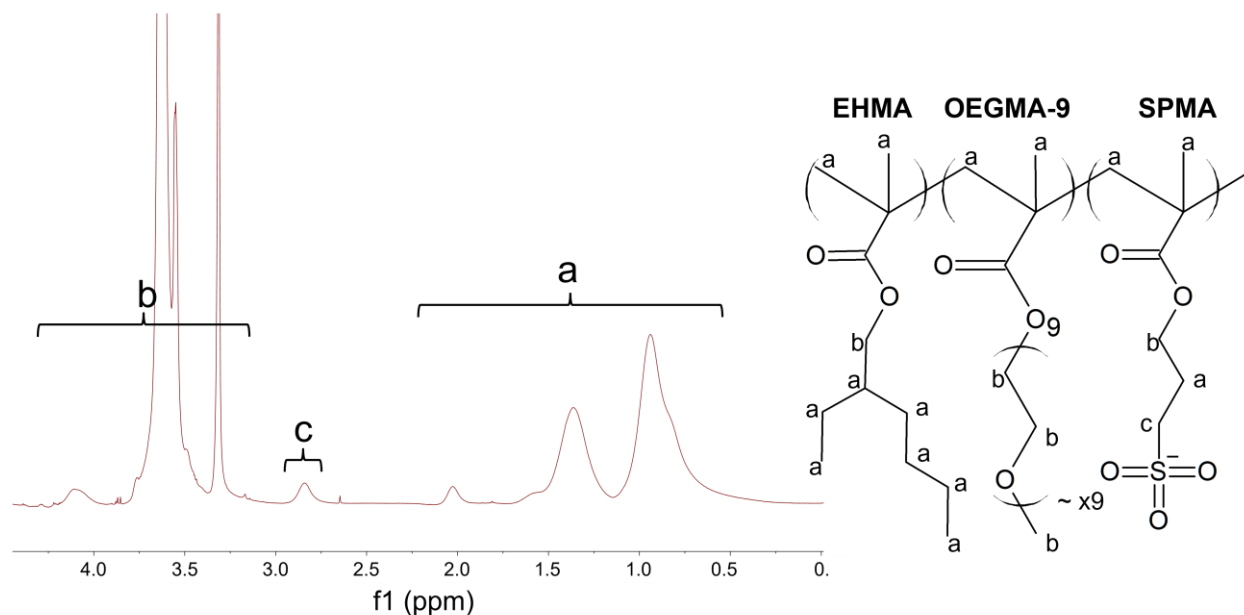


Figure 5.10 Hydrogen nuclear magnetic resonance (HNMR) spectrum of RAFT-synthesized random copolymer.

PETase expression and purification

The PETase sequence used in this study can be found in Figure 5.11 and 5.12.

```

atgaacttccccgtgectcgcgcttatgcaggctgctgtgctggcggccttatggccgtttccgcagcggccaccg
cagaccaatcctgatgcgcgcgcccaaccctaccgccgctcgttggaaaccagcgcgggaccctttaccgttcgta
gctttaccgttagccgtccgctccgatatggtgcaggaccgtctattaccaaccaatgcaggcggcaccgttggcgc
gattgcaatcgtccccgggtacaccgcgctcaaagcagcattaagtggggggtccgcgcttagctagccatggctt
gtggttattaccatcgatacgaacagcactctagaccagcccagcagccgtagctcgcaacagatggccgcgcttcgctc
aagttgagcgttgaacgggaccagcagtagcccgatttacggaaaggtcgatactgcccgcagtggtgtgatgggcca
ctcaatggggggcggcggttcacttattagcggcggaacaaccgagtttaaagcagcggcaccgcagggcctatgg
gactcttcaaccaacttcagcagtggtaccgtgccgacgctgattttcgcgtcgagaatgatagcattgcaccgggta
acagcagcgcgctgccgattatgatagcatgtcccgaacgcaaacagttctgaaattaacggcggtagccactt
ctgtgccaactctgggaacagcaaccaggcactgatcggaaaaaagggttgcagtgatgaaacgattcatggataat
gacaccggttactcaacctcgcctgtgagaatccaacagcacacgcgtgctcgattttcgcaccgcgaactgtccc
tcgagcaccaccatcaccaccactga

```

Figure 5.11 DNA sequence encoding PETase used in this study

MNFPRASRLMQAAVLGGLMAVSAATAQTNPYARGPNPTAASLEASAGPFTVRSFTVS
 RPSGYGAGTVYYPTNAGGTVGAIAIVPGYTARQSSIKWWGPRLASHGFVVITIDTNSTLD
 QPSSRSSQMAALRQVASLNGTSSSPIYGKVDTARMGVMGHSMGGGSLISAANNPSL
 KAAPQAPWDSSTNFSSVTVPTLIFACENDSIAPVNSSALPIYDSMSRNAKQFLEINGGSH
 FCANSGNSNQALIGKKGVAWMKRFMDNDTRYSTFACENPNSTRVSDFRRTANCSLEHHH
 HHH*

Figure 5.12 Amino acid sequence of PETase used in this study

The gene was ordered from Twist Biosciences subcloned into pET-21b(+). The PETase sequence used contained two point mutations (W159H and S238F) shown to enhance PETase activity¹⁷¹ and a C-terminal 6xHistidine tag for purification. The PETase enzyme was expressed and purified as described previously, with the minor modifications indicated here.¹⁷¹ PETase was expressed in *Escherichia coli* C41 (DE3) cells. Overnight cultures were grown from a single colony in lysogeny broth, Miller formulation (LB-Miller) supplemented with 50 $\mu\text{g}/\text{mL}$ carbenicillin (DOT Scientific, Inc.). For expression, overnight cultures were subcultured 1:100 into LBMiller supplemented with 50 $\mu\text{g}/\text{mL}$ carbenicillin and grown at 37 °C with shaking at 225 rpm to an optical density at 600 nm (OD600) of 0.4-0.6. After reaching this target OD600 range, cultures were placed on ice for 15 minutes and then induced with 0.5 mM isopropyl β -D-1-thiogalactopyranoside (IPTG, DOT Scientific, Inc.). Induced cultures were grown for 20 hours at 18 °C with shaking at 225 rpm. Cells were harvested by centrifugation and resuspended in 25 mL binding buffer (20 mM sodium phosphate, 500 mM sodium chloride (Fisher Chemical), 20 mM imidazole (Spectrum Chemical), pH 7.4) per liter of culture. Resuspended cells were frozen and stored at -20 °C until ready for lysis.

Cells were lysed as follows. The resuspended cells were thawed and incubated with 1 mg/mL lysozyme for 1 hour at room temperature, followed by tip sonication. Cell debris was removed

from the lysate via three 15 minute centrifugations at 15,000xg, where the supernatant was transferred to a clean tube after each spin. Clarified lysate was applied to a His GraviTrap column (Cytiva 11003399) to bind the 6xHis-tagged PETase protein. Flow through was discarded and the column was washed three times with 10 mL wash buffer (20 mM sodium phosphate, 500 mM sodium chloride, 40 mM imidazole, pH 7.4).

Purified PETase was then eluted with 2 mL of elution buffer (20 mM sodium phosphate, 500 mM sodium chloride, 500 mM imidazole, pH 7.4). The purified PETase product was exchanged into 50 mM sodium phosphate buffer, pH 7.2 using a PD-10 desalting column (Cytiva 17085101) according to the manufacturer's instructions. Purity of the final protein product was confirmed by sodium dodecyl sulfate polyacrylamide gel electrophoresis (SDSPAGE) and Coomassie blue staining (Figure 5.13). Protein samples were separated on 12.5 % w/w polyacrylamide gels (Bio-Rad, purchased as 30 % w/w Acrylamide/Bis Solution 37.5:1) cast in 0.1 % (w/w) SDS (Fisher Bioreagents), 375 mM tris, pH 8.8 (Fisher Bioreagents). Coomassie G-250 dye was used for gel staining (ICN Biochemicals).

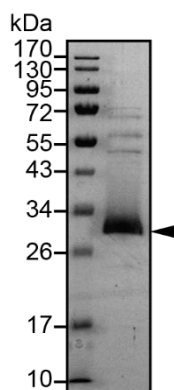


Figure 5.13 Sodium dodecyl sulfate polyacrylamide gel electrophoresis (SDS-PAGE) stained with Coomassie blue on final purified PETase protein product used in this study.

PETase activity against p-nitrophenyl acetate after thermal challenge

Mixtures of PETase and random copolymer for the thermal challenge assay were prepared by mixing concentrated stocks of PETase (200 $\mu\text{g}/\text{mL}$) and random copolymer (80 $\mu\text{g}/\text{mL}$) with 50 mM sodium phosphate buffer pH 7.2 to the specified concentrations. Mixtures were prepared to a final volume of 50 μL , with 20 $\mu\text{g}/\text{mL}$ PETase and a random copolymer concentration specified by the molar ratio described in the main text (8 $\mu\text{g}/\text{mL}$ for 14:1 PETase:random copolymer, 40 $\mu\text{g}/\text{mL}$ for 3:1 PETase:random copolymer). All mixtures were prepared in triplicate. Samples were then either refrigerated at 4 °C or placed in a Bio-Rad C1000 Touch Thermal Cycler set to 20 °C, 30 °C, 40 °C, or 50 °C and incubated for 1 hour. After this one hour incubation, samples were brought to room temperature and 10 μL of sample was added to a well in a 96-well flat bottom plate for assaying. In addition to the PETase or PETase mixture, each well contained 10 μL of 50 mM sodium phosphate buffer pH 7.2 Assays were initiated by adding 180 μL freshly prepared 0.667 mM p-nitrophenyl acetate (Sigma) in 50 mM sodium phosphate buffer pH 7.2 with a multichannel pipette. Activity was monitored by measuring absorbance at 347 nm (the isosbestic point of p-nitrophenol) for 20 minutes in a BioTek Synergy HTX plate reader. Absorbance was converted to p-nitrophenol concentration using a calibration Curve (Figure 5.14, p-nitrophenol ordered from Sigma Aldrich), and the slope of the p-nitrophenol concentration versus time was calculated for each replicate. Slopes were corrected for background hydrolysis by subtracting the average p-nitrophenol versus time slope in a buffer-only control sample. This background-corrected slope was converted to specific PETase activity by dividing the slope by the final concentration of PETase in each well

(1 $\mu\text{g}/\text{mL}$). All error bars reported represent the standard deviation in this calculated specific activity over three separately prepared and incubated mixtures.

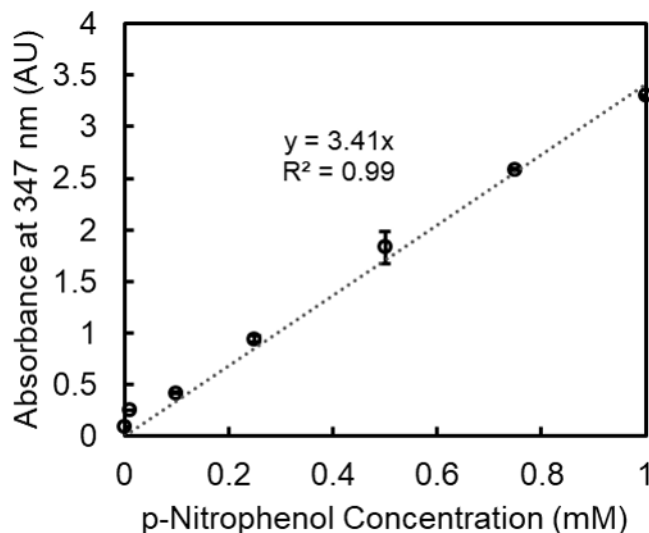


Figure 5.14 Calibration curve used to convert absorbance at 347 nm to p-nitrophenol concentration. Error bars represent standard deviation over three independently prepared samples.

PETase activity on PET films

Activity tests on PET films were conducted in 20 mL glass scintillation vials. A 0.2 mm thick PET film was rinsed several times with ethanol (200 proof, Decon Labs) and deionized water and 0.5 inch discs were cut from the film using a hole punch. The films were placed inside the vials and submerged in 2 mL of the appropriate solution (20 $\mu\text{g}/\text{mL}$ PETase, 20 $\mu\text{g}/\text{mL}$ PETase 8 $\mu\text{g}/\text{mL}$ copolymer, or 20 $\mu\text{g}/\text{mL}$ PETase 40 $\mu\text{g}/\text{mL}$ copolymer in 50 mM sodium phosphate pH 7.2). All samples were prepared in triplicate, and each time point had its own set of corresponding vials that were removed accordingly. The samples were incubated in an oven at 35 °C. Product generation was measured by UV-visible absorbance at 242 nm on a Thermo

Scientific Evolution 201 Spectrophotometer. Absorbance of the assayed PETase or PETase/copolymer mixture at 242 nm was subtracted to determine the contribution from PET degradation products. Conversion of absorbance to degradation product mass was achieved using a calibration curve (Figure 5.15).

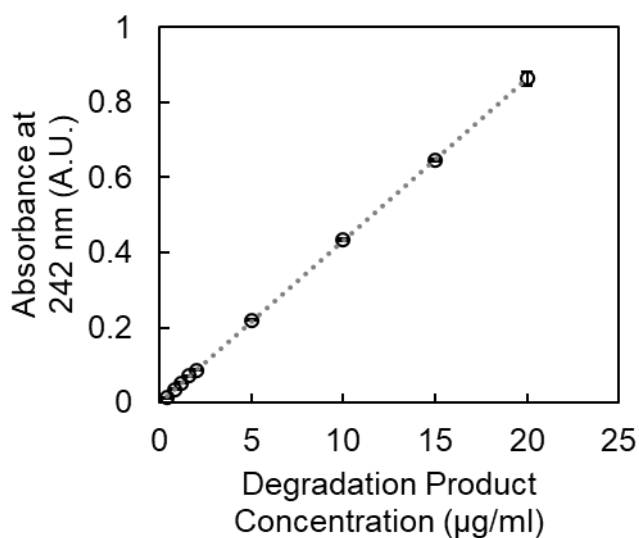


Figure 5.15 Calibration curve used to convert absorbance at 242 nm to mass of PET degraded. Error bars represent standard deviation over three independently prepared samples.

PET degradation product calibration curve construction

1 g of bis hydroxyethyl terephthalate (Sigma Aldrich) was added to 500 mL of 300 mM phosphate buffer pH 7.2 and stirred overnight to form a fine suspension. 1 mL of 1.5 mg/mL PETase solution was added to this suspension and mixing was continued for two days, after which a clear solution was observed. This solution was filtered through a 0.22 µm PES membrane filter. The solution was then acidified with 40 mL of hydrochloric acid (ThermoFisher), resulting in a pH of approximately 1. This resulted in formation of a suspended precipitate. This suspension was chilled in an ice bath overnight to allow settling of

the precipitate. The solution was then filtered and the precipitate collected. The precipitate was dried in a vacuum oven overnight, and stock solutions of varying concentrations were prepared in 50 mM sodium phosphate buffer at pH 7.2 for construction of the calibration curve. UV-visible spectra for each stock solution were taken and absorbance values at 242 nm were recorded as a function of degradation product mass.

Atomistic Simulations

Forcefield

We performed all atom molecular dynamics simulations to study PETase in aqueous solution using the package GROMACS (version 2016.3).¹ We used the most recent CHARMM² forcefield. The recommended CHARMM TIP3P water model³ was applied with the structures constrained via the SETTLE algorithm.⁴ For simulations at different temperatures only the temperature was varied and all other parameters remained the same. The periodic boundary conditions were employed in all dimensions. The neighbor searching was calculated up to 12 °A using the Verlet particle-based method and was updated every 20-time steps. The Lennard-Jones (LJ) 12-6 interactions were switched off from 10 to 12 °A via the potential-switch method in GROMACS. The short-range Coulomb interactions were truncated at the cut-off distance of 12 °A, and the long-range interactions were calculated using the Smooth Particle Mesh Ewald (PME) algorithm.^{5,6} The NPT ensemble (constant number of particles, pressure, and temperature) was employed. The temperature was coupled using the Nosé-Hover algorithm (reference temperature was varied, characteristic time 1 ps). The isotropic Parrinello-Rahman barostat was employed with the reference pressure of 1 bar, the characteristic time was 4 ps,

and the compressibility of $4.5 \times 10^{-5} \text{ bar}^{-1}$. All the covalent bonds were constrained, which supported an integration time step of 1 fs. These parameters were recommended for the accurate reproduction of the original CHARMM simulation on lipid membranes, and have been verified in our simulations on proteins and lipid membranes.

Protocol

Ten different 10 nanosecond simulations, containing only the protein, water, and the counterions necessary for electroneutrality, are carried out at each temperature (298K, 310K, 320K, 325K, 330K, 335K, 340K, and 350K) and data is collected for the last 5 nanoseconds. Using GROMACS,¹³ the root mean square deviation (RMSD) is all atoms relative to that atom in the energy minimized crystal structure with rigid body translation and rotation accounted for. Thus, this is not a measure of diffusion, but a measure of how conserved the PETase conformation is with lower values being more conserved. The value for each atom is then averaged over the entire protein for the "Whole Protein RMSD" (ignoring the first 20 and last five residues, which are less structured and thus have high fluctuations leading too large errors). For the "active site RMSD" we include only the atoms in the active site, according to previous definitions of the active site.¹⁴ The RMSDs of the PETase active site are of particular interest since they correlate with observed catalytically inactivity of PETase at temperatures above room temperature. Error bars are the standard error based on the number of independent runs, N=10.

GoMartini PETase Only Simulations

Forcefield

To model the complexation of the random copolymers with the PETase (PDB: 6EQE) surface, we use the MARTINI forcefield with polarizable water. The temperature dependant melting behavior of PETase is captured by the GoMARTINI protein model. This model builds on network-based models¹⁹ by replacing harmonic bonds between noncovalently bonded residues with Lennard-Jones interactions where epsilon is 12 kJ/mol, increasing the ability of the protein to denature including at elevated temperatures. Remarkably, it has been very recently demonstrated that the Go Martini model with these parameters is capable of protein configuration change for several mutations of copper, zinc, superoxide dismutase, a protein associated with neurodegenerative disorder amyotrophic lateral sclerosis. The topology files for the Go Martini 2.2 model were generated using the program `go_martinize.py` and the epsilon value of 12 kJ/mol. The program `go_martinize.py` was modified such that the neighboring contact map was built up to a cut-off distance of 1.1 nm. In the production simulations, the recommended parameters²³ for the MARTINI 2.2 potential were employed, which are summarized here. The short-range Coulomb interactions were calculated up to 1.1 nm with the reaction field approach (relative permittivity of 2.5) for the long-range electrostatic interactions. The LJ 12-6 potential interactions were truncated at 1.1 nm. The NPT ensemble was applied. The temperature was coupled at 298, 320, or 350K using the velocity rescaling method. The isotropic pressure coupling (reference pressure 1 bar, time constant 5.0 ps, compressibility $3 \times 10^{-4} \text{ bar}^{-1}$) was employed using the Parrinello-Rahman algorithm. The leapfrog integration time step of 10 fs was employed.

Protocol

We use a similar methodology for the GoMartini as for the atomistic simulations. We simulate only the protein, polarizable water, and the counterions necessary for electroneutrality.

Five independent simulations are run for 300 nanoseconds, and data is collected for the second half of the simulation. We calculate the root mean square deviation (RMSD) between the beads which comprise the PETase protein in the molecular dynamics and the respective energy minimized crystal structures using GROMACS.¹³ Thus, the RMSD is a measure of how conserved the PETase conformation is with lower values being more conserved. We then average this quantity over the beads in the GoMartini PETase model (once again ignoring the first 20 and last 5 residues) and all beads in the active site providing us with two different RMSD values corresponding to different parts of the PETase. The active site group uses the same definition of the 7 active site residues (Thr88, Trp159, Ser160, Trp185, Asp206, His237, Ser238) as the all-atom RMSD calculations. Error bars are the standard error based on the number of independent runs, $N=5$.

Calculation of Hydrophobic Surface Fraction

In Figure 4(b) in the main text we calculate the hydrophobic fraction of the surface of PETase as follows. First we define which beads are in the surface. These are beads which make, over a time average, one contact with a water bead. A contact means that the PETase bead is within the $.53 \text{ nm}$, the equilibrium separation distance, of a water bead. Then, all beads defined to be in the surface are labeled as either polar or hydrophobic. There are 4 general types of beads in the Martini forcefield: "Q", "P", "C", and "N". We consider "C" and "N" to be hydrophobic and others to be polar. The hydrophobicity of the polymer beads is defined in the same way.

The fraction is just the number of beads considered to be hydrophobic divided by the total number of beads. The fraction calculated, .49, is significantly higher than .28, which has been reported previously in atomistic simulation for the hydrophobic surface fraction of PET. This is based on a different definition of hydrophobic which labels each bead based on the identity of the amino acid they are a part of. In the Martini model, amino acids often contain both hydrophobic and polar beads making the definitions nonequivalent. These definitions accounts for the vast majority of the difference since, by using the other definition of hydrophobicity on the martini model, we get a surface fraction of .32, in reasonable agreement with atomistic result. We think the bead-by-bead definition makes more physical sense for the Martini simulations, especially since our polymer monomers also contain both hydrophobic and polar beads, which we show is very important to explain the behavior of the system. In other words, we perform the analysis at the length scale of the coarse graining.

Martini Simulations of PETase and Random Copolymers

Forcefield

The MARTINI model for the monomers comes from a variety of sources: one for the methacrylate backbone,²⁴ one for the PEO oligomers, and another for the rational approach to coarse graining organic molecules including those with charge.

Protocol

Each simulation involves PETase and four copolymers with a degree of polymerization (DP) of 100 monomers. Sequences are built at random under the constraint of a given mean composition. This is accomplished by creating a computational pool of 400 monomers (N=100

* 4 polymers) with the given ratio of monomer types. Monomers are randomly chosen one at a time and added to the growing chains until no monomers are left. The result is 4 chains with completely random sequences that likely do not have the same composition, but have the given mean composition as a group. The counterions included are those necessary to neutralize the positively charged protein and one counterion for each negatively charged polymer monomer. The compositions constrain the total percentages of monomers in the box while individual copolymers have gaussian fluctuations in composition. This also means that the volume fraction of polymers plus PETase fluctuates, but is around 5 percent. For all 21 compositions, the simulation is initialized with only the PETase and polymers allowing the copolymers to quickly contact PETase. This box is then solvated and cyclically annealed from 298K to 350K and back down three times at a rate of one cycle per 80ns. Twelve configurations are taken from the last half of the 240ns annealing process. For each of these configurations, the simulation is run for an additional 50ns at each temperature (298K, 320K, and 350K), a total of 1800ns per composition. From these simulations, all relevant values are measured and averaged by temperature.

Definition of Polymer-Protein Contacts

Like in the calculation of the hydrophobic surface fraction, a contact occurs between two beads when they are less than $.53 \text{ nm}$ from each other. These contacts can either be hydrophobic-hydrophobic (Hh), hydrophobic-polar (Hp), polar-polar (Pp), or polar-hydrophobic (Ph). This is determined by bead type, not monomer or amino acid type, consistent with the calculation of the hydrophobic surface fraction. Again we use the definition that "C" or "N" beads are

hydrophobic and all others are polar. Thus most polymer monomers and many amino acids contain both polar and hydrophobic beads.

Chapter 6

The studies presented in this thesis demonstrate the versatile nature of random copolymer polyelectrolytes, particularly when they form charged complexes with other polyelectrolytes and proteins. Random and statistical copolymers can exhibit novel polymer interactions with surfaces due to the correlations in monomer sequence, a sort of disorder that when properly utilized, can lead to functionalities that we see in biological systems. The ability to design polymers with these functionalities is an advancement of polymer science, and can do much to address the environmental issues associated with polymer usage in modern society. However, while the previous three studies show the potential of random copolymer polyelectrolyte complexes in plastic recycling and water remediation, there remain many fundamental and practical questions that deserve investigation to realize the potential of this class of material.

Outlook for enzyme copolymer complexes

Starting with the PETase-copolymer complexes of Chapter 5, we demonstrated that the complexes were able to enhance the activity of PETase on both PET and small molecules. For the case of PET, our best result was an increase in degradation rate of approximately 100%. However, in order to make enzymatic recycling of commercial plastics feasible, this increase in degradation rate may need to be improved by orders of magnitude. Clearly, there is room for improvement, and there several avenues of investigation available to further enhance the degradation rate.

The simplest route may be the optimization of the copolymer composition used to form our PETase copolymer complexes. Only one composition was used in the study, with a roughly equal fraction of hydrophobic and hydrophilic monomers to have as broad of a distribution of sequences as

possible. It is likely that, using the same monomer components, there is an optimal composition which can enhance PETase activity. As previously discussed, one possible mechanism for activity enhancement is the adsorption of the complexes on the PET surface. Our adsorption studies in Chapter 4 indicate that there is a dependence on hydrophobicity on our copolymer adsorption onto PET. The increasing nanoplastic removal performance of the complexes with hydrophobicity may suggest that more hydrophobic complexes adsorb and interact better with PET, and thus more hydrophobic copolymer compositions may further enhance enzyme activity on PET. It would be relatively straightforward to perform degradation tests with different copolymer compositions and then compare the results to find the optimal composition.

These results may also help expand our fundamental understanding of how these enzyme copolymer complexes behave. As mentioned in Chapter 5, there is debate on how important the polymer-surface interactions are in enzyme enhancement compared to the polymer-enzyme interactions. Knowing the degree of enzyme enhancement with respect to copolymer compositions could shed light on this issue. If enhancement tracks well with adsorption capability, then it would be strong evidence that it is a strong factor. It should be noted that in Chapter 4, we saw that the adsorption of the copolymer may not be correlated to the adsorption of the complex onto PET. The difficulties in performing adsorption measurements on the polyelectrolyte complexes, which forms macroscopic particles, prevented a definitive comparison. However, in the case of enzyme-copolymer complexes, the complexes are well dissolved in water, and direct adsorption measurement should be feasible. The results of these adsorption studies may also complement the investigations performed to understand how adsorption of complexes of the polymer may differ from the adsorption of the polymers themselves.

There could be other ways to increase enzymatic activity that leverage the properties of enzyme copolymer complexes. On a fundamental level, enzymatic degradation is slow because at most plastic materials are glassy at room and biological temperatures. Thus the polymer chains are quite immobile and cannot effectively interact with the enzyme active site. Raising the temperature above the glass transition, which is around 70 °C for the case of PET, will cause the chains to become more mobile, but these elevated temperature tend to denature most proteins, rendering them inactive. While our polymers appear to impart some thermal resistance to PETase, the activity still drops precipitously past 50 C, and it is unclear whether a different polymer composition could potentially protect PETase activity at even higher temperatures. There could be studies performed to explore how to strengthen this thermal resistance. One reasonable hypothesis could be that the stronger the binding and coverage is between the polymer and enzyme, the more insulated the enzyme will be from thermal fluctuations. Thus, finding optimal polymer compositions for complex formation in this regard could also yield useful information. However, with increased temperature, hydrophobic interaction, which are a major part of these copolymer interactions, significantly weaken, leading to additional considerations with binding and activity.

The temperature issue appears to be most effectively addressed by engineering proteins to have some degree of thermal resistance. Various plastic degrading enzymes have been engineered to function at the PET glass transition temperature,¹⁷⁷ and such work would be beyond the scope of the work related to this thesis. However, this may not be an effective technique for recycling plastics in general. Some commonly used plastics, such as polystyrene, have glass transition temperatures greater than or equal to 100 °C. Engineering proteins to be functional at these

relatively extreme temperatures seems difficult, and while some enzymes and organisms do survive at these temperatures,¹⁷⁸ the process of translating those characteristics into plastic-degrading enzymes would be challenging work.

One other method to increase the mobility of polymer chains is to use favorable solvents that can penetrate the polymer and effectively act as a plasticizer. The use of solvent mixtures for enzyme degradation faces similar issues as elevated thermal treatment, as enzymes tend to denature in organic-solvent conditions. However, our copolymer-enzyme complexes may also have the ability to protect enzyme activity from exposure to organic solvent, as was hinted in previous work in the literature. Such experiments, if successful, would not only provide another avenue to enhance enzyme activity, but also demonstrate another fundamental property of these enzyme-copolymer complexes.

Some preliminary work was done, not showing any particular solvent resistance of PETase copolymer complexes, but of the potential gains in activity that could be obtained from solvent-exposed plastic. By submerging a sample of PET into various solvents, and then placing the PET in PETase buffer, we can obtain considerable increases in solvent activity. The solvents used were regular buffer, 5% HFIP/buffer, and 50% HFIP/buffer. We can observe solvents swell the PET samples considerably, and in the case of 50% HFIP/buffer, over a magnitude increase in activity was obtained.

Table 6.1 Degradation of Treated PET samples

Treatment	Buffer	5% HFIP	50% HFIP
Thickness	0.20 mm	0.21 mm	0.3 mm
Amount degraded (1 day)	4.9 ug	6.5 ug	85 ug

One other issue that needs to be considered in the enzymatic recycling of plastics is that some polymer are semicrystalline in nature. PET is semicrystalline, as is polyethylene and nylon. Polymer chains within crystalline regions of a polymer have very low mobilities, being confined to the crystalline lattice. Thus it is particularly difficult for enzymes to act on crystalline regions of polymer materials. The melting point of these crystalline domains tend to be quite higher than the glass transition of the polymer matrix. For PET, the melting point is around 260 °C, a temperature at which enzymes will not function. It is an open problem on how enzymatic recycling will deal with polymer materials with crystalline domains.

One potential idea is adding groups to the random copolymer to disrupt crystalline regions of PET. Some cellulose binding domains are thought to peel off cellulose chains from a crystalline state, and it would be an interesting exercise to design polymers and polymer complexes with the same functionality. One approach would be to utilize cation- π interactions, in which cationic ions and molecules can form particularly strong bonds with aromatic rings. PET crystals have regularly

spaced aromatic rings along the chain axis, with a spacing of 1.075 nm. Thus it seems possible to design a polymeric motif with precisely spaced positive charges to match that of aromatic rings in PET crystals and bind strongly to crystalline PET. In order to peel off surface chains, one could make use of dielectric repulsion, which is an electrostatic effect when a charge is brought close to a surface from a high dielectric medium to a low dielectric medium. Thus, by utilizing this physical principle, it should be possible to peel off surface layers of PET if the cationic polymer motif can bind to the surface. This motif can be attached to the random copolymer during the synthesis process, and give the random copolymer complex the ability to disrupt PET crystals. Structures of potential monomers are shown below in Figure 6.1.

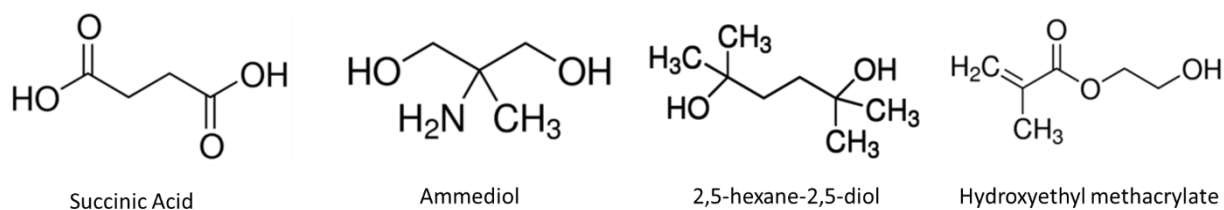


Figure 6.1 Monomers for possible PET binding motif. Succinic acid and ammediol would be the main monomer components with an established spacing between charged groups. Hydroxyethyl methacrylate would cap the chain ends and allow incorporation into free radical polymerizations. The hexanediol is a cleavable linker under acidic conditions.

A chemical synthesis procedure was investigated to synthesize such a motif. The main components was ammediol, a symmetric amine, and succinyl chloride. Ammediol is basic and will be positively charged at near neutral PH. The calculated spacing between the amines if a polymer made of these two monomers through step-growth polymerization is 1.09 nm, which is close to the 1.075 nm spacing of the aromatic segments. In order to attach this motif to the polymer, some other functional monomers will need to be added. These will be hydroxyethyl methacrylate and 2,5-hexane-2,5-diol. The hydroxyethyl methacrylate has a single alcohol group,

which will terminate the polymerization. The vinyl group on the hydroxyethyl methacrylate can then be used in the radical polymerization process used to add to the regular random copolymers. The 2,5-hexane-2,5-diol is an acid labile group and will cleave the chains so we do not have the equivalent of a crosslinking agent with two methacrylate groups.

Unfortunately, the preliminary work to realize this synthesis process encountered difficulties, and unknown side reactions were dominating the polymerization procedure, and no polymer product could be recovered.

One last note on this topic is that solvent-based techniques could also potentially address the crystallinity issue. Solvent molecule could potentially solvate polymer chains that are otherwise crystalline and disrupt their structure and increase mobility. This may be particularly true for the HFIP solvent, which is known to dissolve PET on its own. Thus investigating the solvent resistance of plastic-degrading enzymes and methods to increase such could be particularly fruitful.

Outlook for polyelectrolyte complexes for water remediation

In our investigations of random copolymer complexes for water remediation, we demonstrated their ability to encapsulate and remove small molecule and nanoplastics contaminants. While more work could be done to improve the removal efficiency of some contaminants, particularly some of the emerging contaminants that we were unable to quantitatively remove with our technique, there are other aspects of the copolymer system that need to be considered to maximize its applicability and environmental utility. Such aspects include the ability to extract contaminants

that have been encapsulated, reuse the copolymers for future remediation processes and, minimize residual copolymers dissolved in solution.

In terms of encapsulation performance, an exploration of different copolymer compositions could provide a modest boost in a feasible and straightforward manner. As noted in the outlook for copolymer-enzyme complexes, only one copolymer composition was tested for removing molecular contamination from water and optimization of the composition is still possible. Changing copolymer hydrophobicity will likely yield results, as molecular dynamics simulations appear to suggest hydrophobic forces are significant in terms of molecule-complex interactions. The case of improving the removing of fluorinated compounds may be more involved. Fluorinated compounds are known to be both hydrophobic and lipophobic due to low surface energies, and changing hydrophobicity of the copolymer may not significantly change the interaction strength. For PFOA, it appears that using electrostatics and targeting the negatively charged acid group could be fruitful. This could be done by adding a small amount of positive charge to the anionic copolymer. There would be several factors to consider with this approach. First, the amount of positive charge cannot be so great as to disrupt the ability for the copolymer to form macroscopic complexes with a cationic flocculant, and it is unclear how much charge this would be. The addition of positive charge could potentially change the nature of the copolymer, as attractive charged intrapolymer interactions would likely induce some form of conformation change which could in itself affect the interactions with small molecules. However, while these additional interactions may complicate the polyelectrolyte system, it may also be a rich research avenue. Many proteins have both negative and positive charges, and these charge interactions can play a crucial role in their function. Investigating the behavior and properties of synthetic

polyampholytes with hydrophobic interactions may lead to new results in mimicking protein functions.

In order to recycle and reuse the polyelectrolyte complexes in multiple remediation cycles, several problems need to be solved. One main problem is the ability to separate the anionic and cationic copolymers back into solution form so that the flocculation and encapsulation step may be repeated. The key issue is that the polyelectrolyte mixing and complex formation is a thermodynamically favorable process and will ultimately require some form of energy input to undo. One potential method to dissolve the complexes is to use high-salinity water, which we know reduces the thermodynamic driving force for complexation and can bring the system back into a one-phase region. A drawback of this method is that any excess salt added would ultimately need to be removed from solution before being reused in order to prevent the salinity from increasing in the treated water. Another idea is to use weak acids and bases as the charges for our polyelectrolyte system. pH can then be used to regulate the charge fraction of the polyelectrolytes, and sufficiently high or low pH would cause one of the polyelectrolytes to become uncharged, which removes the thermodynamic driving force for complexation. Adjusting the pH of treated water is a simple and cost-effective process in water treatment plants, in that only a small amount of acid or base is needed to be added.

After dissolving the complexes, the cationic and anionic copolymers would likely need to be separated, along with any contaminants that may have been encapsulated and concentrated within the complexes. These separation processes could add significant cost and complexity to reusing the polyelectrolytes, and constitutes its own research topic. For the case of the polyelectrolytes, there have been some research in designing pH-responsive polyelectrolytes that have significant

hydrophobicity such that once they become uncharged, they phase separate from solution. By adjusting the hydrophobicity of our copolymers, it may be possible to replicate this behavior to sequentially separate our polyelectrolytes by changing from high to low pH, and removing the phase-separated portion. Changing the hydrophobic nature of the polymers may also change their remediation effectiveness, and this would also need to be investigated. Another possibility is to use ion-exchange resins, a separation technique which uses beads with charged surfaces that attract oppositely charged molecules and salts due to electrostatic and salt-release mechanisms. Thus a one-phase solution of polyelectrolytes could be passed through a positively charged and negatively charged ion-exchange resin, with oppositely charged polyelectrolytes adsorbed onto the surface. The polyelectrolytes can then be released from the surfaces into solution through separate washing steps.

However, this does not address removing the contaminants from solution and it is unclear how much would be retained in the separated polymer phases. In principle, there are general solutions that we could apply in this situation. For the case of molecular contaminants, there is a relatively large mismatch in size between the contaminant, anionic copolymer, and cationic copolymer. In terms of molecular weight, the anionic copolymer is around 3 orders of magnitude larger than the contaminants, and the cationic copolymer is around 2 orders of magnitude larger than the anionic copolymer. Thus with membrane filters with carefully controlled pore sizes, it should be possible in a one-phase solution to separate the contaminants from the polyelectrolytes, and then separate the anionic copolymer from the cationic copolymer. This would mostly be a pressure-driven process, and would be similar to reverse osmosis purification of water, which is known to be relatively expensive. In addition, separately polymer solutions could be challenging with

increased viscosities of solution which would decrease the flow rate and increase the needed pressure for purification. One positive note is that the amount of water needed to undergo this filtration would be very small compared to the total amount treated at a water treatment plant. It is possible that the economics of using this sort of membrane filtration as part of the polyelectrolyte complexation system is feasible.

This sort of size-based filtration may not be effective for dealing with nanoplastic contamination, as the size of some of the smaller nanoplastics from under 100 nm can begin to approach to size of the polymers. Even in the one phase solution, it is likely that there would be significant interactions between the polyelectrolyte and the PET nanoplastics, as indicated by the adsorption experiments performed previously. Physically separating the polyelectrolytes from the nanoplastics would be difficult. In this case, it would be extremely advantageous to decompose the nanoplastics into molecular components, which could then be dealt with through size based filtration. There is a natural extension of the PETase copolymer complexes here, in which PETase could be used to break down the PET nanoplastics into monomer components with the aid of the polyelectrolytes. As mentioned before, the issue of degradation speed of PETase still needs to be addressed for this to be a viable option. Additionally, there could be extra factors regarding enzymatic degradation of nanoplastics. The size of the nanoplastics may affect the adsorption behavior of the enzymes, and the curvature of the nanoplastics could be a significant factor in the accessibility of the chains to the enzyme active site. At the same time, nanoplastics present a much higher surface area to volume ratio, which could be an advantage for complete degradation of the nanoplastics.

The issue of dealing with residual polymer in treated water may require yet different approaches. Using membrane filtration with very fine pores is an option, but treatment the large amounts of water that pass through water treatment plants is not usually an option. The technique of using pH-sensitive polymers that phase separate from solution may yield some results, but the amount removed at dilute concentrations may not be quantitative. One study showed a reduction in residual polymer concentration of a flocculant by 66% through a phase-separation coarse filtration step. One potential solution is to use monomers that are biodegradable for the polyelectrolytes. It is common for water treatment plants to have a biological remediation step in which organic matter is broken down by naturally occurring bacteria and organisms. Thus, designing random copolymer polyelectrolytes with biodegradable monomers could be an important step in reducing the environmental impact of using these polymers. Since the properties of random copolymer polyelectrolytes rely mostly on sequence correlations and nonspecific interactions, there is flexibility in monomer choice.

Conclusion

The usage of polymers has enabled great advances in standards of living throughout the world. Advances in polymer science has led to the discovery of new materials with unique properties that are suitable for various applications. However, this pursuit has also contributed to many environmental issues as well. The work in this thesis aims to advance our understanding of what polymers are capable of achieving, particularly with the case of remediating environmental damage that may be caused by polymer usage. By utilizing relatively simple concepts of polymer sequence and statistics and electrostatic interactions, we can develop new functionalities and uses for polymer materials that can address these environmental issues. These functionalities have great

similarities to those found in biological systems, and further research may uncover more links between natural and synthetic charged polymer complexes. Exploring and investigating these connections is one way to achieve innovation in the field of polymer science and engineering. This thesis demonstrates that such explorations and studies can yield concrete and quantitative results and advance our knowledge of a novel polymer system.

References

- (1) Rösler, J.; Harders, H.; Bäker, M. *Mechanical Behaviour of Engineering Materials: Metals, Ceramics, Polymers, and Composites*; Springer Science & Business Media, 2007.
- (2) Crawford, R. J.; Martin, P. *Plastics Engineering*; Butterworth-Heinemann, 2020.
- (3) Palacios-Mateo, C.; van der Meer, Y.; Seide, G. Analysis of the Polyester Clothing Value Chain to Identify Key Intervention Points for Sustainability. *Environ Sci Eur* **2021**, *33* (1), 2. <https://doi.org/10.1186/s12302-020-00447-x>.
- (4) Szczepanski, C. R.; Torkelson, J. M. Engineering Surface Hydrophilicity via Polymer Chain-End Segregation in Coatings Formed by Photopolymerization. *ACS Applied Polymer Materials* **2019**, *1* (11), 3095–3102.
- (5) Winkler, H. Climate Change and Developing Countries. *South African Journal of Science* **2005**, *101* (7), 355–364.
- (6) Chen, Y.; Awasthi, A. K.; Wei, F.; Tan, Q.; Li, J. Single-Use Plastics: Production, Usage, Disposal, and Adverse Impacts. *Science of The Total Environment* **2021**, *752*, 141772. <https://doi.org/10.1016/j.scitotenv.2020.141772>.
- (7) Khait, K.; Torkelson, J. M. Solid-State Shear Pulverization of Plastics: A Green Recycling Process. *Polymer-Plastics Technology and Engineering* **1999**, *38* (3), 445–457.
- (8) Maes, T.; McGlade, J.; Fahim, I. S.; Green, D. S.; Landrigan, P.; Andrady, A. L.; Costa, M. F.; Geyer, R.; Gomes, R.; Hwai, A. T. S. *From Pollution to Solution: A Global Assessment of Marine Litter and Plastic Pollution*; United Nations Environment Programme, 2021.
- (9) Bhatt, P.; Pathak, V. M.; Bagheri, A. R.; Bilal, M. Microplastic Contaminants in the Aqueous Environment, Fate, Toxicity Consequences, and Remediation Strategies. *Environmental Research* **2021**, *200*, 111762. <https://doi.org/10.1016/j.envres.2021.111762>.
- (10) Koelmans, A. A.; Bakir, A.; Burton, G. A.; Janssen, C. R. Microplastic as a Vector for Chemicals in the Aquatic Environment: Critical Review and Model-Supported Reinterpretation of Empirical Studies. *Environ. Sci. Technol.* **2016**, *50* (7), 3315–3326. <https://doi.org/10.1021/acs.est.5b06069>.
- (11) Azeem, I.; Adeel, M.; Ahmad, M. A.; Shakoor, N.; Jiangcuo, G. D.; Azeem, K.; Ishfaq, M.; Shakoor, A.; Ayaz, M.; Xu, M.; Rui, Y. Uptake and Accumulation of Nano/Microplastics in Plants: A Critical Review. *Nanomaterials (Basel)* **2021**, *11* (11), 2935. <https://doi.org/10.3390/nano11112935>.
- (12) Enfrin, M.; Dumée, L. F.; Lee, J. Nano/Microplastics in Water and Wastewater Treatment Processes – Origin, Impact and Potential Solutions. *Water Research* **2019**, *161*, 621–638. <https://doi.org/10.1016/j.watres.2019.06.049>.
- (13) Staples, C. A.; Dome, P. B.; Klecka, G. M.; Oblock, S. T.; Harris, L. R. A Review of the Environmental Fate, Effects, and Exposures of Bisphenol A. *Chemosphere* **1998**, *36* (10), 2149–2173. [https://doi.org/10.1016/S0045-6535\(97\)10133-3](https://doi.org/10.1016/S0045-6535(97)10133-3).
- (14) Cooper, J. E.; Kendig, E. L.; Belcher, S. M. Assessment of Bisphenol A Released from Reusable Plastic, Aluminium and Stainless Steel Water Bottles. *Chemosphere* **2011**, *85* (6), 943–947. <https://doi.org/10.1016/j.chemosphere.2011.06.060>.
- (15) Erler, C.; Novak, J. Bisphenol A Exposure: Human Risk and Health Policy. *Journal of Pediatric Nursing* **2010**, *25* (5), 400–407. <https://doi.org/10.1016/j.pedn.2009.05.006>.

- (16) Lamprea, K.; Bressy, A.; Mirande-Bret, C.; Caupos, E.; Gromaire, M.-C. Alkylphenol and Bisphenol A Contamination of Urban Runoff: An Evaluation of the Emission Potentials of Various Construction Materials and Automotive Supplies. *Environ Sci Pollut Res* **2018**, *25* (22), 21887–21900. <https://doi.org/10.1007/s11356-018-2272-z>.
- (17) Arnold, S. M.; Clark, K. E.; Staples, C. A.; Klecka, G. M.; Dimond, S. S.; Caspers, N.; Hentges, S. G. Relevance of Drinking Water as a Source of Human Exposure to Bisphenol A. *J Expo Sci Environ Epidemiol* **2013**, *23* (2), 137–144. <https://doi.org/10.1038/jes.2012.66>.
- (18) Gaines, L. G. T. Historical and Current Usage of Per- and Polyfluoroalkyl Substances (PFAS): A Literature Review. *American Journal of Industrial Medicine* n/a (n/a). <https://doi.org/10.1002/ajim.23362>.
- (19) Post, G. B.; Cohn, P. D.; Cooper, K. R. Perfluorooctanoic Acid (PFOA), an Emerging Drinking Water Contaminant: A Critical Review of Recent Literature. *Environmental Research* **2012**, *116*, 93–117. <https://doi.org/10.1016/j.envres.2012.03.007>.
- (20) Podder, A.; Sadmani, A. H. M. A.; Reinhart, D.; Chang, N.-B.; Goel, R. Per and Poly-Fluoroalkyl Substances (PFAS) as a Contaminant of Emerging Concern in Surface Water: A Transboundary Review of Their Occurrences and Toxicity Effects. *Journal of Hazardous Materials* **2021**, *419*, 126361. <https://doi.org/10.1016/j.jhazmat.2021.126361>.
- (21) Sinclair, G. M.; Long, S. M.; Jones, O. A. H. What Are the Effects of PFAS Exposure at Environmentally Relevant Concentrations? *Chemosphere* **2020**, *258*, 127340. <https://doi.org/10.1016/j.chemosphere.2020.127340>.
- (22) Mishra, S. P. *A Text Book of Fibre Science and Technology*; New Age International, 2000.
- (23) Stamm, A. J. Wood and Cellulose Science. *Wood and cellulose science*. **1964**.
- (24) Dill, K. A.; MacCallum, J. L. The Protein-Folding Problem, 50 Years On. *science* **2012**, *338* (6110), 1042–1046.
- (25) Fersht, A. *Structure and Mechanism in Protein Science: A Guide to Enzyme Catalysis and Protein Folding*; Macmillan, 1999.
- (26) Hall, J. E.; Hall, M. E. *Guyton and Hall Textbook of Medical Physiology E-Book*; Elsevier Health Sciences, 2020.
- (27) Pearse, B. M. Clathrin: A Unique Protein Associated with Intracellular Transfer of Membrane by Coated Vesicles. *Proceedings of the National Academy of Sciences* **1976**, *73* (4), 1255–1259.
- (28) Mazzon, M.; Marsh, M. Targeting Viral Entry as a Strategy for Broad-Spectrum Antivirals. *F1000Research* **2019**, *8*.
- (29) Bownds, D. Site of Attachment of Retinal in Rhodopsin. *Nature* **1967**, *216* (5121), 1178–1181.
- (30) Ridge, K. D.; Abdulaev, N. G.; Sousa, M.; Palczewski, K. Phototransduction: Crystal Clear. *Trends in biochemical sciences* **2003**, *28* (9), 479–487.
- (31) Kinnamon, S. C. Taste Receptor Signalling—from Tongues to Lungs. *Acta physiologica* **2012**, *204* (2), 158–168.
- (32) Wang, J.; Waltmann, C.; Umana-Kossio, H.; Olvera de la Cruz, M.; Torkelson, J. M. Heterogeneous Charged Complexes of Random Copolymers for the Segregation of Organic Molecules. *ACS Central Science* **2021**, *7* (5), 882–891.

- (33) Waltmann, C.; Mills, C. E.; Wang, J.; Qiao, B.; Torkelson, J. M.; Tullman-Ercek, D.; Olvera de la Cruz, M. Functional Enzyme–Polymer Complexes. *Proceedings of the National Academy of Sciences* **2022**, *119* (13), e2119509119.
- (34) Hill, L. J.; Pinna, N.; Char, K.; Pyun, J. Colloidal Polymers from Inorganic Nanoparticle Monomers. *Progress in Polymer Science* **2015**, *40*, 85–120. <https://doi.org/10.1016/j.progpolymsci.2014.08.003>.
- (35) Brunsveld, L.; Folmer, B. J.; Meijer, E. W.; Sijbesma, R. P. Supramolecular Polymers. *Chemical reviews* **2001**, *101* (12), 4071–4098.
- (36) Brazel, C. S.; Rosen, S. L. *Fundamental Principles of Polymeric Materials*; John Wiley & Sons, 2012.
- (37) Clayden, J.; Greeves, N.; Warren, S. *Organic Chemistry*; Oxford university press, 2012.
- (38) O’Neil, G. A.; Torkelson, J. M. Modeling Insight into the Diffusion-Limited Cause of the Gel Effect in Free Radical Polymerization. *Macromolecules* **1999**, *32* (2), 411–422.
- (39) Braunecker, W. A.; Matyjaszewski, K. Controlled/Living Radical Polymerization: Features, Developments, and Perspectives. *Progress in Polymer Science* **2007**, *32* (1), 93–146. <https://doi.org/10.1016/j.progpolymsci.2006.11.002>.
- (40) Gray, M. K.; Zhou, H.; Nguyen, S. T.; Torkelson, J. M. Synthesis and Glass Transition Behavior of High Molecular Weight Styrene/4-Acetoxy styrene and Styrene/4-Hydroxystyrene Gradient Copolymers Made via Nitroxide-Mediated Controlled Radical Polymerization. *Macromolecules* **2004**, *37* (15), 5586–5595.
- (41) Wong, C. L.; Kim, J.; Torkelson, J. M. Breadth of Glass Transition Temperature in Styrene/Acrylic Acid Block, Random, and Gradient Copolymers: Unusual Sequence Distribution Effects. *Journal of Polymer Science Part B: Polymer Physics* **2007**, *45* (20), 2842–2849.
- (42) Wong, C. L.; Kim, J.; Roth, C. B.; Torkelson, J. M. Comparison of Critical Micelle Concentrations of Gradient Copolymer and Block Copolymer in Homopolymer: Novel Characterization by Intrinsic Fluorescence. *Macromolecules* **2007**, *40* (16), 5631–5633.
- (43) Kim, J.; Mok, M. M.; Sandoval, R. W.; Woo, D. J.; Torkelson, J. M. Uniquely Broad Glass Transition Temperatures of Gradient Copolymers Relative to Random and Block Copolymers Containing Repulsive Comonomers. *Macromolecules* **2006**, *39* (18), 6152–6160.
- (44) Li, L.; Marrou, S. R.; Torkelson, J. M. Remarkable Glass Transition Breadths up to 120 K Exhibited by Block-Gradient Copolymers and by Gradient Copolymers Plasticized by Oligomer. *Polymer* **2018**, *151*, 145–153.
- (45) Coleman, M. M. *Fundamentals of Polymer Science: An Introductory Text*; Routledge, 2019.
- (46) Peters, E. N. *Plastics: Thermoplastics, Thermosets, and Elastomers*; Wiley-Interscience, New York, 2002.
- (47) Chakraborty, A. K. Disordered Heteropolymers: Models for Biomimetic Polymers and Polymers with Frustrating Quenched Disorder. *Physics Reports* **2001**, *342* (1), 1–61. [https://doi.org/10.1016/S0370-1573\(00\)00006-5](https://doi.org/10.1016/S0370-1573(00)00006-5).
- (48) Bratko, D.; Chakraborty, A. K.; Shakhnovich, E. I. Recognition between Random Heteropolymers and Multifunctional Disordered Surfaces. *Chemical Physics Letters* **1997**, *280* (1), 46–52. [https://doi.org/10.1016/S0009-2614\(97\)01075-0](https://doi.org/10.1016/S0009-2614(97)01075-0).

- (49) Mammen, M.; Dahmann, G.; Whitesides, G. M. Effective Inhibitors of Hemagglutination by Influenza Virus Synthesized from Polymers Having Active Ester Groups. Insight into Mechanism of Inhibition. *Journal of medicinal chemistry* **1995**, *38* (21), 4179–4190.
- (50) Irbäck, A.; Peterson, C.; Potthast, F. Evidence for Nonrandom Hydrophobicity Structures in Protein Chains. *proceedings of the National Academy of Sciences* **1996**, *93* (18), 9533–9538.
- (51) Nguyen, T. D.; Qiao, B.; Cruz, M. O. de la. Efficient Encapsulation of Proteins with Random Copolymers. *PNAS* **2018**, *115* (26), 6578–6583. <https://doi.org/10.1073/pnas.1806207115>.
- (52) Panganiban, B.; Qiao, B.; Jiang, T.; DelRe, C.; Obadia, M. M.; Nguyen, T. D.; Smith, A. A.; Hall, A.; Sit, I.; Crosby, M. G.; Dennis, P. B.; Drockenmuller, E.; Cruz, M. O. de la; Xu, T. Random Heteropolymers Preserve Protein Function in Foreign Environments. *Science* **2018**, *359* (6381), 1239–1243. <https://doi.org/10.1126/science.aao0335>.
- (53) Dautzenberg, H.; Jaeger, W.; Koetz, J.; Philipp, B.; Seidel, C.; Stscherbina, D. Polyelectrolytes: Formation, Characterization and Application. **1994**.
- (54) Umana-Kossio, H.; Nguyen, T. D.; Wang, J.; Olvera de la Cruz, M.; Torkelson, J. M. Unusual Glass Transition Breadths of Ionomers: Effects of Thermal Treatment and Charge-Carrying Side Chains. *Macromolecules* **2022**, *55* (15), 6536–6546.
- (55) Brereton, M. G.; Vilgis, T. A. Compatibility and Phase Behavior in Charged Polymer Systems and Ionomers. *Macromolecules* **1990**, *23* (7), 2044–2049.
- (56) Baigl, D.; Seery, T. A. P.; Williams, C. E. Preparation and Characterization of Hydrosoluble, Partially Charged Poly(Styrenesulfonate)s of Various Controlled Charge Fractions and Chain Lengths. *Macromolecules* **2002**, *35* (6), 2318–2326. <https://doi.org/10.1021/ma011707o>.
- (57) Visakh, P. M. *Polyelectrolyte: Thermodynamics and Rheology: State of Art, New Challenges and Opportunities*; Springer, 2014.
- (58) Li, L.; Srivastava, S.; Andreev, M.; Marciel, A. B.; de Pablo, J. J.; Tirrell, M. V. Phase Behavior and Salt Partitioning in Polyelectrolyte Complex Coacervates. *Macromolecules* **2018**, *51* (8), 2988–2995. <https://doi.org/10.1021/acs.macromol.8b00238>.
- (59) Stewart, R. J.; Wang, C. S.; Shao, H. Complex Coacervates as a Foundation for Synthetic Underwater Adhesives. *Advances in Colloid and Interface Science* **2011**, *167* (1), 85–93. <https://doi.org/10.1016/j.cis.2010.10.009>.
- (60) Kulkarni, A. D.; Vanjari, Y. H.; Sancheti, K. H.; Patel, H. M.; Belgamwar, V. S.; Surana, S. J.; Pardeshi, C. V. Polyelectrolyte Complexes: Mechanisms, Critical Experimental Aspects, and Applications. *Artificial Cells, Nanomedicine, and Biotechnology* **2016**, *44* (7), 1615–1625. <https://doi.org/10.3109/21691401.2015.1129624>.
- (61) Tompa, P. Intrinsically Disordered Proteins: A 10-Year Recap. *Trends in Biochemical Sciences* **2012**, *37* (12), 509–516. <https://doi.org/10.1016/j.tibs.2012.08.004>.
- (62) Banani, S. F.; Lee, H. O.; Hyman, A. A.; Rosen, M. K. Biomolecular Condensates: Organizers of Cellular Biochemistry. *Nature Reviews Molecular Cell Biology* **2017**, *18* (5), 285–298. <https://doi.org/10.1038/nrm.2017.7>.
- (63) Mao, Y. S.; Zhang, B.; Spector, D. L. Biogenesis and Function of Nuclear Bodies. *Trends in Genetics* **2011**, *27* (8), 295–306. <https://doi.org/10.1016/j.tig.2011.05.006>.

- (64) Protter, D. S. W.; Parker, R. Principles and Properties of Stress Granules. *Trends in Cell Biology* **2016**, *26* (9), 668–679. <https://doi.org/10.1016/j.tcb.2016.05.004>.
- (65) Ryan, V. H.; Fawzi, N. L. Physiological, Pathological, and Targetable Membraneless Organelles in Neurons. *Trends Neurosci* **2019**, *42* (10), 693–708. <https://doi.org/10.1016/j.tins.2019.08.005>.
- (66) Chakraborty, A. K. Disordered Heteropolymers: Models for Biomimetic Polymers and Polymers with Frustrating Quenched Disorder. *Physics Reports* **2001**, *342* (1), 1–61. [https://doi.org/10.1016/S0370-1573\(00\)00006-5](https://doi.org/10.1016/S0370-1573(00)00006-5).
- (67) Srebnik, S.; Chakraborty, A. K.; Shakhnovich, E. I. Adsorption-Freezing Transition for Random Heteropolymers near Disordered 2D Manifolds Due to “Pattern Matching”. *Phys. Rev. Lett.* **1996**, *77* (15), 3157–3160. <https://doi.org/10.1103/PhysRevLett.77.3157>.
- (68) Polotsky, A.; Schmid, F.; Degenhard, A. Polymer Adsorption onto Random Planar Surfaces: Interplay of Polymer and Surface Correlations. *J. Chem. Phys.* **2004**, *121* (10), 4853–4864. <https://doi.org/10.1063/1.1778137>.
- (69) Sing, C. E.; Perry, S. L. Recent Progress in the Science of Complex Coacervation. *Soft Matter* **2020**, *16* (12), 2885–2914. <https://doi.org/10.1039/D0SM00001A>.
- (70) Thünemann, A. F.; Müller, M.; Dautzenberg, H.; Joanny, J.-F.; Löwen, H. Polyelectrolyte Complexes. In *Polyelectrolytes with Defined Molecular Architecture II*; Schmidt, M., Ed.; Advances in Polymer Science; Springer: Berlin, Heidelberg, 2004; pp 113–171. <https://doi.org/10.1007/b11350>.
- (71) Priftis, D.; Xia, X.; Margossian, K. O.; Perry, S. L.; Leon, L.; Qin, J.; de Pablo, J. J.; Tirrell, M. Ternary, Tunable Polyelectrolyte Complex Fluids Driven by Complex Coacervation. *Macromolecules* **2014**, *47* (9), 3076–3085. <https://doi.org/10.1021/ma500245j>.
- (72) Chang, L.-W.; Lytle, T. K.; Radhakrishna, M.; Madinya, J. J.; Vélez, J.; Sing, C. E.; Perry, S. L. Sequence and Entropy-Based Control of Complex Coacervates. *Nature Communications* **2017**, *8* (1), 1273. <https://doi.org/10.1038/s41467-017-01249-1>.
- (73) Lytle, T. K.; Chang, L.-W.; Markiewicz, N.; Perry, S. L.; Sing, C. E. Designing Electrostatic Interactions via Polyelectrolyte Monomer Sequence. *ACS Cent. Sci.* **2019**, *5* (4), 709–718. <https://doi.org/10.1021/acscentsci.9b00087>.
- (74) Ghasemi, M.; Larson, R. G. Role of Electrostatic Interactions in Charge Regulation of Weakly Dissociating Polyacids. *Progress in Polymer Science* **2021**, *112*, 101322. <https://doi.org/10.1016/j.progpolymsci.2020.101322>.
- (75) Perry, S. L.; Li, Y.; Priftis, D.; Leon, L.; Tirrell, M. The Effect of Salt on the Complex Coacervation of Vinyl Polyelectrolytes. *Polymers* **2014**, *6* (6), 1756–1772. <https://doi.org/10.3390/polym6061756>.
- (76) Ghasemi, M.; Friedowitz, S.; Larson, R. G. Analysis of Partitioning of Salt through Doping of Polyelectrolyte Complex Coacervates. *Macromolecules* **2020**, *53* (16), 6928–6945. <https://doi.org/10.1021/acs.macromol.0c00797>.
- (77) Friedowitz, S.; Salehi, A.; Larson, R. G.; Qin, J. Role of Electrostatic Correlations in Polyelectrolyte Charge Association. *J. Chem. Phys.* **2018**, *149* (16), 163335. <https://doi.org/10.1063/1.5034454>.
- (78) Li, L.; Rumyantsev, A. M.; Srivastava, S.; Meng, S.; de Pablo, J. J.; Tirrell, M. V. Effect of Solvent Quality on the Phase Behavior of Polyelectrolyte Complexes. *Macromolecules* **2021**, *54* (1), 105–114. <https://doi.org/10.1021/acs.macromol.0c01000>.

- (79) Meka, V. S.; Sing, M. K. G.; Pichika, M. R.; Nali, S. R.; Kolapalli, V. R. M.; Kesharwani, P. A Comprehensive Review on Polyelectrolyte Complexes. *Drug Discovery Today* **2017**, *22* (11), 1697–1706. <https://doi.org/10.1016/j.drudis.2017.06.008>.
- (80) Gucht, J. van der; Spruijt, E.; Lemmers, M.; Cohen Stuart, M. A. Polyelectrolyte Complexes: Bulk Phases and Colloidal Systems. *Journal of Colloid and Interface Science* **2011**, *361* (2), 407–422. <https://doi.org/10.1016/j.jcis.2011.05.080>.
- (81) Romyantsev, A. M.; Jackson, N. E.; de Pablo, J. J. Polyelectrolyte Complex Coacervates: Recent Developments and New Frontiers. *Annu. Rev. Condens. Matter Phys.* **2021**, *12* (1), 155–176. <https://doi.org/10.1146/annurev-conmatphys-042020-113457>.
- (82) Delair, T. Colloidal Polyelectrolyte Complexes of Chitosan and Dextran Sulfate towards Versatile Nanocarriers of Bioactive Molecules. *European Journal of Pharmaceutics and Biopharmaceutics* **2011**, *78* (1), 10–18. <https://doi.org/10.1016/j.ejpb.2010.12.001>.
- (83) Raik, S. V.; Gasilova, E. R.; Dubashynskaya, N. V.; Dobrodumov, A. V.; Skorik, Y. A. Diethylaminoethyl Chitosan–Hyaluronic Acid Polyelectrolyte Complexes. *International Journal of Biological Macromolecules* **2020**, *146*, 1161–1168. <https://doi.org/10.1016/j.ijbiomac.2019.10.054>.
- (84) Vecchies, F.; Sacco, P.; Decleva, E.; Menegazzi, R.; Porrelli, D.; Donati, I.; Turco, G.; Paoletti, S.; Marsich, E. Complex Coacervates between a Lactose-Modified Chitosan and Hyaluronic Acid as Radical-Scavenging Drug Carriers. *Biomacromolecules* **2018**, *19* (10), 3936–3944. <https://doi.org/10.1021/acs.biomac.8b00863>.
- (85) Zhao, M.; Zacharia, N. S. Protein Encapsulation via Polyelectrolyte Complex Coacervation: Protection against Protein Denaturation. *J. Chem. Phys.* **2018**, *149* (16), 163326. <https://doi.org/10.1063/1.5040346>.
- (86) Lindhoud, S.; E. Claessens, M. M. A. Accumulation of Small Protein Molecules in a Macroscopic Complex Coacervate. *Soft Matter* **2016**, *12* (2), 408–413. <https://doi.org/10.1039/C5SM02386F>.
- (87) K. Nakashima, K.; F. Baaij, J.; Spruijt, E. Reversible Generation of Coacervate Droplets in an Enzymatic Network. *Soft Matter* **2018**, *14* (3), 361–367. <https://doi.org/10.1039/C7SM01897E>.
- (88) Petzold, G.; Schwarz, S. Polyelectrolyte Complexes in Flocculation Applications. In *Polyelectrolyte Complexes in the Dispersed and Solid State II: Application Aspects*; Müller, M., Ed.; Advances in Polymer Science; Springer: Berlin, Heidelberg, 2014; pp 25–65. https://doi.org/10.1007/12_2012_205.
- (89) Balea, A.; Concepcion Monte, M.; Fuente, E.; Luis Sanchez-Salvador, J.; Blanco, A.; Negro, C. Cellulose Nanofibers and Chitosan to Remove Flexographic Inks from Wastewaters. *Environmental Science: Water Research & Technology* **2019**, *5* (9), 1558–1567. <https://doi.org/10.1039/C9EW00434C>.
- (90) Ghosh, M. M.; Cox, C. D.; Prakash, T. M. Polyelectrolyte Selection for Water Treatment. *Journal AWWA* **1985**, *77* (3), 67–73. <https://doi.org/10.1002/j.1551-8833.1985.tb05510.x>.
- (91) Vajihinejad, V.; Gumfekar, S. P.; Bazoubandi, B.; Najafabadi, Z. R.; Soares, J. B. P. Water Soluble Polymer Flocculants: Synthesis, Characterization, and Performance Assessment. *Macromolecular Materials and Engineering* **2019**, *304* (2), 1800526. <https://doi.org/10.1002/mame.201800526>.

- (92) Yu, L.; Liu, X.; Yuan, W.; Brown, L. J.; Wang, D. Confined Flocculation of Ionic Pollutants by Poly(l-Dopa)-Based Polyelectrolyte Complexes in Hydrogel Beads for Three-Dimensional, Quantitative, Efficient Water Decontamination. *Langmuir* **2015**, *31* (23), 6351–6366. <https://doi.org/10.1021/acs.langmuir.5b01084>.
- (93) Zhao, M.; Eghtesadi, S. A.; Dawadi, M. B.; Wang, C.; Huang, S.; Seymore, A. E.; Vogt, B. D.; Modarelli, D. A.; Liu, T.; Zacharia, N. S. Partitioning of Small Molecules in Hydrogen-Bonding Complex Coacervates of Poly(Acrylic Acid) and Poly(Ethylene Glycol) or Pluronic Block Copolymer. *Macromolecules* **2017**, *50* (10), 3818–3830. <https://doi.org/10.1021/acs.macromol.6b02815>.
- (94) Huang, S.; Zhao, M.; Dawadi, M. B.; Cai, Y.; Lapitsky, Y.; Modarelli, D. A.; Zacharia, N. S. Effect of Small Molecules on the Phase Behavior and Coacervation of Aqueous Solutions of Poly(Diallyldimethylammonium Chloride) and Poly(Sodium 4-Styrene Sulfonate). *Journal of Colloid and Interface Science* **2018**, *518*, 216–224. <https://doi.org/10.1016/j.jcis.2018.02.029>.
- (95) Zhao, M.; Zacharia, N. S. Sequestration of Methylene Blue into Polyelectrolyte Complex Coacervates. *Macromolecular Rapid Communications* **2016**, *37* (15), 1249–1255. <https://doi.org/10.1002/marc.201600244>.
- (96) Zhao, M.; Wang, C.; Jiang, H.; B. Dawadi, M.; D. Vogt, B.; A. Modarelli, D.; S. Zacharia, N. Polyelectrolyte–Micelle Coacervates: Intrapolymer-Dominant vs. Interpolymer-Dominant Association, Solute Uptake and Rheological Properties. *Soft Matter* **2019**, *15* (14), 3043–3054. <https://doi.org/10.1039/C8SM02229A>.
- (97) Terashima, T.; Sugita, T.; Fukae, K.; Sawamoto, M. Synthesis and Single-Chain Folding of Amphiphilic Random Copolymers in Water. *Macromolecules* **2014**, *47* (2), 589–600. <https://doi.org/10.1021/ma402355v>.
- (98) Swift, B. W.; Cruz, M. O. de la. Random Copolymers in Concentrated Solutions. *EPL* **1996**, *35* (7), 487. <https://doi.org/10.1209/epl/i1996-00140-7>.
- (99) Ma, B.; Nguyen, T. D.; Pryamitsyn, V. A.; Olvera de la Cruz, M. Ionic Correlations in Random Ionomers. *ACS Nano* **2018**, *12* (3), 2311–2318. <https://doi.org/10.1021/acsnano.7b07432>.
- (100) Ma, B.; Nguyen, T. D.; Olvera de la Cruz, M. Control of Ionic Mobility via Charge Size Asymmetry in Random Ionomers. *Nano Lett.* **2020**, *20* (1), 43–49. <https://doi.org/10.1021/acs.nanolett.9b02743>.
- (101) Cochin, D.; De Schryver, F. C.; Laschewsky, A.; van Stam, J. Polysoaps in Aqueous Solutions: Intermolecular versus Intramolecular Hydrophobic Aggregation Studied by Fluorescence Spectroscopy. *Langmuir* **2001**, *17* (9), 2579–2584. <https://doi.org/10.1021/la0011329>.
- (102) Cowie, J. M. G. *Polymers: Chemistry and Physics of Modern Materials, 2nd Edition*; Taylor & Francis, 1991.
- (103) Nayak, R. R.; Roy, S.; Dey, J. Characterization and Self-Assembly of Poly[Sodium N-(11-Acrylamidoundecanoyl)-l-Alaninate] in Water. *Polymer* **2005**, *46* (26), 12401–12409. <https://doi.org/10.1016/j.polymer.2005.10.127>.
- (104) Aydogan, C.; Ciftci, M.; Yagci, Y. Hyperbranched Polymers by Type II Photoinitiated Self-Condensing Vinyl Polymerization. *Macromolecular Rapid Communications* **2016**, *37* (7), 650–654. <https://doi.org/10.1002/marc.201500721>.

- (105) Maniego, A. R.; Sutton, A. T.; Gaborieau, M.; Castignolles, P. Assessment of the Branching Quantification in Poly(Acrylic Acid): Is It as Easy as It Seems? *Macromolecules* **2017**, *50* (22), 9032–9041. <https://doi.org/10.1021/acs.macromol.7b01411>.
- (106) Matilainen, A.; Vepsäläinen, M.; Sillanpää, M. Natural Organic Matter Removal by Coagulation during Drinking Water Treatment: A Review. *Advances in Colloid and Interface Science* **2010**, *159* (2), 189–197. <https://doi.org/10.1016/j.cis.2010.06.007>.
- (107) Dautzenberg, H.; Karibyants, N. Polyelectrolyte Complex Formation in Highly Aggregating Systems. Effect of Salt: Response to Subsequent Addition of NaCl. *Macromolecular Chemistry and Physics* **1999**, *200* (1), 118–125. [https://doi.org/10.1002/\(SICI\)1521-3935\(19990101\)200:1<118::AID-MACP118>3.0.CO;2-K](https://doi.org/10.1002/(SICI)1521-3935(19990101)200:1<118::AID-MACP118>3.0.CO;2-K).
- (108) Petcu, A. R.; Rogozea, E. A.; Lazar, C. A.; Olteanu, N. L.; Meghea, A.; Mihaly, M. Specific Interactions within Micelle Microenvironment in Different Charged Dye/Surfactant Systems. *Arabian Journal of Chemistry* **2016**, *9* (1), 9–17. <https://doi.org/10.1016/j.arabjc.2015.09.009>.
- (109) Roshchyna, K. V.; Eltsov, S. V.; Laguta, A. N.; Mchedlov-Petrossyan, N. O. Micellar Rate Effects in the Alkaline Fading of Crystal Violet in the Presence of Various Surfactants. *Journal of Molecular Liquids* **2015**, *201*, 77–82. <https://doi.org/10.1016/j.molliq.2014.11.013>.
- (110) Kudlay, A.; Olvera de la Cruz, M. Precipitation of Oppositely Charged Polyelectrolytes in Salt Solutions. *J. Chem. Phys.* **2003**, *120* (1), 404–412. <https://doi.org/10.1063/1.1629271>.
- (111) Shakya, A.; Girard, M.; King, J. T.; Olvera de la Cruz, M. Role of Chain Flexibility in Asymmetric Polyelectrolyte Complexation in Salt Solutions. *Macromolecules* **2020**, *53* (4), 1258–1269. <https://doi.org/10.1021/acs.macromol.9b02355>.
- (112) Romyantsev, A. M.; de Pablo, J. J. Microphase Separation in Polyelectrolyte Blends: Weak Segregation Theory and Relation to Nuclear “Pasta.” *Macromolecules* **2020**, *53* (4), 1281–1292. <https://doi.org/10.1021/acs.macromol.9b02466>.
- (113) Painter, Paul C.; Coleman, Michael M. *Fundamentals of Polymer Science: An Introductory Text*, 2nd ed.; Technomic: Lancaster, Pennsylvania, 1997.
- (114) Halperin, A. On the Collapse of Multiblock Copolymers. *Macromolecules* **1991**, *24* (6), 1418–1419. <https://doi.org/10.1021/ma00006a033>.
- (115) Nesarikar, A.; Olvera de la Cruz, M.; Crist, B. Phase Transitions in Random Copolymers. *J. Chem. Phys.* **1993**, *98* (9), 7385–7397. <https://doi.org/10.1063/1.464729>.
- (116) Shen, M.; Zhang, Y.; Zhu, Y.; Song, B.; Zeng, G.; Hu, D.; Wen, X.; Ren, X. Recent Advances in Toxicological Research of Nanoplastics in the Environment: A Review. *Environmental Pollution* **2019**, *252*, 511–521. <https://doi.org/10.1016/j.envpol.2019.05.102>.
- (117) Bo, G.; Wesslén, B.; Wesslén, K. B. Amphiphilic Comb-Shaped Polymers from Poly(Ethylene Glycol) Macromonomers. *Journal of Polymer Science Part A: Polymer Chemistry* **1992**, *30* (9), 1799–1808. <https://doi.org/10.1002/pola.1992.080300903>.
- (118) Marrink, S. J.; Risselada, H. J.; Yefimov, S.; Tieleman, D. P.; de Vries, A. H. The MARTINI Force Field: Coarse Grained Model for Biomolecular Simulations. *J. Phys. Chem. B* **2007**, *111* (27), 7812–7824. <https://doi.org/10.1021/jp071097f>.

- (119) Grunewald, F.; Rossi, G.; de Vries, A. H.; Marrink, S. J.; Monticelli, L. Transferable MARTINI Model of Poly(Ethylene Oxide). *J. Phys. Chem. B* **2018**, *122* (29), 7436–7449. <https://doi.org/10.1021/acs.jpcc.8b04760>.
- (120) Anderson, J. A.; Lorenz, C. D.; Travesset, A. General Purpose Molecular Dynamics Simulations Fully Implemented on Graphics Processing Units. *Journal of Computational Physics* **2008**, *227* (10), 5342–5359. <https://doi.org/10.1016/j.jcp.2008.01.047>.
- (121) Weeks, J. D.; Chandler, D.; Andersen, H. C. Role of Repulsive Forces in Determining the Equilibrium Structure of Simple Liquids. *J. Chem. Phys.* **1971**, *54* (12), 5237–5247. <https://doi.org/10.1063/1.1674820>.
- (122) N. LeBard, D.; G. Levine, B.; Mertmann, P.; A. Barr, S.; Jusufi, A.; Sanders, S.; L. Klein, M.; Z. Panagiotopoulos, A. Self-Assembly of Coarse-Grained Ionic Surfactants Accelerated by Graphics Processing Units. *Soft Matter* **2012**, *8* (8), 2385–2397. <https://doi.org/10.1039/C1SM06787G>.
- (123) Yesylevskyy, S. O.; Schäfer, L. V.; Sengupta, D.; Marrink, S. J. Polarizable Water Model for the Coarse-Grained MARTINI Force Field. *PLOS Computational Biology* **2010**, *6* (6), e1000810. <https://doi.org/10.1371/journal.pcbi.1000810>.
- (124) Campos-Villalobos, G.; R. Siperstein, F.; Patti, A. Transferable Coarse-Grained MARTINI Model for Methacrylate-Based Copolymers. *Molecular Systems Design & Engineering* **2019**, *4* (1), 186–198. <https://doi.org/10.1039/C8ME00064F>.
- (125) Zhang, K.; Hamidian, A. H.; Tubić, A.; Zhang, Y.; Fang, J. K. H.; Wu, C.; Lam, P. K. S. Understanding Plastic Degradation and Microplastic Formation in the Environment: A Review. *Environmental Pollution* **2021**, *274*, 116554. <https://doi.org/10.1016/j.envpol.2021.116554>.
- (126) Tziourrou, P.; Kordella, S.; Ardali, Y.; Papatheodorou, G.; Karapanagioti, H. K. Microplastics Formation Based on Degradation Characteristics of Beached Plastic Bags. *Marine Pollution Bulletin* **2021**, *169*, 112470. <https://doi.org/10.1016/j.marpolbul.2021.112470>.
- (127) Naik, R. A.; Rowles, L. S.; Hossain, A. I.; Yen, M.; Aldossary, R. M.; Apul, O. G.; Conkle, J.; Saleh, N. B. Microplastic Particle versus Fiber Generation during Photo-Transformation in Simulated Seawater. *Science of The Total Environment* **2020**, *736*, 139690. <https://doi.org/10.1016/j.scitotenv.2020.139690>.
- (128) Rai, P. K.; Lee, J.; Brown, R. J. C.; Kim, K.-H. Micro- and Nano-Plastic Pollution: Behavior, Microbial Ecology, and Remediation Technologies. *Journal of Cleaner Production* **2021**, *291*, 125240. <https://doi.org/10.1016/j.jclepro.2020.125240>.
- (129) Jiang, B.; Kauffman, A. E.; Li, L.; McFee, W.; Cai, B.; Weinstein, J.; Lead, J. R.; Chatterjee, S.; Scott, G. I.; Xiao, S. Health Impacts of Environmental Contamination of Micro- and Nanoplastics: A Review. *Environ Health Prev Med* **2020**, *25* (1), 29. <https://doi.org/10.1186/s12199-020-00870-9>.
- (130) Gao, X.; Hassan, I.; Peng, Y.; Huo, S.; Ling, L. Behaviors and Influencing Factors of the Heavy Metals Adsorption onto Microplastics: A Review. *Journal of Cleaner Production* **2021**, *319*, 128777. <https://doi.org/10.1016/j.jclepro.2021.128777>.
- (131) Ramirez Arenas, L.; Ramseier Gentile, S.; Zimmermann, S.; Stoll, S. Nanoplastics Adsorption and Removal Efficiency by Granular Activated Carbon Used in Drinking Water

- Treatment Process. *Science of The Total Environment* **2021**, 791, 148175. <https://doi.org/10.1016/j.scitotenv.2021.148175>.
- (132) Yu, F.; Yang, C.; Zhu, Z.; Bai, X.; Ma, J. Adsorption Behavior of Organic Pollutants and Metals on Micro/Nanoplastics in the Aquatic Environment. *Science of The Total Environment* **2019**, 694, 133643. <https://doi.org/10.1016/j.scitotenv.2019.133643>.
- (133) Yee, M. S.-L.; Hii, L.-W.; Looi, C. K.; Lim, W.-M.; Wong, S.-F.; Kok, Y.-Y.; Tan, B.-K.; Wong, C.-Y.; Leong, C.-O. Impact of Microplastics and Nanoplastics on Human Health. *Nanomaterials* **2021**, 11 (2), 496. <https://doi.org/10.3390/nano11020496>.
- (134) Mitrano, D. M.; Wick, P.; Nowack, B. Placing Nanoplastics in the Context of Global Plastic Pollution. *Nat. Nanotechnol.* **2021**, 16 (5), 491–500. <https://doi.org/10.1038/s41565-021-00888-2>.
- (135) Kang, J.; Zhou, L.; Duan, X.; Sun, H.; Ao, Z.; Wang, S. Degradation of Cosmetic Microplastics via Functionalized Carbon Nanosprings. *Matter* **2019**, 1 (3), 745–758. <https://doi.org/10.1016/j.matt.2019.06.004>.
- (136) Tofa, T. S.; Kunjali, K. L.; Paul, S.; Dutta, J. Visible Light Photocatalytic Degradation of Microplastic Residues with Zinc Oxide Nanorods. *Environ Chem Lett* **2019**, 17 (3), 1341–1346. <https://doi.org/10.1007/s10311-019-00859-z>.
- (137) Akarsu, C.; Deniz, F. Electrocoagulation/Electroflotation Process for Removal of Organics and Microplastics in Laundry Wastewater. *CLEAN – Soil, Air, Water* **2021**, 49 (1), 2000146. <https://doi.org/10.1002/clen.202000146>.
- (138) Perren, W.; Wojtasik, A.; Cai, Q. Removal of Microbeads from Wastewater Using Electrocoagulation. *ACS Omega* **2018**, 3 (3), 3357–3364. <https://doi.org/10.1021/acsomega.7b02037>.
- (139) Zhang, Y.; Diehl, A.; Lewandowski, A.; Gopalakrishnan, K.; Baker, T. Removal Efficiency of Micro- and Nanoplastics (180 Nm-125 Mm) during Drinking Water Treatment. *Sci Total Environ* **2020**, 720, 137383. <https://doi.org/10.1016/j.scitotenv.2020.137383>.
- (140) Bratby, J. *Coagulation and Flocculation in Water and Wastewater Treatment*; IWA publishing, 2016.
- (141) Zhang, Y.; Wang, X.; Li, Y.; Wang, H.; Shi, Y.; Li, Y.; Zhang, Y. Improving Nanoplastic Removal by Coagulation: Impact Mechanism of Particle Size and Water Chemical Conditions. *Journal of Hazardous Materials* **2022**, 425, 127962. <https://doi.org/10.1016/j.jhazmat.2021.127962>.
- (142) Chen, Z.; Liu, J.; Chen, C.; Huang, Z. Sedimentation of Nanoplastics from Water with Ca/Al Dual Flocculants: Characterization, Interface Reaction, Effects of PH and Ion Ratios. *Chemosphere* **2020**, 252, 126450. <https://doi.org/10.1016/j.chemosphere.2020.126450>.
- (143) M. Hofman-Caris, C. H.; S. Bäuerlein, P.; G. Siegers, W.; M. Mintenig, S.; Messina, R.; C. Dekker, S.; Bertelkamp, C.; R. Cornelissen, E.; Wezel, A. P. van. Removal of Nanoparticles (Both Inorganic Nanoparticles and Nanoplastics) in Drinking Water Treatment – Coagulation/Flocculation/Sedimentation, and Sand/Granular Activated Carbon Filtration. *Environmental Science: Water Research & Technology* **2022**, 8 (8), 1675–1686. <https://doi.org/10.1039/D2EW00226D>.

- (144) Bayarkhuu, B.; Byun, J. Optimization of Coagulation and Sedimentation Conditions by Turbidity Measurement for Nano- and Microplastic Removal. *Chemosphere* **2022**, *306*, 135572. <https://doi.org/10.1016/j.chemosphere.2022.135572>.
- (145) Murray, A.; Örmeci, B. Removal Effectiveness of Nanoplastics (<400 Nm) with Separation Processes Used for Water and Wastewater Treatment. *Water* **2020**, *12* (3), 635. <https://doi.org/10.3390/w12030635>.
- (146) Rathee, V. S.; Zervoudakis, A. J.; Sidky, H.; Sikora, B. J.; Whitmer, J. K. Weak Polyelectrolyte Complexation Driven by Associative Charging. *The Journal of Chemical Physics* **2018**, *148* (11), 114901.
- (147) Zhang, P.; Alsaifi, N. M.; Wu, J.; Wang, Z.-G. Salting-out and Salting-in of Polyelectrolyte Solutions: A Liquid-State Theory Study. *Macromolecules* **2016**, *49* (24), 9720–9730.
- (148) Prusty, D.; Nap, R. J.; Szleifer, I.; De La Cruz, M. O. Charge Regulation Mechanism in End-Tethered Weak Polyampholytes. *Soft Matter* **2020**, *16* (38), 8832–8847.
- (149) Rumyantsev, A. M.; Jackson, N. E.; Yu, B.; Ting, J. M.; Chen, W.; Tirrell, M. V.; De Pablo, J. J. Controlling Complex Coacervation via Random Polyelectrolyte Sequences. *ACS Macro Letters* **2019**, *8* (10), 1296–1302.
- (150) Cardellini, A.; Jiménez-Ángeles, F.; Asinari, P.; Olvera de la Cruz, M. A Modeling-Based Design to Engineering Protein Hydrogels with Random Copolymers. *ACS nano* **2021**, *15* (10), 16139–16148.
- (151) McTigue, W. C. B.; Perry, S. L. Design Rules for Encapsulating Proteins into Complex Coacervates. *Soft Matter* **2019**, *15* (15), 3089–3103.
- (152) Horn, J. M.; Kapelner, R. A.; Obermeyer, A. C. Macro- and Microphase Separated Protein-Polyelectrolyte Complexes: Design Parameters and Current Progress. *Polymers* **2019**, *11* (4), 578. <https://doi.org/10.3390/polym11040578>.
- (153) Mills, C. E.; Obermeyer, A.; Dong, X.; Walker, J.; Olsen, B. D. Complex Coacervate Core Micelles for the Dispersion and Stabilization of Organophosphate Hydrolase in Organic Solvents. *Langmuir* **2016**, *32* (50), 13367–13376.
- (154) Kriksin, Y. A.; Khalatur, P. G.; Khokhlov, A. R. Recognition of Complex Patterned Substrates by Heteropolymer Chains Consisting of Multiple Monomer Types. *J. Chem. Phys.* **2006**, *124* (17), 174904. <https://doi.org/10.1063/1.2191849>.
- (155) DelRe, C.; Jiang, Y.; Kang, P.; Kwon, J.; Hall, A.; Jayapurna, I.; Ruan, Z.; Ma, L.; Zolkin, K.; Li, T.; Scown, C. D.; Ritchie, R. O.; Russell, T. P.; Xu, T. Near-Complete Depolymerization of Polyesters with Nano-Dispersed Enzymes. *Nature* **2021**, *592* (7855), 558–563. <https://doi.org/10.1038/s41586-021-03408-3>.
- (156) Shull, K. R.; Taghon, M.; Wang, Q. Investigations of the High-Frequency Dynamic Properties of Polymeric Systems with Quartz Crystal Resonators. *Biointerphases* **2020**, *15* (2), 021012.
- (157) De Gennes, P. G. Scaling Theory of Polymer Adsorption. *Journal de physique* **1976**, *37* (12), 1445–1452.
- (158) Johner, A.; Joanny, J. F. Polymer Adsorption in a Poor Solvent. *Journal de Physique II* **1991**, *1* (2), 181–194.
- (159) Ge, T.; Rubinstein, M. Strong Selective Adsorption of Polymers. *Macromolecules* **2015**, *48* (11), 3788–3801. <https://doi.org/10.1021/acs.macromol.5b00586>.

- (160) Cao, J.; Yang, Q.; Jiang, J.; Dalu, T.; Kadushkin, A.; Singh, J.; Fakhrullin, R.; Wang, F.; Cai, X.; Li, R. Coronas of Micro/Nano Plastics: A Key Determinant in Their Risk Assessments. *Particle and Fibre Toxicology* **2022**, *19* (1), 55.
<https://doi.org/10.1186/s12989-022-00492-9>.
- (161) Coon, M. J. Cytochrome P450: Nature's Most Versatile Biological Catalyst. *Annu. Rev. Pharmacol. Toxicol.* **2005**, *45*, 1–25.
- (162) Martinez, C. A.; Rupasinghe, S. G. Cytochrome P450 Bioreactors in the Pharmaceutical Industry: Challenges and Opportunities. *Current topics in medicinal chemistry* **2013**, *13* (12), 1470–1490.
- (163) Sureka, H. V.; Obermeyer, A. C.; Flores, R. J.; Olsen, B. D. Catalytic Biosensors from Complex Coacervate Core Micelle (C3M) Thin Films. *ACS applied materials & interfaces* **2019**, *11* (35), 32354–32365.
- (164) Blank, L. M.; Narancic, T.; Mampel, J.; Tiso, T.; O'Connor, K. Biotechnological Upcycling of Plastic Waste and Other Non-Conventional Feedstocks in a Circular Economy. *Current opinion in biotechnology* **2020**, *62*, 212–219.
- (165) Cózar, A.; Echevarría, F.; González-Gordillo, J. I.; Irigoien, X.; Úbeda, B.; Hernández-León, S.; Palma, Á. T.; Navarro, S.; García-de-Lomas, J.; Ruiz, A. Plastic Debris in the Open Ocean. *Proceedings of the National Academy of Sciences* **2014**, *111* (28), 10239–10244.
- (166) Jambeck, J. R.; Geyer, R.; Wilcox, C.; Siegler, T. R.; Perryman, M.; Andrady, A.; Narayan, R.; Law, K. L. Plastic Waste Inputs from Land into the Ocean. *Science* **2015**, *347* (6223), 768–771.
- (167) Smith, M.; Love, D. C.; Rochman, C. M.; Neff, R. A. Microplastics in Seafood and the Implications for Human Health. *Curr Environ Health Rep* **2018**, *5* (3), 375–386.
<https://doi.org/10.1007/s40572-018-0206-z>.
- (168) Arnold, F. H. Directed Evolution: Bringing New Chemistry to Life. *Angewandte Chemie International Edition* **2018**, *57* (16), 4143–4148.
- (169) Dubey, N. C.; Tripathi, B. P. Nature Inspired Multienzyme Immobilization: Strategies and Concepts. *ACS Applied Bio Materials* **2021**, *4* (2), 1077–1114.
- (170) Son, H. F.; Cho, I. J.; Joo, S.; Seo, H.; Sagong, H.-Y.; Choi, S. Y.; Lee, S. Y.; Kim, K.-J. Rational Protein Engineering of Thermo-Stable PETase from *Ideonella Sakaiensis* for Highly Efficient PET Degradation. *ACS Catalysis* **2019**, *9* (4), 3519–3526.
- (171) Austin, H. P.; Allen, M. D.; Donohoe, B. S.; Rorrer, N. A.; Kearns, F. L.; Silveira, R. L.; Pollard, B. C.; Dominick, G.; Duman, R.; Omari, K. E.; Mykhaylyk, V.; Wagner, A.; Michener, W. E.; Amore, A.; Skaf, M. S.; Crowley, M. F.; Thorne, A. W.; Johnson, C. W.; Woodcock, H. L.; McGeehan, J. E.; Beckham, G. T. Characterization and Engineering of a Plastic-Degrading Aromatic Polyesterase. *PNAS* **2018**, *115* (19), E4350–E4357.
<https://doi.org/10.1073/pnas.1718804115>.
- (172) Kapelner, R. A.; Yeong, V.; Obermeyer, A. C. Molecular Determinants of Protein-Based Coacervates. *Current Opinion in Colloid & Interface Science* **2021**, *52*, 101407.
- (173) Cummings, C. S.; Obermeyer, A. C. Phase Separation Behavior of Supercharged Proteins and Polyelectrolytes. *Biochemistry* **2018**, *57* (3), 314–323.

- (174) Fecker, T.; Galaz-Davison, P.; Engelberger, F.; Narui, Y.; Sotomayor, M.; Parra, L. P.; Ramírez-Sarmiento, C. A. Active Site Flexibility as a Hallmark for Efficient PET Degradation by *I. Sakaiensis* PETase. *Biophysical Journal* **2018**, *114* (6), 1302–1312.
- (175) Kim, S.; Sureka, H. V.; Kayitmazer, A. B.; Wang, G.; Swan, J. W.; Olsen, B. D. Effect of Protein Surface Charge Distribution on Protein–Polyelectrolyte Complexation. *Biomacromolecules* **2020**, *21* (8), 3026–3037.
- (176) Blaha-Nelson, D.; Kruger, D. M.; Szeler, K.; Ben-David, M.; Kamerlin, S. C. L. Active Site Hydrophobicity and the Convergent Evolution of Paraoxonase Activity in Structurally Divergent Enzymes: The Case of Serum Paraoxonase 1. *Journal of the American Chemical Society* **2017**, *139* (3), 1155–1167.
- (177) Tournier, V.; Topham, C. M.; Gilles, A.; David, B.; Folgoas, C.; Moya-Leclair, E.; Kamionka, E.; Desrousseaux, M.-L.; Texier, H.; Gavalda, S.; Cot, M.; Guémard, E.; Dalibey, M.; Nomme, J.; Cioci, G.; Barbe, S.; Chateau, M.; André, I.; Duquesne, S.; Marty, A. An Engineered PET Depolymerase to Break down and Recycle Plastic Bottles. *Nature* **2020**, *580* (7802), 216–219. <https://doi.org/10.1038/s41586-020-2149-4>.
- (178) Vieille, C.; Zeikus, G. J. Hyperthermophilic Enzymes: Sources, Uses, and Molecular Mechanisms for Thermostability. *Microbiol Mol Biol Rev* **2001**, *65* (1), 1–43. <https://doi.org/10.1128/MMBR.65.1.1-43.2001>.

Vita

Jeremy Wang

jeremywang2022@u.northwestern.edu

Phone: (562) 650-8117

EDUCATION

Northwestern University, PhD, Materials Science

GPA: 3.66

Graduation: 2023

Harvey Mudd College, B.S., Physics

GPA: 3.68

Graduation: 2017

Chemistry of Life Processes-Cornew Innovation Award (2020)

- Significantly contributed to and developed a proposal on PETase-copolymer complexes to depolymerize PET that won \$75,000 in internal university funding

RESEARCH AND PROFESSIONAL EXPERIENCE

Northwestern University, Olvera de la Cruz and Torkelson Group

Doctoral Researcher

Fall 2017 - Present

- Synthesized various methacrylate copolymers using free and controlled radical polymerization techniques
- Characterized polymers and molecules using standard techniques such as ¹H NMR, Size Exclusion Chromatography, Light Scattering, MALDI, and LCMS-Electrospray Ionization
- Designed and implemented various polyelectrolyte complex experiments to remove contaminants from water and to conjugate with enzymes to depolymerize PET
- Led projects with collaboration across multiple groups with different fields of expertise, including enzyme production, electron microscopy, and polymer simulations
- Ran coarse-grained polymer simulations with LAMMPS to understand the effects of confinement and electric fields on bulk polyelectrolyte complexes

Harvey Mudd College, Gerbode Lab

Student Researcher

Summer 2015 – Summer 2017

- Developed experimental protocols to use optical microscopy and optical traps to understand and perturb grain boundaries in crystals of colloidal particles
- Used image processing techniques in MATLAB to track colloidal particles and grain boundaries
- Developed a ray optics model to account for optical trap forces in molecular dynamics simulations of colloidal systems

Northwestern INVO office

Intern Patent Evaluator

Winter 2020 – Summer 2020

- Analyzed and evaluated various patent applications and inventions for feasibility, novelty, and impact.
- Performed market research to gauge the value of potential patents and the likelihood of commercial success

PUBLICATIONS

Cash, C. E., Wang, J., Martirosyan, M. M., Ludlow, B. K., Baptista, A. E., Brown, N. M., ... & Gerbode, S. J. (2018). Local melting attracts grain boundaries in colloidal polycrystals. *Physical review letters*, 120(1), 018002.

Wang, J., Waltmann, C., Umana-Kossio, H., Olvera de la Cruz, M., & Torkelson, J. M. (2021). Heterogeneous Charged Complexes of Random Copolymers for the Segregation of Organic Molecules. *ACS central science*, 7(5), 882-891.

Waltmann, C., Mills, C. E., Wang, J., Qiao, B., Torkelson, J. M., Tullman-Ercek, D., & Olvera de la Cruz, M. (2022). Functional enzyme-polymer complexes. *Proceedings of the National Academy of Sciences*, 119(13), e2119509119.

Umana-Kossio, H., Nguyen, T.D., Wang, J., Olvera de la Cruz, M., & Torkelson, J. M. (2022). Unusual Glass Transition Breadths of Ionomers: Effects of Thermal Treatment and Charge-Carrying Side Chains. *Macromolecules*. *Accepted*.

PATENTS

“Assembly of Random Copolymer Polyelectrolyte Complexes for Removal of Contaminants from Water” – Patent No. PCT/US2021/020191. Filed 03/01/2021. Patent pending.

PROFESSIONAL SOCIETY MEMBERSHIPS

Member of the American Physical Society	Summer 2016 - Present
Member of the American Chemical Society	Winter 2020 – Present

OTHER RELEVANT EXPERIENCES

Team Leader for Solvay Additive Manufacturing Cup

- Worked with colleagues to build a 3D printer capable of using high temperature and high performance polymer materials

Project Lead for High Performance Computing server assembly and administration

- Worked with colleagues in the Olvera de la Cruz group to build and maintain an internal computing cluster for running simulations used in research work